The Role of Gene Expression and Aging in SCA1

A DISSERTATION
SUBMITTED TO THE FACULTY OF
UNIVERSITY OF MINNESOTA
BY

Melissa Anne Cornwell Ingram

IN PARTIAL FULFILLMENT OF THE REQUIREMENTS
FOR THE DEGREE OF
DOCTOR OF PHILOSOPHY

Advisor: Harry T. Orr

December 2013

Acknowledgements

There are many people who assisted in my journey and deserve acknowledgements. Thank you to everyone in the Orr lab for helpful comments, fun conversations, and encouragement – Lisa Duvick, Jill Frisch, Brennon O'Callaghan, Nissa Mollema, Orion Rainwater, Emily Leathley, Judit Pérez Ortiz and Tyler Tschumperlin. You all made it an enjoyable place to learn and execute (and sometimes fail) experiments. Thank you Orion, for spending many a day in the mouse room helping me keep track of my massive behavioral cohort and the less glamorous duties that go along with mouse work.

The University of Minnesota Genomics Center and Supercomputing Institute were instrumental in completing and analyzing the RNA-sequencing. Thank you to the many people that were involved in running, transferring and storing the massive amount of sequencing data I generated.

Thank you to all my friends and family. You have made this experience worthwhile. I'm happy to say my success is due to your support and inspiration.

Finally, thank you to my mentor, Harry Orr. You took me in when I needed a lab and a project and some focus. You have also allowed me to explore my career aspirations for which I will be always grateful.

Dedication

To my Mom, who taught me to work with my hands – crafting and cooking and gardening – these were my very first experiments.

To my Dad, who brought home science magazines and a doctor's kit and gave in to just about everything I wanted.

To Kirk.

Abstract

Spinocerebellar ataxia type 1 is an autosomal dominant disorder caused by a CAG repeat expansion encoding a polyglutamine tract, where patients present with a lack of motor coordination including ataxia. The disease is characterized pathologically by loss of Purkinje cells (PCs) in the cerebellar cortex and neuronal loss in brain stem nuclei and cerebellar dentate nuclei. Besides expansion of the polyglutamine tract, other features of ATXN1 are critical for pathogenesis and severity of disease including phosphorylation of ATXN1 at S776. Mouse models expressing an expanded form of ATXN1, *ATXN1[82Q]* share initial disease features, such as ataxia, with mice with a normal repeat length with a phosophomimetic aspartic acid substitution, *ATXN1[30Q]-D776*. However, *ATXN1[30Q]-D776* mice do not display late-stage, progressive disease features including PC death. In order to determine molecular pathways leading to the ataxic similarities as well as progressive disease differences in the models, I used RNA-sequencing to examine the cerebellar transcriptome. In addition to identifying candidate genes, *Col18a1* and *Cck*, involved in PC – climbing fiber dynamics, I found splicing correlates with ataxia in the *ATXN1[82Q]* and *ATXN1[30Q]-D776* mice. In order to validate RNA-seq targets and focus on the more biologically relevant splicing candidates, I developed and analyzed RNA-seq from a conditional *ATXN1[30Q]-D776* model. In addition, I used this model to examine disease recovery. Interestingly, I found a lack of recovery at older ages without PC death, suggesting older neurons are inherently less able to recover.

Table of Contents

List of Tables

List of Figures

Chapter 1: Introduction

Spinocerebellar ataxia

The spinocerebellar ataxias (SCA) are a group of autosomal dominantly inherited neurodegenerative conditions that have ataxia as a major component of the clinical presentation. These patients usually have loss of coordination of the limbs and trunk, unstable gait, dysarthric speech, and nystagmus but may have other symptoms, including extrapyramidal dysfunction, dysautonomia, cognitive impairment, and motor and sensory impairments. The pathological process primarily involves the cerebellum, brainstem and spinal cord. There are approximately 30 different types identified to date with only about half having defined mutations. A number of these diseases, including SCA types 1, 2, 3, 6, 7, and 17 have an abnormal expansion of a CAG-repeat sequence, which codes for an expanded tract of glutamine (Q) residues within the mutated protein (Koeppen, 1998; Orr, 2000).

Spinocerebellar ataxia type 1 (SCA1) is an autosomal dominant disorder caused by a CAG repeat expansion encoding a polyglutamine tract. It is characterized pathologically by loss of Purkinje cells (PC) in the cerebellar cortex and neuronal loss in brain stem nuclei and cerebellar dentate nuclei (Zoghbi and Orr, 1995). The *SCA1* gene encodes ataxin-1, a protein of 792 to 826 amino acids depending on the number of CAG trinucleotides (Servadio et al., 1995). Unaffected alleles contain between 6-42 CAG repeats; the larger alleles

interrupted with 1-3 CAT (or histidine), while disease-related expansions range from approximately 40-80 pure polyglutamine residues (Chung et al., 1993). The age of onset for SCA1 is dependent on the repeat length, though typically occurs in the third or fourth decade (Zoghbi and Orr, 1995). Instability of the CAG repeat leads to genetic anticipation in SCA1, where age of onset decreases in subsequent generations as diseased allele repeat length increases from parent to offspring (Haines et al., 1984; Schut, 1950). Disease manifestations are progressive and there is no cure for SCA1, which is lethal 10-15 years after diagnosis.

Mouse Models of SCA1

Several mouse models have been generated in an effort to understand the molecular mechanisms underlying SCA1 disease and ataxin-1 function. Because SCA1 is a neurodegenerative diseases with an onset several decades into life, modeling in mice may not allow enough time for disease to develop during their relatively short life span. This concern has been realized in a number of models, thus requiring over-expression of the transgene or a worsening of the genetic mutation (e.g., increasing the length of the CAG-repeat expansion) in order to create a clinical phenotype. These manipulations create a potential for misinterpretation of results and require careful controls, such as lines with matched over-expression of normal allelic transgenes. Another tactical issue is

whether to express the mutant transgene in all neurons or cells of the CNS, or to target critical populations such as the Purkinje cell (PC). The advantage of the former approach is that it more closely models the human disease, but in turn it makes interpretation of mechanisms more complex. The advantage of the latter approach is that PCs are critical cells for cerebellar function, they are the primary site of pathology in SCA1, and damage to them usually creates a behavioral phenotype. In addition, PCs have an elaborate dendritic structure, which can be readily studied for morphological and even physiological alterations. A disadvantage of this modeling is that human disease has a more complex pathology.

The first mouse model was generated to test the CAG expansion, gain-of-function hypothesis. Burright *et al.* (Burright et al., 1995) expressed the human SCA1 gene specifically in mouse PC using a Purkinje cell-specific Pcp2/L7 promoter (Oberdick et al., 1990; Smeyne et al., 1991; Vandaele et al., 1991). Two lines were created with various repeat lengths; a control line with over-expression of the normal interrupted allele containing 30 repeats, $(CAG)_{12}$ $CATCAGCAT(CAG)_{15}$, while the expansion construct contained 82 uninterrupted CAG repeats. The control ATXN1[30Q] line, and the expansion ATXN1[82Q] line progeny both inherited the transgene either paternally or maternally and in all animals the repeat was stable and showed no change in repeat size.

After one year of age, the 30Q line had a normal phenotype, suggesting intact PC function. In contrast, the mutant 82Q lines developed reduced cage activity and general uncoordinated movements, which become more pronounced with age until they had clearly ataxic cage behavior at 12 weeks. Footprint patterns indicated gait abnormalities and motor performance measured using a rotating-rod apparatus was abnormal as early as 5 weeks (Clark and Orr, 2000). Pathologic changes were observed in the ATXN1[82Q] cerebellum as early as postnatal day 25 when clear cytoplasmic vacuoles were found in some of the somata of PC (Clark and Orr, 2000). The degeneration progressed with age and by 27 weeks the majority of PC had stunted, atrophic dendritic morphology. At 1 year, the cerebellar cortex was dramatically decreased in size secondary to both atrophy and loss of PC, frequent heterotopic localization of PC in the molecular layer, and diminished calbindin immunoreactivity in surviving PCs. Interestingly, PC loss was preceded by the ataxic phenotype. Adult mice expressing disease-causing forms of ATXN1 in PCs also display alterations in climbing fiber (CF) innervation including a lack of CF terminals on PC dendrites and a reduction in CF-PC synaptic strength (Barnes et al., 2011; Duvick et al., 2010). In addition, ATXN1[82Q] PC accumulated ataxin-1- and ubiquitin-positive aggregates, or neuronal intranuclear inclusions (NII), that co-localized with the proteasome and the molecular chaperone, HDJ-2/HSDJ, demonstrating that there is ataxin-1 misfolding in SCA1 disease (Cummings et al., 1998).

Öz *et.al.* demonstrated that changes in cerebellar neurochemical levels measured by proton magnetic resonance spectroscopy (^{1}H MRS) can distinguish patients with SCA1 from controls (Öz et al., 2010). Specifically, patients exhibit decreased levels of N-acetylaspartate and glutamate, and increased levels of *myo*-inositol, which correlated with ataxia rating scores. These MRS biomarkers were similarly altered in ATXN1[82Q] mice indicating parallel neurochemical changes in the ATXN1[82Q] model and patients (Oz et al., 2010).

To study the effect of mutant ataxin-1 expression under control of its endogenous promoter, a knock-in model was generated by inserting an expanded CAG trinucleotide repeat into the mouse *Sca1* locus. The original model, *Sca*$^{78Q/2Q}$, expressed endogenous levels of expanded ataxin-1 in the expected temporal and spatial patterns. However, the mice lacked any ataxic phenotype or neuropathological abnormalities. A second model was then generated with 154 CAGs (Watase et al., 2002). The *Sca*$^{154Q/2Q}$ phenotype included muscle wasting, ataxia, abnormal gait, severe kyphosis and premature death between 35 and 45 weeks. *Sca*$^{154Q/2Q}$ animals displayed significant motor deficits by rotating-rod analysis at 5 and 7 weeks as well as impaired spatial learning deficits. This was intriguing as when an ATXN1 knock-out model was generated the mice did not display any ataxic symptoms but displayed learning deficits (Matilla et al., 1998). In addition, the *Sca*$^{154Q/2Q}$ mice exhibited a decrease in long-term potentiation at 24 weeks. The *Sca*$^{154Q/2Q}$ animals were distinct from the ATXN1[82Q] model in

that they exhibited repeat instability similar to human patients (Watase et al., 2003). Brains from *Sca*$^{154Q/2Q}$ animals were smaller than controls, though brain sections showed uniform atrophy rather than specific atrophy of the cerebellum more characteristic of SCA1 disease. While slight PC loss was observed, the molecular layer thickness was relatively intact even in 24-week-old animals.

SCA1 disease reversal

To determine if SCA1 disease is reversible, a conditional model of SCA1 was developed using the tetracycline-regulated (Tet) system (Zu et al., 2004). In this case, the *Pcp2/L7* promoter drives the tetracycline-transactivator specifically in Purkinje cells, which can then bind a universally expressed tetracycline response element to induce expression of ATXN1[82Q] solely in PC. Administration of doxycycine (dox) abolishes this interaction and turns off expression of transgenic ataxin-1. Effects of reversal of transgene expression were assessed at early, mid, and late stages of disease. At the early stage, 6-week-old mice demonstrated a rotating-rod deficit that could be reversed after 6 weeks of dox treatment. In addition, PC pathology improved by assessment of molecular layer thickness and dendritic arborization, although heterotopic PC still were present. At mid stage disease, 12 week on – 4 week off animals continued to have rotating-rod deficits similar to 12 and 16 week-on animals. After 8 weeks and 12 weeks of dox treatment, however, rotating-rod performance improved, but only

partially. Interestingly, this 8-week timepoint coincided with the return of mGluR1α glutamate receptors at the Purkinje cell-parallel fiber synapses, albeit at a lower expression level. There was recovery of molecular layer thickness and improved arborization of PC dendrites demonstrating that halting *ATXN1[82Q]* expression at the time of typical onset of ataxia prevents the progression of and partially reverses degenerative changes in PC. When the dox was given to animals at 32 weeks of age, there was no significant improvement of ataxia, but there was some improvement of PC pathology. At all disease stages, the presence of ataxin-1[82Q]-containing NII was rapidly reversible with dox treatment.

ATXN1 domains and localization

ATXN1 contains a highly conserved domain of 12 amino acids at site 768-780, near the c-terminus (Carlson et al., 2009; de Chiara et al., 2009). This region contains a nuclear localization signal (NLS) at amino acids 771-774 (Klement et al., 1998), a 14-3-3 binding motif at amino acids 774-778 (Chen et al., 2003), and a UHM ligand motif (ULM) at amino acids 771-776 (de Chiara et al., 2009). ULMs are found only in proteins involved in RNA splicing (Corsini et al., 2007). ATXN1 also contains a self-association domain between amino acids 495 and 605 (Burright et al., 1997) and a 120 amino acid AXH domain (de Chiara et al., 2003). This AXH domain crystalizes as a dimer with an OB fold, which is a characteristic

of many oligonucleotide-binding proteins and further supports the idea that ATXN1 is an RNA-binding protein.

Neuronal aggregates containing the mutant protein occur in many of the inherited polyglutamine disorders and have been suggested to be a common mechanism for neuropathology (Ross, 1997). To examine the role aggregates play in SCA1, Ataxin-1[77]Δ model was developed by deleting the self-association region of ataxin-1 (Klement et al., 1998). SCA1[77]Δ transgenic mice expressed ataxin-1 in the PC cytoplasm and nucleus, similar to ATXN1[82Q] animals. However, SCA1[77]Δ mice did not develop NII. The absence of NII, however, did not protect transgenic mice from developing PC pathology or ataxia. Indeed, SCA1[77]Δ had the same PC atrophy seen in ATXN1[82Q] animals and performed similarly to ATXN1[82Q] animals in behavioral examinations. Further studies crossed the ATXN1[82Q] to a transgenic mouse overexpressing HSP70 chaperone protein (Cummings et al., 2001). These animals had improvement in ataxic phenotype and Purkinje cell morphology supporting the hypothesis that protein misfolding and impaired clearance of proteins might be contribute to pathogenesis in polyglutamine diseases. These studies suggested that protein misfolding and aggregation may contribute to pathology, but is not the primary form of pathogenicity in SCA1 (Klement et al., 1999).

To determine how cellular localization impacts disease an NLS mutant model was generated. Using the ATXN1[82Q] transgene, a lysine- to-threonine substitution at amino acid residue 772 disrupted the NLS function SCA1^{K772T} (Klement et al., 1998). This resulted in transgenic mice that expressed ataxin-1 primarily in the cytoplasm of Purkinje cells in contrast to control ATXN1[82Q] mice that expressed significant levels in both the cytoplasm and nucleus. More importantly, SCA1^{K772T} mice did not develop ataxia, as measured by rotating-rod deficits or ataxic cage behavior and they had no cerebellar pathology (Klement et al., 1998). This data provided the first evidence that regions outside the polyglutamine tract are important for ATXN1 pathogenesis. Additionally, it provided the first data that ATXN1 must enter the nucleus to cause disease, suggesting that pathogenesis is mediated by an aberrant ATXN1 function in the nucleus.

ATXN1 pathways

To determine ATXN1 function in the nucleus, further studies investigated the role of binding partners in disease. Many proteins bind to ataxin-1 via its AXH domain, including the RORα-Tip60 complex (Serra et al., 2006). Mouse models expressing mutant forms of ataxin-1 expressed decreased levels of RORα and therefore decreased levels of RORα-mediated genes. To evaluate the role of

RORα in SCA1 pathogenesis, ATXN1[82Q] animals were crossed to staggerer heterozygous mice which lack one functional copy of *Rora* (sg/+). ATXN1[82Q]:sg/+ mice had more severe Purkinje cell pathology suggesting that depletion of *Rora* enhances SCA1 disease. Crossing ATXN1[82Q] animals to *Tip60*$^{+/-}$ animals transiently delayed the ATXN1[82Q] cerebellar degeneration by increasing RORa and RORa -mediated gene expression (Gehrking et al., 2011).

ATXN1 also forms a native complex with a transcriptional repressor Capicua (Cic) in a large protein complex (Lam et al., 2006). Both wild-type and expanded ATXN1 form these complexes. Abolishing phosphorylation with an alanine substitution at serine 776 does not prevent these complexes from forming. Rather, Cic interacts with ATXN1 via the AXH domain (Kim et al., 2013). A study that crossed a transgenic line with a duplication of the murine ataxin-1-like protein to the 154Q- knock-in line found that increased levels of ataxin-1-like diminished disease severity in the knock-in line by displacing mutant ataxin-1 from its native complex with Cic (Bowman et al., 2007). These findings support the concept that the selective neuropathology of SCA1 arises from modulation of a core functional activity of Ataxin-1.

Wild-type and mutant ataxin-1 are known to interact with 14-3-3 proteins, and overexpression of 14-3-3 stabilizes ataxin-1 levels in cells and increases neurotoxicity of mutant ataxin-1 in Drosophila (Chen et al., 2003). Similarly,

Sca1[154Q/+] mice with a haploinsufficiency of 14-3-3-episilon show improvement of cerebellar pathology and motor phenotypes but no improvement of weight loss, respiratory function or premature death (Jafar-Nejad et al., 2011). Although both wild-type and mutant ataxin-1 were reduced in the cerebellum of these mice, they were not reduced in the brainstem, which is an area also affected in the Sca1[154Q] mice. This suggests that different pathogenic mechanisms may operate in different regions of the brain affected by the disease (Jafar-Nejad et al., 2011).

Other studies implicate ATXN1's role in gene expression. Since SCA1 and SCA7 share a cerebellar degenerative phenotype, shared transcriptional changes were studied between the two knock-in models. Both *Sca*$^{154Q/2Q}$ and Sca7$^{266Q/2Q}$ mice significantly down-regulated insulin-like growth factor protein 5 (*Igfbp5*) in the granule neurons (Gatchel et al., 2008). This down-regulation in granule cells also was observed in the ATXN1[82Q] transgenic line, suggesting that it occurred by a non-cell-autonomous mechanism, as the change was a result of a pathogenic process initiated in Purkinje cells which solely expressed the mutant protein.

Phosphorylation status critical for pathogenesis

The amino acid sequence of ataxin-1 revealed several possible phosphorylation sites (Banfi et al., 1994). Further analysis by mass spectrometry identified a

serine at amino acid 776 as the major site of phosphorylation (Emamian et al., 2003). This was also of interest due to its location in the highly conserved c-terminus region mentioned above. In addition, evidence indicated that phosphorylation at this site modulated the stability of ATXN1 (Jorgensen et al., 2009). A phosphomimetic aspartic acid mutation at this site was shown to increase the interaction with RNA-binding motif protein 17 (RBM17) to levels comparable to ATXN1[82Q]-S776 (Lim et al., 2008). Thus, ATXN1[82Q] protein or ATXN1 phosphomimetic with a normal repeat tract could similarly alter the normal ATXN1 function and increase the RBM17 mediated pathway.

To examine whether phosphorylation regulates the function and pathogenicity of ataxin-1, mouse models either blocking phosphorylation by substituting alanine for serine (A776) (Emamian et al., 2003) or mimicking phosphorylation by substituting aspartic acid for serine (D776) (Duvick et al., 2010) were generated from the original 82Q and 30Q transgenes. At 5 weeks, ATXN1[82Q]-A776 was localized to the nuclei of PC similarly to ATXN1[82Q]. However, *ATXN1[82Q]-A776* mice formed substantially fewer NII compared to *ATXN1[82Q]* transgenic mice at 32 weeks. In addition, *ATXN1[82Q]-A776* transgenic mice did not develop ataxic cage behavior, did not show deficits by rotating-rod testing, and had only mild PC pathology. These results indicate that the serine at position 776 is critical for disease manifestation, while the expanded polyglutamine tract is not sufficient for disease.

On the other hand, *ATXN1[30Q]-D776* transgenic mice had impaired motor coordination on the Rotarod compared to wild-type and *ATXN1[30Q]* control animals. The level of impairment was similar to that of *ATXN1[82Q]* animals and progressed as animals aged until they could no longer perform the task. Similarly, *ATXN1[30Q]-D776* animals had a significantly widened gait typical of ATXN1[82Q] animals. This was intriguing because a single point mutation, mimicking phosphorylation, converted a wild-type protein to a pathogenic protein. *ATXN1[82Q]-D776* mice had enhanced disease with significant PC atrophy and neuronal loss, while *ATXN1[30Q]-D776* PC were atrophic but did not progress to significant neuronal loss. Therefore, ATXN1[30Q]-D776 can induce disease initiation and Purkinje cell dysfunction, but only mice expressing ATXN1 with an expanded polyQ tract have late stage disease and Purkinje cell death.

Mutant ATXN1 Affects Gene Expression

As previously indicated, clues from mouse models point to RNA-binding and protein-protein interaction as key for ATXN1 function and SCA1 pathogenesis. In addition, the fact that ATXN1 must enter the nucleus suggests that disruption of nuclear structures and functions may lead to changes in gene expression. In an effort to identify expression changes, *ATXN1[82Q]* cerebellar RNA was examined using a PCR-based cDNA subtractive-hybridization assay (Lin et al., 2000). This

study identified six genes that were significantly downregulated in *ATXN1[82Q]* cerebellum including *Icmt*, *Itpr1*, *Atp2a2*, *Slc1a6*, *Trpc3* and *5-phosphatase I*, and one gene, *Serpina1a*, was upregulated. These were not global changes, as many other PC specific genes remained unchanged. In addition, these changes occurred between post-natal day 11 to three weeks of age, prior to detection of any histologic or behavioral abnormalities.

A genetic screen in a Drosophila model of SCA1 identified several genetic loci capable of modulating SCA1 neurodegeneration (Fernandez-Funez et al., 2000). Many of the modifiers identified were those involved in protein folding, heat-shock response and ubiquitination common in polyQ diseases with misfolding. Other enhancer genes implicated oxidative and chemical stress play a role in pathology. Several of the modifiers identified were genes that encoded proteins with RNA-binding domains, suggesting RNA processing is a critical function of ATXN1 and alterations in this pathway lead to pathogenesis. An additional Drosophila study implicated DNA damage repair in SCA1 (Barclay et al., 2013).

These data led to a larger, more in depth study of gene expression changes in disease models using microarrays at 5 and 12 weeks of age (Serra, 2004). This study compared gene expression profiles of affected *ATXN1[82Q]* to unaffected *ATXN1[30Q]* and *ATXN1[82Q]-K772T*. The gene lists were generated and compared, and 12 changes exclusively found to be altered in the *ATXN1[82Q]*

mice but not in either control, were considered relevant. Similar to Lin *et al*, most of the gene changes were downregulated including *Homer3*, carbonic anhydrase-like sequence, G-substrate, *Slc1a6*, *Itpr1*, Purkinje cell protein 1, *Atp2a3*, EST (A1842002), homeotic protein Gtx. Three had increased expression including *Tac1*, *Nrgn*, and EST (AI852661). These findings implicate glutamate signaling pathways in pathogenesis.

Towards identification of disease progression pathways

Previous data indicates that even within the same neuronal cell type, PCs, disease initiation and early progression are distinct from late stage disease progression. *ATXN1[30Q]-D776* induces disease initiation and dysfunction leading to ataxia but only in mice expressing the expanded polyQ tract does disease progress to late stage, PC death (Duvick et al., 2010). The lack of late disease progression to PC death in *ATXN1[30Q]-D776* animals indicates that this later stage requires the presence of an expanded polyQ repeat. Therefore, we hypothesized that comparing *ATXN1[30Q]-D776* with *ATXN1[82Q]* mice would identify PC pathways or molecules that correlate with PC dysfunction and ataxia, as well as features that distinguish disease in the two models. To identify molecular pathways leading to the ataxic similarities as well as progressive disease differences in the models, we used RNA-sequencing to examine the cerebellar transcriptome. Described in chapter 3 is RNA sequence analyses of

the cerebellar transcriptome from two ataxic *SCA1* mouse models, *ATXN1[82Q]* and *ATXN1[30Q]-D776*. The analysis revealed that while *ATXN1[82Q]* and *ATXN1[30Q]-D776* cerebella differed considerably in the expression of a number of genes, they had essentially identical alterations in RNA splicing. In addition, to validate RNA-seq targets and focus on the more biologically relevant candidates I developed a *conditional ATXN1[30Q]-D776* mouse model and analyzed RNA-seq expression and splicing profiles. This led to the identification of a candidate ataxia RNA, *Anks1b*, which is mis-spliced in every ataxic model we tested. We propose that genes whose expression levels differ between *ATXN1[82Q]* and *ATXN1[30Q]-D776* cerebella, such as *Cck* and *Col18a1*, encode proteins that contribute to phenotypes that differ between these two *SCA1* transgenic lines.

Assessing recovery of disease in *conditional ATXN1[30Q]-D776*

Prior studies described the ability of conditional *ATXN1[82Q]* to recover from disease after halting expression of mutant *ATXN1* (Zu et al., 2004). However, the extent of recovery was decreased as animals increase in age. It is unclear if age dependence recovery is due to prolonged exposure to mutant ATXN1 or if older neurons are inherently less able to recover. In addition, delaying *ATXN1* expression until after cerebellar development (which is completed 3 weeks after birth) greatly decreases disease severity (Serra et al., 2006). Since disease the progressive feature of disease is dependent on the presence of an expanded

polyQ tract, we set out to determine if the *ATXN1[30Q]-D776* mice recover with age. We hypothesized that since the *ATXN1[30Q]-D776* mice do not progress or activate cell death pathways, these mice would have enhanced recovery compared to *ATXN1[82Q]* at later ages. However, we found muted recovery at later ages suggesting that recovery is age dependent. These studies are described in chapter 4.

Chapter 2: Methods

Mice

The Institutional Animal Care and Use Committee approved all animal use protocols. *ATXN1[82Q]* (Burright et al., 1995), *ATXN1[30Q]-D776, ATXN1[82Q]-D776* (Duvick et al., 2010), *conditional ATXN1[30Q]-D776* (Ebner et al., 2013), *Pcp2-tTA* (Zu et al., 2004) *Cck*$^{-/-}$ (Jax B6.129-*Cck*^{tm1Lcs}/J) and FVB/NJ mice were housed and managed by Research Animal Resources under SPF conditions in an AAALAC-approved facility. *Conditional ATXN1[30Q]-D776* mice were generated by adding a point mutation to *TRE-ATXN1[30Q]* construct, which were cloned in the same manner as *TRE-ATXN1[82Q]* mice (Zu et al., 2004). The transgene was linearized with *Hind II* and *Xho I*, gel isolated, purified by ethanol precipitation, and suspended in injection buffer (10 mM Tris-Cl [pH 8.0]; 0.1 mM EDTA) at a concentration of 4 ng/ml. Embryo injections were performed by the Mouse Genetics Laboratory, University of Minnesota. PCR and Southern blot analyses were used to identify transgene positive animals. PCR primer sequences include the following: TRE forward 5'- GTGAAAGTCGAGCTCGGT-3', TRE reverse 5'- AGGCAGGCATTCGTTGCT-3', tTA forward 5'- TTGCTCCATTGCGATGAC-3', tTA reverse 5'- AACAGCGCATTAGAGCTG-3'. The Southern blot TRE probe was generated by digest of the *TRE-ATXN1[30Q]* construct with XhoI and EcoRI, isolating PhCMV-1 which contains the TRE sequence, followed by gel purification. Gene off mice were given 1.5mg/ml doxycycline (dox) (purchased from the University of Minnesota Boynton Health Service Pharmacy) in a 4% sucrose solution in their drinking water. Gene-on

animals were given 2% sucrose (to account for equal sucrose intake) for the same amount of time gene-off mice were administered dox. Pcp2 tTA/+ control mice were administered dox similar to the gene-on cohort. In all experiments involving the use of mice, animals of either sex were used.

RNA Isolation

Total RNA was isolated from dissected cerebella using TRIzol Reagent (Life Technologies, Carlsbad, California) following the manufacturer's protocols. Cerebella were homogenized on ice in 500mL TRIzol reagent using an RNase-Free Disposable Pellet Pestles in a motorized chuck. Once tissue was homogenized, 500mL TRIzol reagent was added for a total of 1mL TRIzol reagent per cerebella. Samples were then incubated for 5 minutes at room temperature to permit dissociation of nucleoprotein complexes. Phase separation was completed by adding 0.5mL chloroform, shaking vigorously for 15 seconds, and incubating at room temperature for 2-3 minutes. Samples were centrifuged at 12,000 x g for 15 minutes at 4°C, allowing for collection of the clear upper aqueous layer into a new RNase-free tube. RNA was precipitated from the aqueous layer by the addition of 0.5mL 100% isopropanol, incubating at room temperature for at least 10 minutes and centrifugation at 12,000 x g for 10 minutes at 4°C. The RNA pellet was washed with 75% ethanol, briefly vortexed, and centrifuged at 7,500 x g for 5 minutes at 4°C. The pellet was allowed to air-

dry for 5-10 minutes at room temperature, making sure not to allow the pellet to dry completely. RNA was resuspended in 100-200ul RNase-free water by passing the solution through a pipette tip several times. RNA was incubated for 10-15 minutes at 60°C and stored at -80°C.

For RNA-sequencing RNA was further purified to remove any organic carryover, which can inhibit the enzymatic reactions used in Illumina library preparation and can increase the risk of failure of library generation. RNA was purified using the RNeasy Mini Kit (Qiagen, Venlo, Limburg), and following the manufacturer's RNA Cleanup protocol. Briefly, buffer RLT and ethanol are added to the sample to promote selective binding of RNA to the RNeasy membrane. The sample is then applied to the RNeasy Mini spin column. Total RNA binds to the membrane, contaminants are efficiently washed away, and high-quality RNA is eluted in RNase-free water.

cDNA Synthesis

Random-primed cDNA was generated from 1µg RNA using the SuperScript VILO cDNA Synthesis Kit (Life Technologies) according to manufacturer's protocols. Each reaction contained 4ul 5X VILO Reaction Mix, 2ul 10X SuperScript Enzyme Mix, 1ug RNA and DEPC-treated water to 20ul. Tube contents were mixed,

placed in a PCR block, and incubated at 25°C for 10 minutes, followed by 42°C for 60 minutes, then 85°C for 5 minutes to terminate the reaction. The cDNA generated was then diluted 1:5 for use in RT-qPCR.

RT-PCR

Primers were designed to exon 18 and 20 to amplify four of the splice forms of *Anks1b*. Primer sequences – left: gaaacgcattttggcatctt right: agtttttccggatgatgctg. cDNA was amplified with GoTaq Green Master Mix (Promega, Madison, Wisconsin) following manufacturer's protocols for a 25ul reaction. Samples were amplified and removed from the thermal cycler (Bio-Rad, Hercules, California) after 22, 25 or 30 cycles. Bands were separated by gel electrophoresis and imaged on an UV transilluminator.

RT-qPCR

RT-qPCR reactions were completed using LightCycler 480 Probes Master Mix and hydrolysis probe (Roche, Penzberg, Germany) following manufacturer's protocols. Primer sequences and probe combinations were generated using Universal ProbeLibrary for mouse Assay Design Center (Roche). Universal ProbeLibrary Mouse GAPD Gene Assay (Roche) was used as a control. Mouse *Anks1b* primers include the following: isoform 1 left: CCAGATTGCAACGCTCTTG right: CATGCTCTTCCAGGACTGCT probe #4,

isoform 4 left: CGATGCAAGGAGGAGAAGAA right: CTCCCCAGTCCCCTGTCT probe #78, isoform 3 left: TGATATTCCCCGATCAAAGC right: CGTTCTGATTGGTCCAGATTT probe #34, common assay left: GACAGAGAATTCTACAAGCGATCC right: CAGAGGTGGGATGGTAGCC probe #12. To human *ATXN1* left: AGAGATAAGCAACGACCTGAAGA right: CCAAAACTTCAACGCTGACC probe 67. To mouse *Cck* left: TGATTTCCCCATCCAAAGC right: GCTTCTGCAGGGACTACCG probe 9. To mouse *Col18a1* left: ACCAGGACCAGGATTTGCT right: ATCAGAGCTTCGGGCTGTT probe 97.

RNA-sequencing

Whole cerebellar RNA from three biological replicates for each genoptype was isolated using TRIzol Reagent (Life Technologies) followed by purification with RNeasy Kit according to the manufacturer's protocol (Qiagen) [methods detailed above]. Purified RNA was sent to the BioMedical Genomic Center at the University of Minnesota for quality control, including quantification using fluorimetry (RiboGreen assay, Life Technologies) and RNA integrity assessed with capillary electrophoresis (Agilent BioAnalyzer 2100, Algilent Technologies, Inc.) generating an RNA integrity number (RIN). All submitted samples had greater than 1ug total mass and RINs greater than 8. Library creation was completed using oligo-dT purification of polyadenylated RNA, which was reverse transcribed to create cDNA. The cDNA was fragmented, blunt-ended, and ligated

to barcoded adaptors. The library was size selected to 320bp +/- 5% to produce average inserts of approximately 200bp, and size distribution validated using capillary electrophoresis and quantified using fluorimetry (PicoGreen, Life Technologies) and Q-PCR. The libraries were then normalized, pooled and sequenced. *ATXN1[82Q]*, *ATXN1[30Q]-D776*, and WT/FVB samples were sequenced on an Illumina GAIIX using a 76nt paired-end read strategy, while conditional *ATXN1[30Q]-D776* samples were sequence on an Illumina HiSeq 2000 using a 100nt paired-end read strategy. Data was stored and maintained on University of Minnesota Supercomputing Institute (MSI) Servers. Research Informatics Support Systems (RISS) bioinformaticians were available at MSI for analysis questions and support.

Gene expression analysis with the Tuxedo pipeline was done using the Galaxy platform hosted by the MSI. Initial read quality was determined using FastQC (Andrews) to determine the following: basic statistics, per base sequence quality, per sequence quality scores, per base sequence content, per base GC content, per sequence GC content, per base N content, sequence length distribution, sequence duplication levels, overrepresented sequences, kmer content. Using the FastQC results, reads were trimmed to an acceptable length, e.g. per base sequence quality greater than 28. *ATXN1[82Q]* and *ATXN1[30Q]-D776* reads were processed to remove contaminating adapter sequences. All paired-end

reads were correctly synchronized; this was checked using PE-Sync Report, a tool created by MSI.

Reads were aligned to the mouse reference genome (Illumina igenomes mm9) with Tophat by using mostly default parameters, except a Std. Dev for Distance between Mate Pairs of 60 and using a gene annotation model only looking for supplied junctions. Differential gene expression was determined with Cuffdiff using default parameters. Splicing analysis was completed using GSNAP and DEXseq by using most default parameters. Genes/introns with a $q \leq 0.05$ were considered significant. Genome tracks were visualized with IGV. Results were graphed with CummeRbund. Pathway and clustering analysis was completed with Ingenuity Pathway Analysis (Ingenuity Systems, Redwood City, California) and DAVID Bioinformatics Resource (NIAID, NIH).

Histology and Immunostaining

Animals were deeply anesthetized and transcardially exsanguinated with PBS (pH 7.4) and perfused using 10% formalin (30 mL). Brains were post-fixed overnight in 10% formalin and subsequently placed in PBS at 4ºC before sectioning. The cerebellum was sagittally sectioned into 50 μm thick sections using a vibratome. Epitotopes were exposed using antigen retrieval by boiling sections four times for 10 sec each in 0.01M urea. The sections were blocked overnight in 2% normal donkey serum and 0.3% Triton X-100 in PBS. All

subsequent staining was carried out in 2% normal donkey serum and 0.3% Triton X-100 in PBS. The following primary antibodies were used: rabbit anti-ATXN1 (11750) (Servadio et al., 1995) at 1:2000, rabbit, mouse or goat anti-calbindin (Santa Cruz) at 1:250, mouse anti-Vesicular Glutamate Transporter 2 (VGLUT2) (MAB5504, Millipore) at 1:1000, rabbit anti-Col18a1 (PA5-24199, Thermo Scientific) at 1:100, and (GA5, Cell Signaling) mouse anti-GFAP at 1:200.

Sections were incubated for 24 hr in primary antibodies at 4ºC. Following incubation, the sections were washed three times in PBS and exposed to secondary antibodies (DyLight 488, Dylight 549, and Dylight 649 - Jackson Immunoresearch, West Grove, PA) for 24 hr at 4ºC. Lastly, sections were washed three times in PBS and mounted onto charged slides (Colorfrost Plus, Fisher, Waltham, MA). Fluorescently labeled tissue was imaged using a confocal Olympus 1000 IX inverted microscope.

Quantification of Purkinje cell length and climbing fiber extension distance

PC length and CF extension into the PC dendrites were measured using 20x confocal images from 50 μm cerebellar sections stained for calbindin and VGLUT2 from 6, 12, 16, 20, 24, 28, 32 and 36 week of age animals. Confocal image stacks of 16-μm depth and step size of 2 μm were captured from lobule VI and analyzed using the imaging program, Fluoview Viewer 1.7. The PC length was measured as the distance from the base of the PC soma to tip of the PC

dendrite. CF extension into the molecular layer of lobule VI was measured from the base of the PC soma to the tip of the CF arbor, as previously described (Duvick et al, 2010). Six separate measurements of PC length and CF extension were taken from each image of the PC primary fissure and averaged. On average, eighteen measurements were obtained from three midline sections from the lobule VI of each animal.

Disease Severity Scale

As an assessment of disease status the following disease severity scale was used: 0.5, near-normal but molecular layer (ML) somewhat thinner; 1, mild changes including heterotopic PCs, vacuoles in PCs, thinning of ML, largely confined to the posterior lobules; 2, similar to 1 but more widespread, heterotopic PCs more numerous and often higher in the ML; 3, widespread ML thinning, numerous heterotopic PCs involving anterior lobules nearly as frequently as posterior, mild PC loss, primarily in the posterior lobules; 4, severe disorganization of cerebellar cortex with generalized severe atrophy of ML and frequent heterotopic PCs and PC loss.

Behavioral Analyses

Motor ability was assessed using an accelerating Rotarod apparatus as previously described (Clark et al, 1997). Cohorts of 10 mice, 5 female and 5 male, were tested using four trials per day, with a minimum of 10 minutes resting

period between trials, for 4 consecutive days. Each trial lasted a maximum of 10 min, as the rod accelerated from 4 to 40 rpm over 5 minutes and then remained at the maximum speed of 40 rpm for an additional 5 minutes. Animals were scored in seconds for latency to fall from the rod. If an animal remained on the rod without running for three consecutive turns, it was considered a fall.

Footprint analysis was completed using the DigiGait Imaging System (Mouse Specifics, Inc. Watertown, MA). Mice were placed onto the transparent treadmill moving at 25cm/sec and filmed for at least 6 seconds of continuous walking. Software analysis calculated the hind stance width in cm.

Chapter 3:
RNA sequencing reveals roles for Cck, Col18a1 and Anks1b in Purkinje cell dysfunction in SCA1 mice

Introduction

An important step towards understanding the molecular basis of neurodegenerative disease was the identification of genes in which mutations cause disease. While the genetic basis for many of the inherited neurodegenerative disease is known, it has remained challenging to link a specific molecular alteration with a disease-associated phenotype. Among the inherited neurodegenerative diseases are a group of disorders caused by the expansion of a CAG nucleotide repeat encoding a stretch of glutamine amino acids and, as a group, are known as the polyglutamine diseases. The polyglutamine neurodegenerative disease Spinocerebellar ataxia type 1 (SCA1) is a progressive autosomal dominant disorder caused by a CAG repeat expansion, where patients display loss of coordination of the limbs and trunk, unstable gait, dysarthric speech, and nystagmus pathologically associated with loss of Purkinje cells (PC) in the cerebellar cortex (Zoghbi and Orr, 1995).

Mice expressing human Ataxin-1 with an expanded polyglutamine (*ATXN1[82Q]*) manifest a progressive form of disease similar to that seen in SCA1 patients. Besides expansion of the polyglutamine tract, other features of ATXN1 are critical for pathogenesis and severity of disease. Among these is phosphorylation of ATXN1 at S776, which when substituted with a phospho-resistant alanine renders ATXN1[82Q] nonpathogenic (Emamian et al., 2003). In contrast, placing

a potentially phospho-mimicking aspartic acid at position 776 enhances pathogenesis of ATXN1[82Q] and transforms wildtype ATXN1[30Q] into a pathogenic protein (ATXN1[30Q]-D776) (Duvick et al., 2010). An intriguing feature of disease in mice expressing *ATXN1[30Q]-D776* is that while mice develop signs associated with early disease progression, including an ataxia similar to *ATXN1[82Q]* animals, disease in *ATXN1[30Q]-D776* does not show the late-stage progression to PC death as seen in *ATXN1[82Q]* mice (Duvick et al., 2010). Thus, comparing *ATXN1[30Q]-D776* with *ATXN1[82Q]* mice affords an opportunity to identify PC pathways or molecules that correlate aspects of disease in common between these two SCA1 lines, as well as features that distinguish disease in the two models.

Structural motifs identified in ATXN1, as well as cellular molecules that interact with ATXN1, indicate it functions in the nucleus as a regulator of transcription and RNA-processing with both playing critical roles in pathogenesis. Such motifs include the AXH (Ataxin-1/HBP1) domain that folds into an oligomer-binding (OB)-fold, forming both a putative RNA-binding and a protein-protein interaction surface (Chen et al., 2004; Kim et al., 2013), a nuclear localization signal (NLS) (Klement et al., 1998) that overlaps with or is immediately adjacent to a U2AF homology motif (UHM) ligand motif (ULM). UHM/ULMs are present in proteins associated with RNA splicing (de Chiara et al., 2009). Moreover, ATXN1 interacts with a variety of nuclear components including RNA (Irwin et al., 2005; Yue et al.,

2001), several regulators of transcription including SMRT (Tsai et al., 2004), Capicua (Kim et al., 2013; Lam et al., 2006), Gfi-1 (Tsuda et al., 2005), and the Rora/Tip60 complex (Gehrking et al., 2011; Serra et al., 2006). Additionally, ATXN1 interacts with proteins involved in RNA processing such as the RNA splicing factors RBM17 (Lim et al., 2008) and U2AF65 (de Chiara et al., 2009), and p80 coilin involved in the assembly of U snRNPs (Hong et al., 2003). Of interest is the observation that ATXN1[82Q] as well as ATXN1[30Q]-D776 interact more strongly with RBM17 than wild type Ataxin-1 (Lim et al., 2008).

Based on a role of ATXN1 in regulating gene expression, we reasoned that RNA sequence analysis of the cerebellar transcriptomes of *ATXN1[82Q]* and *ATXN1[30Q]-D776* mice would elucidate pathways that contribute to PC dysfunction in SCA1 mice. Results of this RNA sequence analyses presented here support a model whereby alterations in the level of expression of cholecystokinin and collagen 18a1 are uniquely enhanced in *ATXN1[30Q]-D776* cerebella and likely contribute to alterations in climbing fiber/PC synapse development. On the other hand, changes in RNA splicing patterns are identical in *ATXN1[82Q]* and *ATXN1[30Q]-D776* mice. These latter results suggest that alterations in splicing, notably the splicing of ankyrin repeat and sterile alpha motif domain containing 1B (*Anks1b* or *AIDA-1*), contribute to the development of ataxia seen in both *ATXN1[82Q]* and *ATXN1[30Q]-D776* mice.

Results

Overview of *SCA1* Mouse Cerebellar RNA-seq Analysis

We harvested whole cerebellar RNA from *ATXN1[82Q]*, *ATXN1[30Q]-D776* and wt/FVB animals at 12 weeks of age; at this stage both disease models have ataxia with minimal Purkinje cell atrophy (Fig. 3.1).

Samples were sent to the University of Minnesota Biomedical Genomics Center for library creation and Illumina GAIIx sequencing. In order to pass quality control, each sample was required to have an RNA integrity number (RIN) greater than 8; the cerebellar RNA-seq samples had RINs ranging from 8.3-9.4 with an average RIN of 9.2 (Table 3.1). Using three biological replicates per genotype, a total of 157.4 million paired-end reads were generated with a minimum of 10 million reads per replicate (Table 3.2).

Figure 3.1

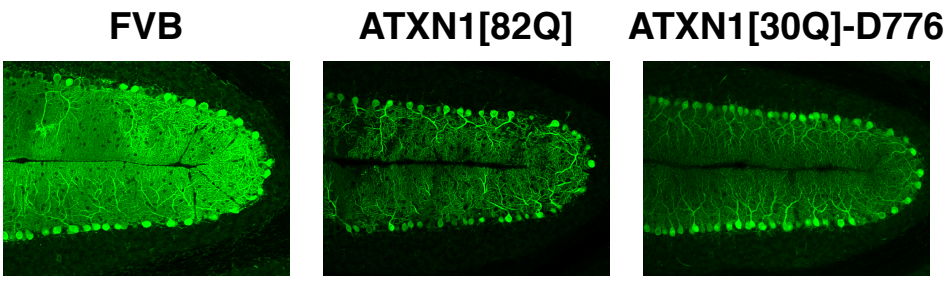

Figure 3.1: Calbindin staining of representative sequenced genotypes shows minimal PC atrophy and absence of cell death at 12 weeks of age.

Table 3.1

Genotype	Replicate ID	RIN
WT/FVB	FVB-1	9.2
	FVB-2	9.1
	FVB-3	9.2
ATXN1[82Q]	B05-414	9.1
	B05-415	9
	B05-416	9.2
ATXN1[30Q]-D776	D30-217	9.4
	D30-220	9.2
	D30-221	9.2
conditionalD30	38997	8.5
	38999	8.3
	38822	8.7
conditionalD30+dox	38823	9
	38824	8.8
	38831	9.1

Table 3.1: RNA-seq samples RNA Integrity Numbers (RIN) indicated RNA sequenced was of high quality.

Table 3.2

	WT/FVB			Total
Replicate ID	FVB-1	FVB-2	FVB-3	
Reads (millions)	13.77	17.61	13.13	**44.51**
	ATXN1[82Q]			
Replicate ID	B05-414	B05-415	B05-416	
Reads (millions)	25.92	12.94	22.24	**61.10**
	ATXN1[30Q]-D776			
Replicate ID	D30-217	D30-220	D30-221	
Reads (millions)	17.47	18.41	15.94	**51.82**
	condATXN1[30Q]-D776			
Replicate ID	38997	38999	38822	
Reads (millions)	115.6	115.5	102	**333.1**
	condATXN1[30Q]-D776+dox			
Replicate ID	38823	38824	38831	
Reads (millions)	101.1	94.83	97.18	**293.1**

Table 3.2: Amount of total RNA-seq reads by sample and genotype.

Initial read quality was determined using FastQC (Andrews). Reads were processed to remove adapter sequences and trimmed. Following data quality control and prepping, the samples were mapped to the UCSC mm9 mouse annotated genome (iGenomes, Illumina). Expression analysis was completed using the Tophat, Cuffdiff pipeline (Langmead et al., 2009; Trapnell et al., 2009, 2010) on the Galaxy interface (Blankenberg et al., 2010; Giardine et al., 2005; Goecks et al., 2010). Alignment was completed using default parameters except for using a Std. Dev for Distance between Mate Pairs of 60 and a gene annotation model only looking for supplied junctions. Greater than 70% read pairs correctly mapped following these parameters (Fig. 3.2). The *ATXN1[82Q]* and *ATXN1[30Q]-D776* samples had 10% less efficient mapping than wt/FVB (Fig. 3.2), due to processing to remove adapter sequences. Differential gene expression was determined with Cuffdiff using default parameters.

Differential gene expression was completed in pairwise comparisons: *ATXN1[82Q]* vs. wt/FVB, *ATXN1[30Q]-D776* vs. wt/FVB, and *ATXN1[82Q]* vs. *ATXN1[30Q]-D776*. *ATXN1[82Q]* and *ATXN1[30Q]-D776* when compared to wt/FVB showed several thousand significant gene changes; a minimum of a two-fold change decreased this number to several hundred (Table 3.3).

Figure 3.2

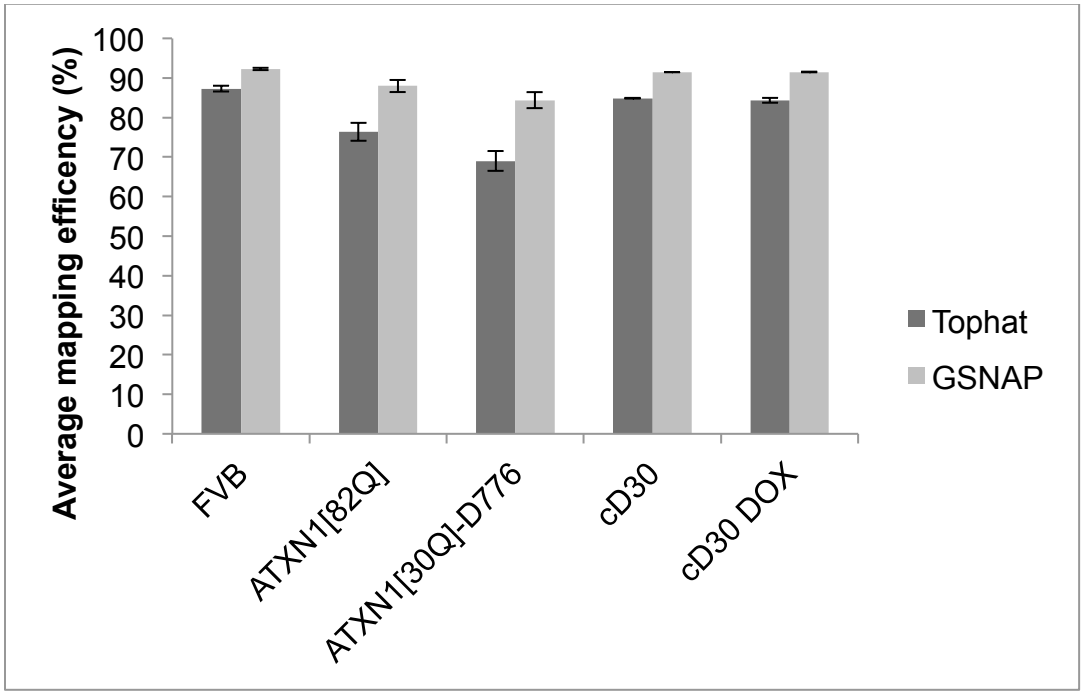

Figure 3.2: Average mapping efficiency using Tophat or GSNAP by genotype.

Table 3.3

Comparison	Number of genes with expression changes	Number of genes with expression changes, ≥2 fold	Number of genes with expression changes FPKM<3	Number of genes with expression changes ≥2 fold, FPKM<3
ATXN1[82Q] vs wt/FVB	6215	454	4789	225
ATXN1[30Q]-D776 vs wt/FVB	5667	888	4385	434
ATXN1[82Q] vs ATXN1[30Q]-D776	457	220	307	98

Table 3.3: Overview of gene expression changes in SCA1 cerebella. Number of significant ($q \leq 0.05$) gene expression changes in pairwise comparisons, and gene expression changes with filters such as requiring greater than a fold change and removing low expressing genes by requiring an FPKM expression value of greater than 3.

The majority of *ATXN1[82Q]* and *ATXN1[30Q]-D776* significant gene changes were downregulated in comparison to wt/FVB (Fig. 3.3).

This is similar to previous results, which found downregulation of gene expression in SCA1 mouse models to predominate (Crespo-Barreto et al., 2010; Lin et al., 2000; Serra, 2004). Direct comparison of *ATXN1[82Q]* and *ATXN1[30Q]-D776* datasets yielded 457 genes whose expression level significantly changed with 220 of those having a minimum of a two-fold change. Of the 457 genes differentially expressed between *ATXN1[82Q]* and *ATXN1[30Q]-D776* cerebella, 157 genes were also significantly different in comparison to wt/FVB (Fig. 3.4A).

Splicing analysis was accomplished by mapping with GSNAP/GMAP (Wu and Watanabe, 2005) and using DEXSeq for differential exon usage (Anders et al., 2012). Pairwise comparisons showed global splicing changes in both *ATXN1[82Q]* and *ATXN1[30Q]-D776* when compared to wt/FVB (Table 3.4). Interestingly, we observed a highly significant amount of overlap (Fisher's exact test p=0) in splicing profiles with 6853 significant splicing changes in common between *ATXN1[82Q*] and *ATXN1[30Q]-D776*. Moreover, pairwise comparisons of the *ATXN1[82Q]* and *ATXN1[30Q]-D776* yielded only 1 significant result, *Slc20a1* (Table 3.4). However, only a single exon was identified as significantly changed in *Slc20a1*, and as it did not correlate with isoform specificity it was not further pursued as a target gene.

Figure 3.3

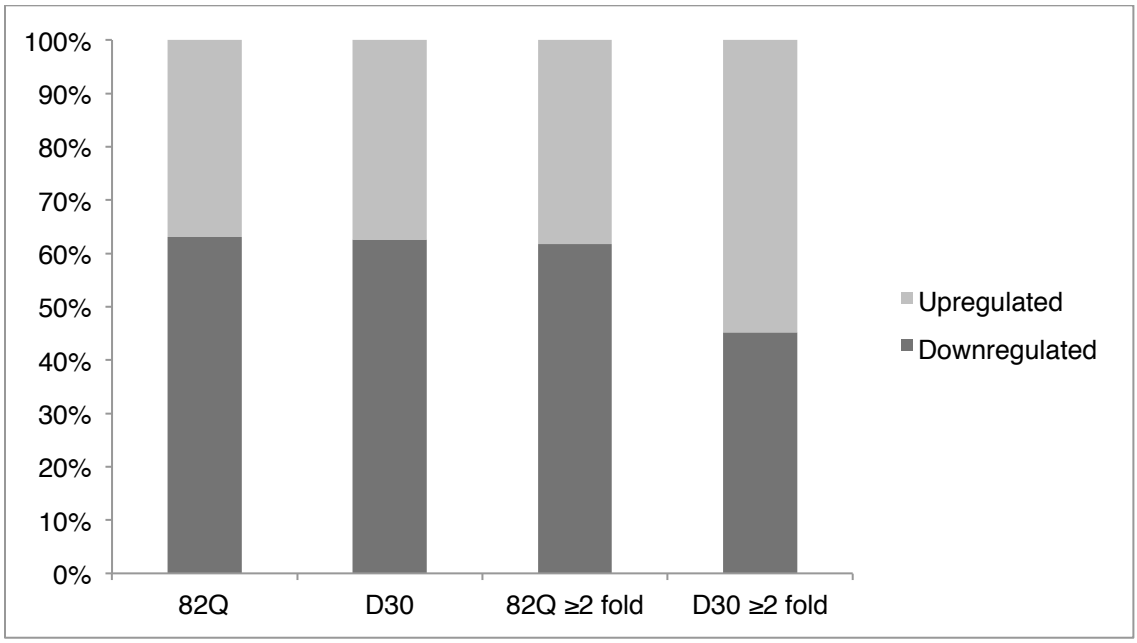

Figure 3.3: Percentages of upregulated and downregulated genes relative to wt/FVB.

Table 3.4

Comparison	Number of genes with splicing changes
ATXN1[82Q] vs wt/FVB	8085
ATXN1[30Q]-D776 vs wt/FVB	7464
ATXN1[82Q] vs ATXN1[30Q]-D776	1
condATXN1[30Q]-D776 vs condATXN1[30Q]-D776+Dox	96

Table 3.4: Overview of splicing changes in SCA1 cerebella. Number of genes with significant ($q \leq 0.05$) splicing changes in pairwise comparisons.

Figure 3.4

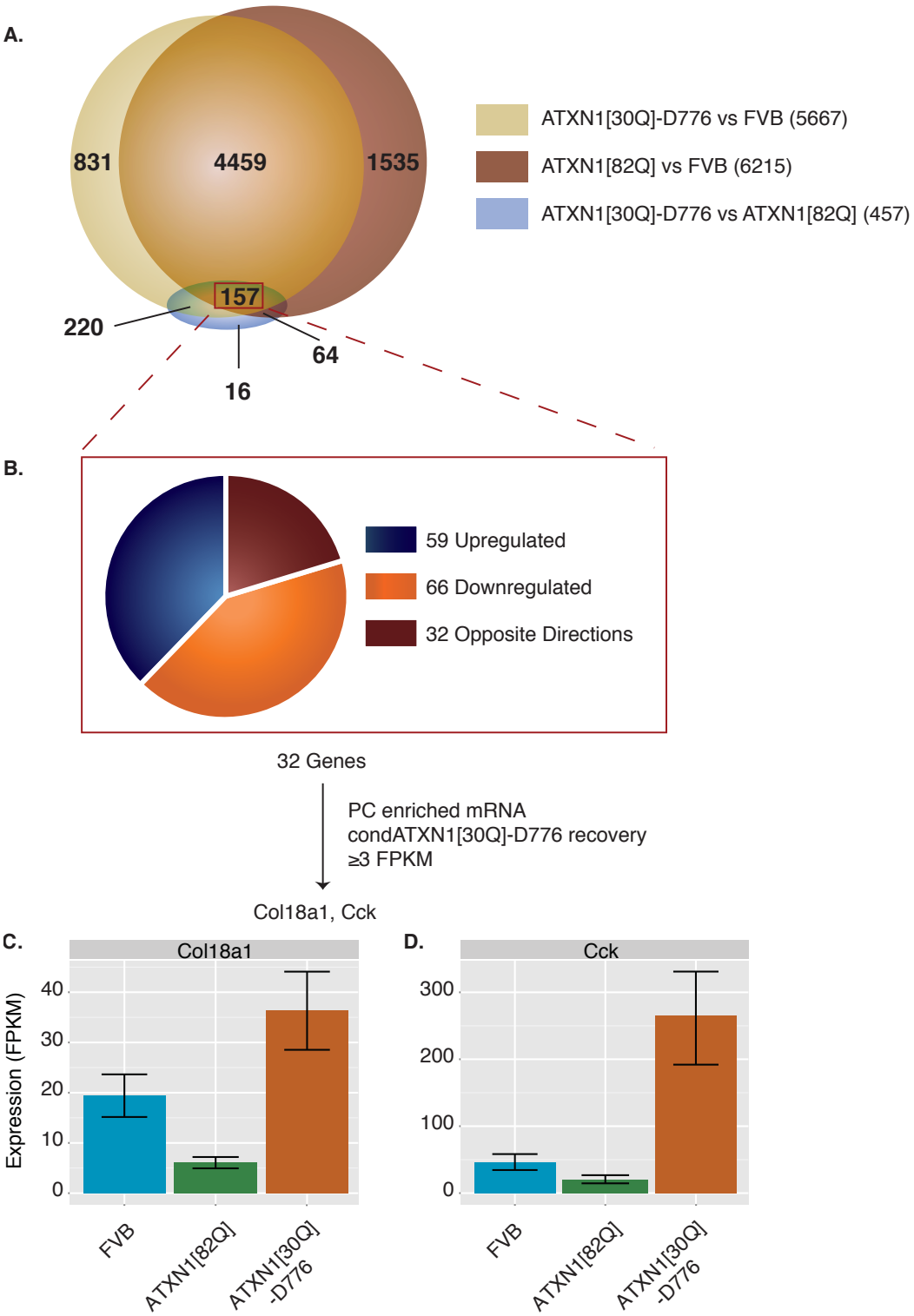
A.
831
4459
1535
157
220
64
16
ATXN1[30Q]-D776 vs FVB (5667)
ATXN1[82Q] vs FVB (6215)
ATXN1[30Q]-D776 vs ATXN1[82Q] (457)
B.
59 Upregulated
66 Downregulated
32 Opposite Directions
32 Genes
PC enriched mRNA
condATXN1[30Q]-D776 recovery
≥3 FPKM
Col18a1, Cck
C.
Col18a1
Expression (FPKM)
40
30
20
10
0
FVB
ATXN1[82Q]
ATXN1[30Q]
-D776
D.
Cck
300
200
100
0
FVB
ATXN1[82Q]
ATXN1[30Q]
-D776

Figure 3.4: Gene expression. (A) Venn diagram reporting significant ($q<0.05$) genes for each pairwise comparison. A total of 157 genes (red box) are significantly different in all three gene lists. (B) The majority of shared changes go in the same direction (125 of 157 or 79.6%). Further candidate selection including moderate FPKM values of ≥3.0, inclusion in a PC enriched translated mRNA list, and recovery in the conditional *ATXN1[30Q]-D776* model after cessation of gene expression resulted in identification of two target genes, *Col18a1* and *Cck*. RNA-seq expression results for *Col18a1* (C) and *Cck* (D).

In summary, these analyses revealed a considerable number of differences in gene expression in cerebellar RNA isolated from *ATXN1[82Q]* and *ATXN1[30Q]-D776* when compared to wt/FVB cerebellar RNA. In addition, there were a large number of genes whose cerebellar expression differed between *ATXN1[82Q]* and *ATXN1[30Q]-D776* mice. This suggests expression differences may underlie some of the phenotypic differences in the models. In contrast, while *ATXN1[82Q]* and *ATXN1[30Q]-D776* each had a substantial number of RNAs whose splicing differed when compared to wt/FVB cerebellar RNA, when compared to each other, *ATXN1[82Q]* and *ATXN1[30Q]-D776* showed virtually identical splicing patterns at 12 weeks of age. Thus, splicing may correlate with common aspects of disease in the two models.

Col18a1 **and** ***Cck*** **Contribute to Enhanced CF synapse on PC Soma in** ***ATXN1[30Q]-D776*** **Mice**

Since cerebellar RNAs from *ATXN1[82Q]* and *ATXN1[30Q]-D776* mice differed considerably in the number of RNAs with altered levels of expression, we reasoned that a detailed examination of the 157 RNAs that differed significantly in expression level between *ATXN1[82Q]* and *ATXN1[30Q]-D776* mice and with each compared to wt/FVB would reveal proteins that contribute to the differences in phenotype (Fig. 3.4 A). Most of the RNAs in *ATXN1[30Q]-D776* and *ATXN1[82Q]* that differed significantly in expression compared to wt/FVB

changed in identical directions, i.e. 59 were upregulated and 66 were downregulated in both ataxic models relative to wt/FVB (Fig. 3.4 B). We further reasoned that focusing on the remaining 32 genes that responded in opposite directions *ATXN1[30Q]-D776* and *ATXN1[82Q]* relative to wt/FVB would reveal genes whose expression likely underlies the differences between the two ataxic models (Fig. 3.4 B & Table 3.5).

Table 3.5

Gene Name	Wildtype	ATXN1[82Q]	ATXN1[30Q] -D776	condATXN1[30Q]-D776 recovery
6030405A18Rik	1.17113	0.766082	2.09542	no
AI593442	8.55231	6.96229	14.4775	no
B3gat1	18.9886	15.5848	24.3486	yes
Camk2a	31.3633	15.394	61.9661	yes
Cck*	45.4973	20.7823	265.736	yes
Coch	3.2505	4.70457	1.99663	no
Col18a1*	19.2714	6.04303	36.3187	yes
Col5a1	2.61754	0.607579	5.07817	yes
Cpne4	0.908513	0.50765	1.67215	no
Elfn2	4.22289	2.75463	6.3964	no
Enc1	6.8663	4.2024	14.1487	no
Fzd7	17.3004	20.9037	13.3422	no
Grin2b	0.825747	0.557256	1.42982	no
Hrh3	7.28959	5.82844	11.4311	no
Hs3st4	1.29894	0.82005	3.16942	no
Ildr2	3.30077	2.62193	4.27992	no
Lmo7*	2.82506	2.07159	4.03173	yes
Mal2	3.3759	1.94973	5.06744	no
Miat	3.74863	2.65277	8.67382	no
Necab2	2.46155	1.50403	4.89033	no
Pde2a	13.6148	11.1162	18.8879	no
Rasgrf2	1.96399	1.21796	3.46647	no
Resp18	38.3563	30.6832	54.0057	no
Rgs4	9.51738	7.32466	12.3916	yes
Slc18a2	1.64983	1.09999	2.66408	no
Sorcs2	3.68513	2.92577	6.71481	no
Spnb3	136.922	114.395	193.129	yes
Spry4	2.38957	1.7532	3.29265	yes
Syt16	1.60265	0.932945	2.78156	no
Tph2	0.885536	0.157855	4.78416	no
Wnt3	5.86374	4.35632	7.75199	yes
Pcp2*	668.13	534.349	859.828	no

Table 3.5: Full gene list of 32 genes with expression (FPKM) differing in opposite directions. Asterisks denote PC enriched translated mRNA (Heiman et al., 2008).

Of the 32 genes whose expression differed in opposite directions, two were selected as being of specific interest, cholecystokinin (*Cck*) and collagen, type XVIII, alpha 1 (*Col18a1*). First of all, detection of both transcripts was robust, these genes were moderately expressed having FPKM values of ≥3.0 (Mortazavi et al., 2008). Importantly, both transcripts are in a list of PC enriched translated mRNAs (Heiman et al., 2008). In addition, expression of *Cck* and *Col18a1* was restored to wt/FVB levels in a *condATXN1[30Q]-D776* mice upon cessation of transgene expression (Fig. 3.4 C). Lastly, the differences in expression of these two genes were dramatic in *ATXN1[82Q]* cerebellar RNA compared to *ATXN1[30Q]-D776* samples. *Cck* expression was elevated in *ATXN1[30Q]-D776* samples, being roughly five fold higher than in wt/FVB RNA and 12-fold higher than in *ATXN1[82Q]* cerebellar RNA (Fig. 3.4 C). Expression of *Col18a1* compared to wt/FVB was 3-fold lower in *ATXN1[82Q]* and almost 2-fold higher in *ATXN1[30Q]-D776* cerebellar RNA samples (Fig. 3.4 D). We examined Col18a1 protein expression in *ATXN1[82Q], ATXN1[30Q]-D776* and wt/FVB cerebella. In accordance with the RNA-seq data, only the *ATXN1[30Q]-D776* PC bodies and dendrites stain positive (Fig. 3.5).

Figure 3.5

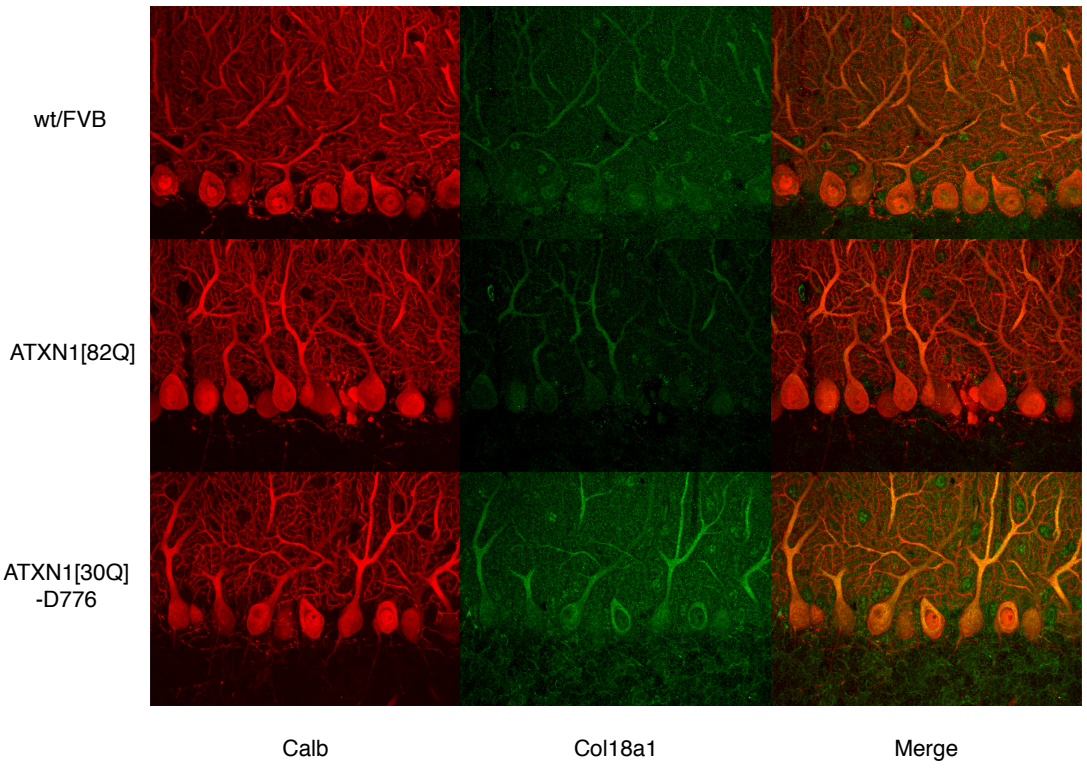

Figure 3.5: Col18a1 expression in mouse cerebella. Calbindin (red) and Col18a1 immunostaining (green) showing upregulation of Col18a1 in *ATXN1[30Q]-D776* and positive staining in the PC bodies and dendrites.

While *Col18a1*, and its proteolytically derived fragment endostatin, are critical for proper formation of CF synapses on the dendrites of PCs (Su et al., 2012), little is known regarding the role of Cck in the CNS, and in particular the cerebellum is less well understood (Matsui et al., 1993; Wood et al., 1988). To determine if *Cck* overexpression has a role in any of the cerebellar phenotypes in *ATXN1[30Q]-D776* animals, we bred them to *Cck*$^{-/-}$ mice. The *ATXN1[30Q]-D776*/Cck$^{-/-}$ mice exhibit ataxic cage behavior as early as 5 weeks, similar to *ATXN1[30Q]-D776* animals. At 12 weeks of age, we examined cerebella of *ATXN1[30Q]-D776/Cck*$^{-/-}$ for histopathology. While no molecular layer changes were observed, there was a significant decrease in the number of CF puncta on the PC body in comparison to *ATXN1[30Q]-D776* mice (Fig. 3.6).

Figure 3.6

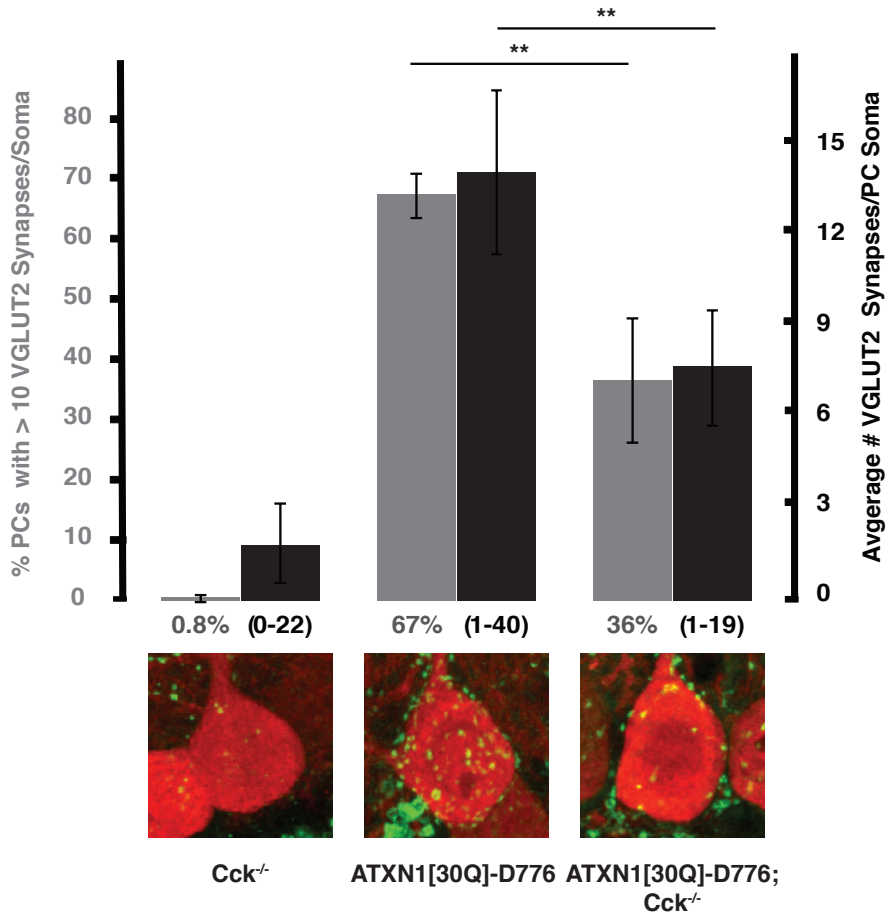

Figure 3.6: Reduction in CF synapses in *ATXN1[30Q]-D776;CCK*$^{-/-}$ PCs. Graph shows number of PCs with >10 VGLUT2 synapses (left axis, grey bars) and average number of VGLUT2 synapses per PC soma (right axis, black bars) in mice 12 weeks of age; wt/FVB (n=83 PCs), *ATXN1[30Q]-D776* (n=132 PCs), *ATXN1[30Q]-D776;CCK*$^{-/-}$ (n=129 PCs). Below are representative images of isolated PCs (calbindin, red) and VGLUT2 (green).

Alterations in Splicing of *Anks1b* Correlate with Ataxia in *SCA1* mice

Both *ATXN1[82Q]* and *ATXN1[30Q]-D776* mice develop ataxia to a similar level of severity (Duvick et al., 2010), both ATXN1[82Q] and ATXN1[30Q]D776 proteins interact strongly with the splicing factor RBM17 (Lim et al., 2008), and the pattern of splicing we detected by sequencing of cerebellar RNA from these two lines essentially overlapped (Table 3.4). Therefore, we hypothesized that common splicing alterations underlie development of ataxia in *ATXN1[82Q]* and *ATXN1[30Q]-D776* animals. However, the large number of RNAs (6853) whose splicing is significantly altered in common in *ATXN1[82Q]* and *ATXN1[30Q]-D776* compared to wt/FVB mice complicates the identification of candidate “ataxia” RNAs.

As a strategy to hone in on candidate RNAs whose altered splicing might contribute to ataxia in these mice, we sequenced cerebellar RNA from *condATXN1[30Q]-D776* tet-off mice (Ebner et al., 2013). Whole cerebellar RNA was harvested from three biological replicates of gene-on *condATXN1[30Q]-D776* at 12 weeks-of-age and *condATXN1[30Q]-D776* animals that were allowed to age for 6 weeks with the gene on and then aged an additional six weeks with the ATXN1[30Q]D776 gene off. Prior to RNA isolation, all animals were assessed for motor deficit via the accelerating Rotarod. Importantly, six-week gene on/six-

week gene off *condATXN1[30Q]-D776* animals fully recovered the ability to perform this test (Fig. 3.7, *condATXN1[30Q]-D776* model discussed further in chapter 4).

RNA was prepared for sequencing as above. However, in this case sequencing was performed using an Illumina HiSeq 2000 with a 100nt paired-end read strategy. Splicing analysis revealed 96 genes with significant splicing changes (Table 2), 77 of which overlap with the 6854 common splicing changes. Gene ontology analysis using DAVID (Database for Annotation, Visualization and Integrated Discovery) (Huang et al., 2008, 2009) identified 16 of the 96 genes with a GO term synapse, consistent with the concept that synaptic dysfunction(s) contribute to development of ataxia in these mice (Barnes et al., 2011; Hourez et al., 2011). This included ankyrin repeat and sterile alpha motif domain containing 1B (Anks1b), which was also included in the *ATXN1[82Q]* and *ATXN1[30Q]-D776* vs. wt/FVB significant splicing lists.

Figure 3.7

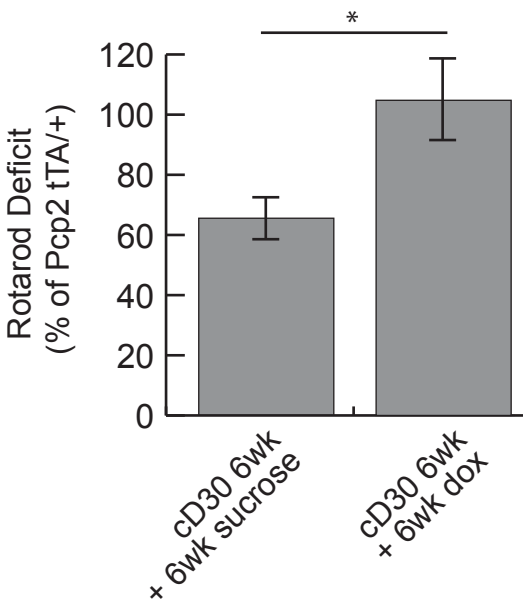

Figure 3.7: Recovery of *condATXN1[30Q]-D776* Rotarod deficit and ataxia after six weeks of treatment with dox to turn the gene off.

Figure 3.8

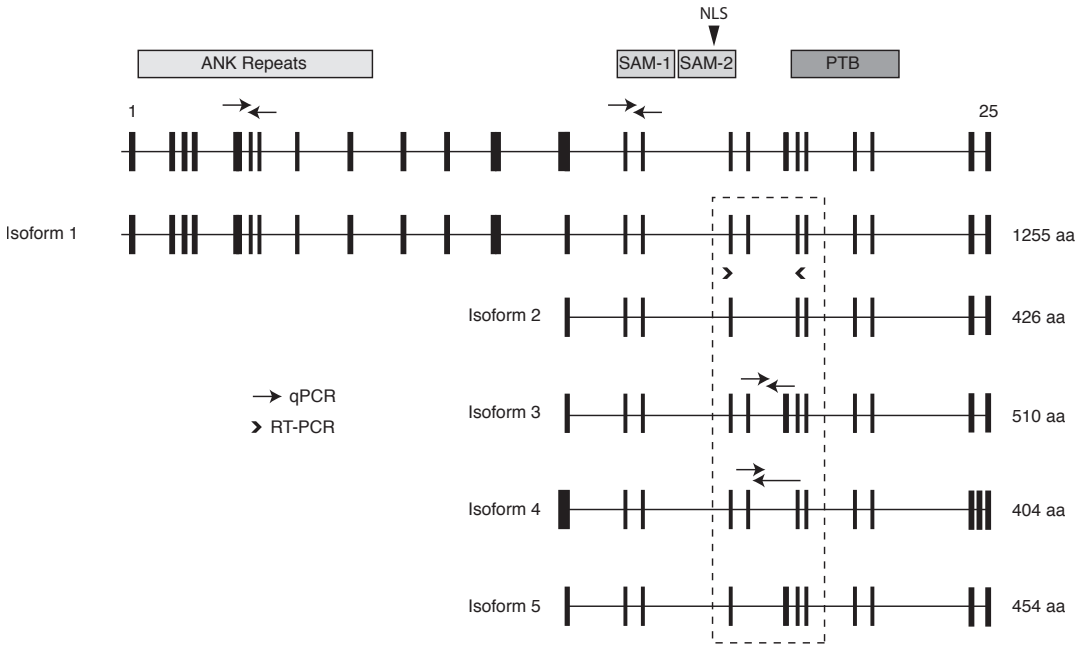

Figure 3.8: Diagram of Anks1b isoforms and locations of structural domains. Arrows represent primer locations for either RT-PCR or q-PCR.

Figure 3.9

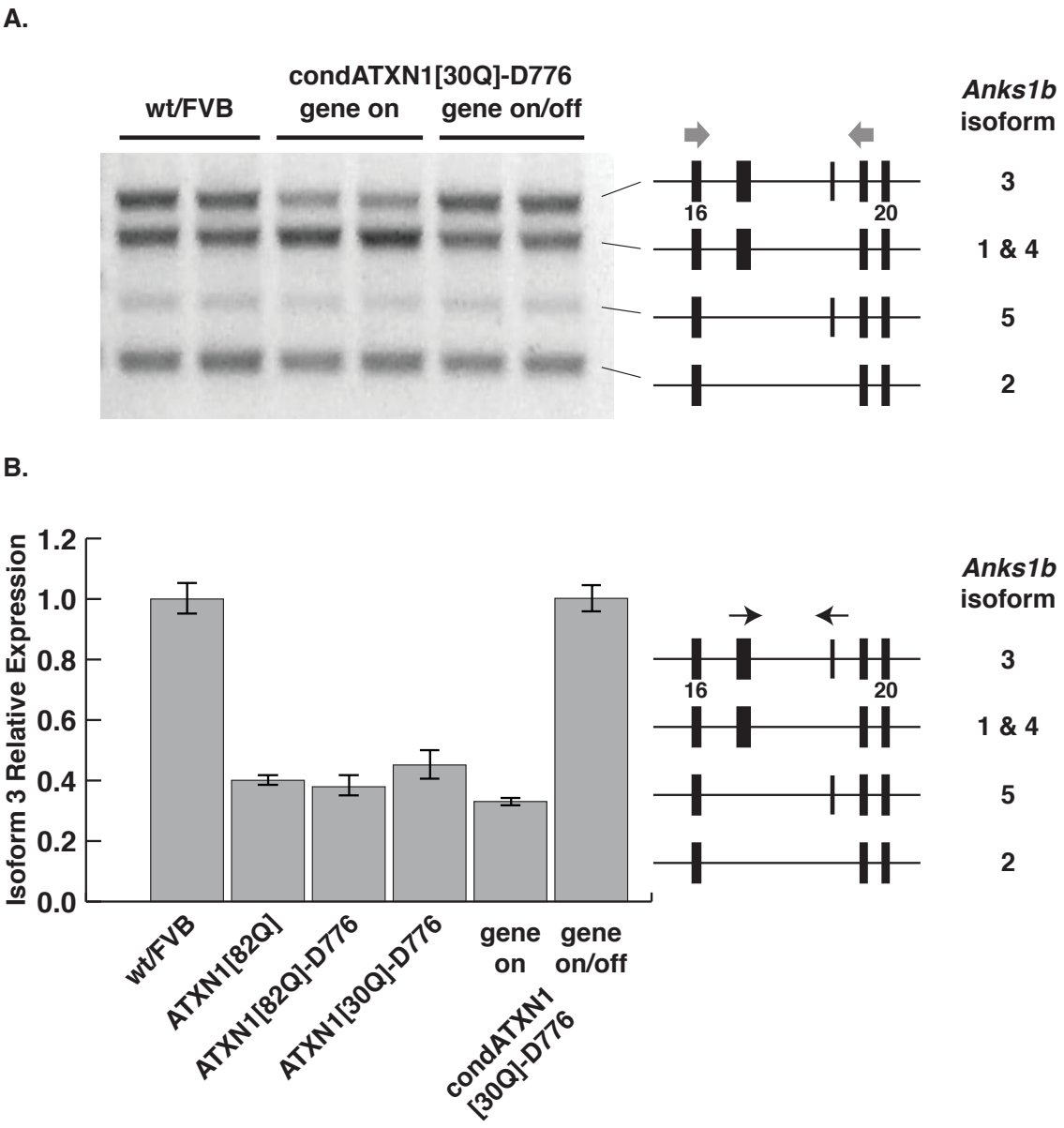

Figure 3.9: *Anks1b* isoform 3 is downregulated in SCA1 models. (A) RT-PCR of *Anks1b* isoforms 1-5 after 25 cycles shows a decrease in isoform 3 (top band) in *condATXN1[30Q]-D776* that increases after treatment with dox. (B) Graph shows relative expression (RT-qPCR) of isoform 3 in wt/FVB, *ATXN1[82Q], ATXN1[82Q]-D776, ATXN1[30Q]-D776,* condATXN1[30Q]-D776 and condATXN1[30Q]-D776 + dox cerebella at 12 weeks of age.

To validate splicing changes in each of the mouse models, we designed RT-PCR primers to identify splicing changes in a region that has isoform specific exon inclusion (Fig. 3.8, dashed box). RT-PCR showed a reduction in isoform 3 levels in *condATXN1[30Q]-D776* cerebellar RNA that was restored with dox treatment, while the other isoform levels stayed consistent (Fig. 3.9 A). We also designed RT-qPCR assays to quantify several of the isoforms including 1, 3, 4, and a RT-qPCR assay detecting an exon in common among all isoforms (Fig. 3.8). Isoforms 2 and 5 had no unique exons in which to base a test. The common assay showed changes consistent with RNA-seq data (data not shown). Interestingly, isoform 3 showed reduced levels in each ataxic mouse model, which was rescued to wt/FVB levels in the *condATXN1[30Q]-D776* treated with dox (Fig. 3.9 B). Thus, expression of isoform 3 of *Anks1b* in six different mouse lines correlated perfectly with the presence or absence of ataxia with a decreased level of *Anks1b* isoform 3 denoting lines with ataxia.

Implicated Pathways

In addition to identifying candidate genes, pathway analysis using Ingenuity® Pathway Analysis (IPA®) software was completed to determine if any pathways were predominantly affected. Core analysis was completed by setting minimum values at 2 FPKM, and 0.05 false discovery rate (q-value).

First, we examined the top diseases and biological functions. IPA categorizes the *Top Diseases and Bio Functions* into the following three groups: Diseases and Disorders, Molecular and Cellular Functions, and Physiological System Development and Function. As may be expected, neurological diseases top the diseases and disorders section for the *ATXN1[82Q]* and *ATXN1[30Q]-D776* compared to wt/FVB. When I examined top networks (summarized in Table 3.6), five were identified in the *ATXN1[82Q]* vs *wt/FVB* comparison, all with a score of 28 including one, hereditary disorder, neurologic disease, psychological disorder, and two, RNA post-transcriptional modification, cellular assembly and organization, nucleic acid metabolism. In the *ATXN1[30Q]-D776* vs *wt/FVB* comparison the top networks are one, connective tissue disorders, developmental disorders, hereditary disorders and two, RNA post-transcriptional modification, RNA damage and repair, molecular transport. Direct comparison of *ATXN1[30Q]-D776* and *ATXN1[82Q]* identified hematological system development and function, developmental disorder, hematological disease as the top network and hereditary disorder as the top disease and disorder. The *condATXN1[30Q]-D776* treated with or without dox, once again identified neurological disease as the top disease and disorder and identified cell death and survival, cellular assembly and organization, cellular compromise as the top network.

Table 3.6

Comparison	Top Networks	IPA score
ATXN1[82Q] vs *wt/FVB*	Hereditary disorder, neurologic disease, psychological disorder	28
	RNA post-transcriptional modification, cellular assembly and organization, nucleic acid metabolism	28
	Cancer, cellular movement, cellular compromise	28
	Cellular growth and proliferation, reproductive system development and function, cancer	28
	Connective tissue disorders, dental disease, developmental disorder	28
ATXN1[30Q]-D776 vs *wt/FVB*	Connective tissue disorders, developmental disorders, hereditary disorders	29
	RNA post-transcriptional modification, RNA damage and repair, molecular transport	29
	Cell death and survival, dermatological diseases and conditions, developmental disorder	29
	Post-translational modification, cell-mediated immune response, cellular movement	29
	Hematological disease, organ morphology, skeletal and muscular system development and function	27
ATXN1[30Q]-D776 vs *ATXN1[82Q]*	Hematological system development and function, developmental disorder, hematological disease	41
	Cell cycle, cellular development, cell death and survival	31
	Cell-to-cell signaling and interaction, nervous system development and function, neurological disease	29
	Gene expression, behavior, cell-to-cell signaling and interaction	28
	Cancer, cellar development, tumor morphology	28
condATXN1 [30Q]-D776 treated vs untreated	Cell death and survival, cellular assembly and organization, cellular compromise	43
	Cellular assembly and organization, cellular function and maintenance, audiotry and vestibular system development	38
	Skeletal and muscular system development and function, organismal development, developmental disorder	36
	Cell-to-cell signaling and interaction, nervous system development and function, auditory disease	34
	Auditory disease, hereditary disorder, neurological disease	32

Table 3.6: Top associated networks from IPA analysis.

Since the networks and diseases and bio functions had similar results in the comparisons, I next focused on canonical pathways. Both *ATXN1[82Q]* vs *wt/FVB* and *ATXN1[30Q]-D776* vs *wt/FVB* have molecular mechanisms of cancer as the top canonical pathway affected (Figure 3.10). This includes major signaling pathways that contribute to malignant phenotypes such as GPCR signaling, Ras/integrin signaling, Akt signaling, TGF-β/BMP signaling, WNT signaling, Notch and Hedgehog signaling and Death receptor signaling. The most highly upregulated genes were *Jun* and *Fos*, while the most downregulated genes were *Camk2a* and *Bmp5* (Figure 3.10). The direct comparison of *ATXN1[30Q]-D776* vs *ATXN1[82Q]* resulted in the Cck/Gastrin pathway being the most affected, reinforcing our selection of *Cck* as a top candidate. The *condATXN1[30Q]-D776* treated with or without dox identified axonal guidance, synaptic long term depression, and synaptic long term potentiation (Figure 3.10).

Figure 3.10

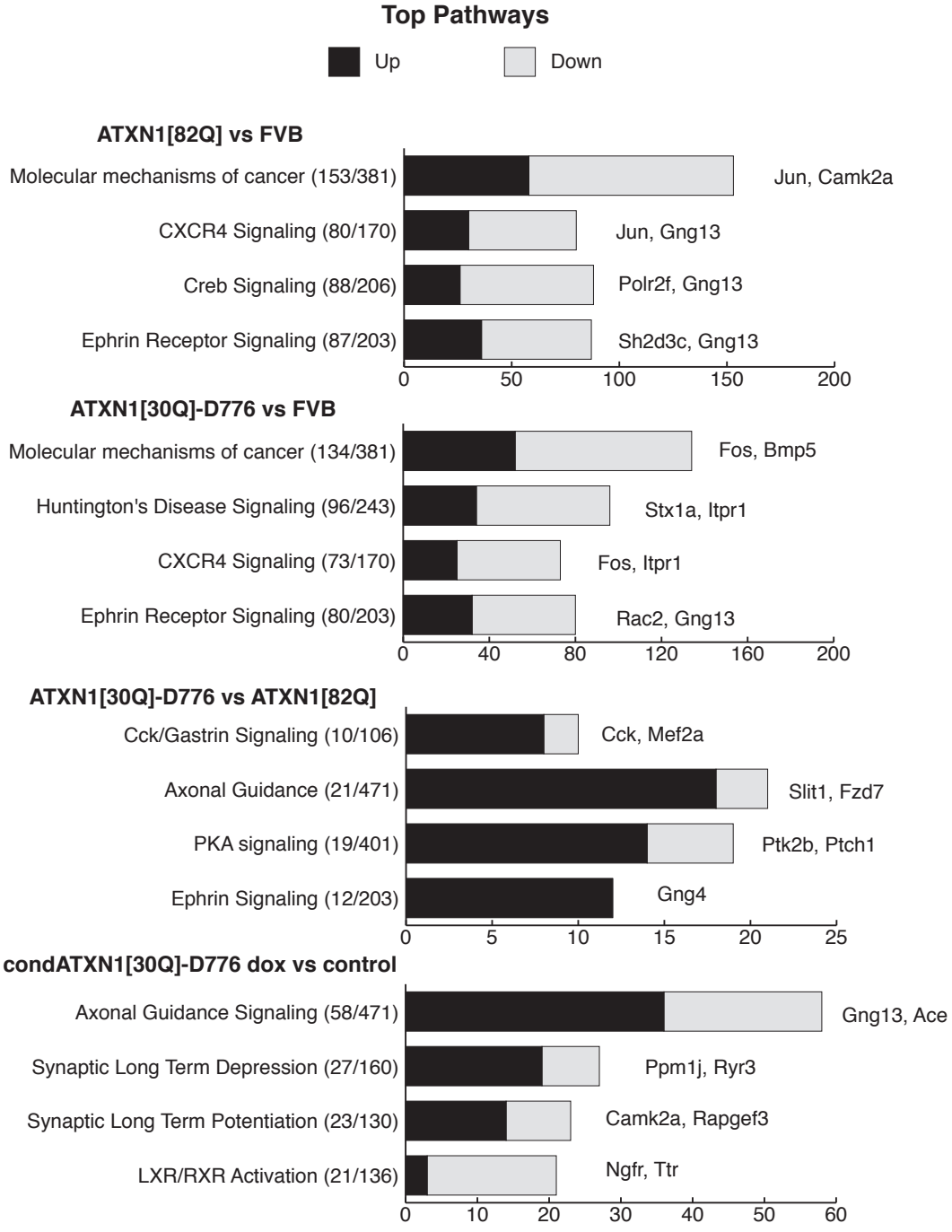
Top Pathways
Up
Down
ATXN1[82Q] vs FVB
Molecular mechanisms of cancer (153/381)
Jun, Camk2a
CXCR4 Signaling (80/170)
Jun, Gng13
Creb Signaling (88/206)
Polr2f, Gng13
Ephrin Receptor Signaling (87/203)
Sh2d3c, Gng13
0
50
100
150
200
ATXN1[30Q]-D776 vs FVB
Molecular mechanisms of cancer (134/381)
Fos, Bmp5
Huntington's Disease Signaling (96/243)
Stx1a, Itpr1
CXCR4 Signaling (73/170)
Fos, Itpr1
Ephrin Receptor Signaling (80/203)
Rac2, Gng13
0
40
80
120
160
200
ATXN1[30Q]-D776 vs ATXN1[82Q]
Cck/Gastrin Signaling (10/106)
Cck, Mef2a
Axonal Guidance (21/471)
Slit1, Fzd7
PKA signaling (19/401)
Ptk2b, Ptch1
Ephrin Signaling (12/203)
Gng4
0
5
10
15
20
25
condATXN1[30Q]-D776 dox vs control
Axonal Guidance Signaling (58/471)
Gng13, Ace
Synaptic Long Term Depression (27/160)
Ppm1j, Ryr3
Synaptic Long Term Potentiation (23/130)
Camk2a, Rapgef3
LXR/RXR Activation (21/136)
Ngfr, Ttr
0
10
20
30
40
50
60

Figure 3.10: Top pathways associated with gene expression changes in SCA1 mice. Canonical pathway name followed by the number of molecules changed in the gene list from total molecules in the pathway. Black bar represents gene upregulation and gray bar represents gene downregulation. The genes listed are the top changed genes up and down respectively.

Discussion

RNA-seq reveals more expression similarities in *ATXN1[82Q]* and *ATXN1[30Q]-D776* than anticipated

RNA sequence analyses of the cerebellar transcriptome from *ATXN1[82Q]* and *ATXN1[30Q]-D776* compared to wt/FVB generated large significant gene expression lists with 6215 and 5667 significant gene expression changes respectively. We also found that a great number of these genes (4459) overlap, e.g. they are found in both groups. In addition, many of the same pathways and networks were implicated using pathway analysis.

While many genes were differentially changed in *ATXN1[82Q]* and *ATXN1[30Q]-D776* it was surprising to find that extent of similarity. It suggests that despite lacking an expanded polyglutamine tract, the *ATXN1[30Q]-D776* is a good model of SCA1 disease and can be used to further our understanding of the differences between initial disease features and late stage disease features like PC death.

RNA-seq expression differences reveal roles for *Cck* and *Col18a1* in CF/PC synapse dysfunction

RNA sequence analyses of the cerebellar transcriptome from two ataxic *SCA1* mouse models, *ATXN1[82Q]* and *ATXN1[30Q]-D776*, in comparison to each other as well as to control wt/FVB revealed that while *ATXN1[82Q]* and *ATXN1[30Q]-D776* cerebella differed considerably in the expression of a number of genes, they had essentially identical alterations in RNA splicing. Thus, we propose that genes whose expression levels differ between *ATXN1[82Q]* and *ATXN1[30Q]-D776* cerebella encode proteins that contribute to phenotypes that differ between these two *SCA1* transgenic lines. In contrast we suggest that the common alterations in splicing promote phenotypes shared by *ATXN1[82Q]* and *ATXN1[30Q]-D776* mice, most notably the motor deficits associated with the ataxia seen in both lines.

In the case of RNAs whose expression differed significantly between *ATXN1[82Q]* and *ATXN1[30Q]-D776* cerebella, we found two to be particularly intriguing - collagen, type XVIII, alpha 1 (*Col18a1*) and cholecystokinin (*Cck*). First, the RNA-seq data revealed that both were expressed significantly higher in *ATXN1[30Q]-D776* than in either ATXN1[82Q] and wt/FVB cerebella, suggesting they could have a role in a phenotype unique to the *ATXN1[30Q]-D776* cerebellum/PCs. Second, consistent with *Col18a1*and *Cck* contributing to the

molecular phenotype of PCs they both are among the top RNAs present in a bacTRAP translational profile of PCs (Heiman et al., 2008). Third, a mutation in *COL18A1* was reported to segregate with a recessive neurological disorder that included ataxia in an Indian family (Paisán-Ruiz et al., 2009). In addition, a recent study found that Col18a1, specifically a proteolytic endostatin fragment of Col18a1, is necessary and sufficient to induce formation of climbing fiber synapses on PCs. In absence of Col18a1 CFs still targeted PCs and seem to extend along the PC dendritic tree, but failed to form synaptic terminals as assessed by the presence of VGlut2 puncta (Su et al., 2012). Moreover, *Col1a1*$^{-/-}$ mice also demonstrated ataxia as assessed by the rotarod (Su et al., 2012). The requirement of Col18a1/endostatin for the formation of CF/PC synaptic terminals suggests that overexpression of Col18a1 in *ATXN[30Q]-D776* mice may contribute to the enhanced number of CF terminals found on *ATXN[30Q]-D776* PCs (Figure 3.11) (Ebner et al., 2013). Our finding that the reduced number of CF terminals on PC soma induced by ATXN1[30Q]-D776 in *ATXN[30Q]-D776:Cck*$^{-/-}$ mice indicates that Cck also has a role CF/PC synapse configuration. In many neurodegenerative diseases, synaptic dysfunction precedes cell death and correlates with development of neurological deficits (Wishart et al., 2006). The conclusion that Col18a1 and Cck have a role in CF/PC synapse organization along with the finding that both were downregulated in *ATXN1[82Q]* cerebella is consistent with them having a role in CF/PC dysfunction seen in *ATXN1[82Q]* SCA1 mice (Barnes et al., 2011).

Figure 3.11

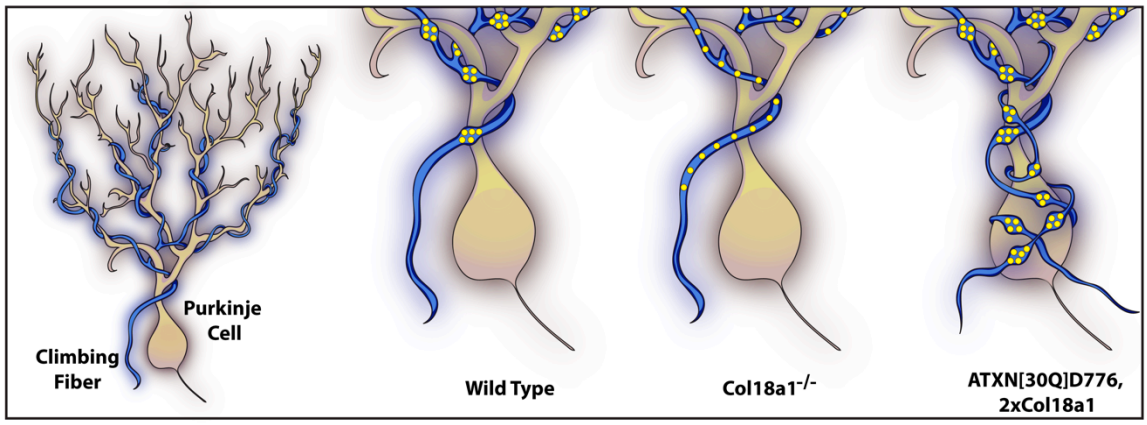

Figure 3.11: Diagram of the CF-PC synapses forming with absence or enhanced levels of *Col18a1*. *Col18a1*$^{-/-}$ PCs display a lack of synapses while ATXN1[30Q]-D776 mice have twice as much *Col18a1* and have increased levels of synapse formation.

RNA-seq splicing profile similarities in *ATXN1[82Q]* and *ATXN1[30Q]-D776* suggest abnormal splicing may cause ataxia in SCA1

Analysis of the RNA-seq data revealed that *ATXN1[82Q]* and *ATXN1[30Q]-D776* cerebellar transcriptomes have a high number of splicing changes when compared to wt/FVB. Yet, there was essentially a complete overlap in RNAs that were alternatively spliced in *ATXN1[82Q]* and *ATXN1[30Q]-D776* cerebella. While ATXN1 is known to interact with two splicing factors, RBM17 and U2AF65 (de Chiara et al., 2009; Lim et al., 2008), its interaction with RBM17 is thought to be dependent on both polyQ tract length and phosphorylation status of S776 in that RBM17 interacts strongly with both ATXN1[82Q] and ATXN[30Q]-D776 (Lim et al., 2008). We suggest that the ability of ATXN1[82Q] and ATXN[30Q]-D776 to interact strongly with RBM17 is an important factor in the high degree of similarity found in the alternative splicing patterns of *ATXN1[82Q] and ATXN[30Q]-D776* cerebellar RNA.

Conditional *ATXN1[30Q]-D776* RNA-seq identified *Anks1b* isoform 3 mis-splicing correlated with ataxia

Applying RNA-seq analysis to a recently developed conditional *ATXN[30Q]-D776* transgenic line (Ebner et al., 2013), proved to an effective strategy for focusing in on RNAs with alterations in splicing that likely correlate with ataxia. Interestingly

of the 96 RNAs whose splicing returned to a wt pattern with recovery from ataxia, sixteen grouped into the synaptic function category by GO analysis, indicating further that synaptic dysfunction is key to the pathogenesis of ataxia in SCA1. Among the sixteen "synaptic" RNAs with a splicing pattern that returned to wt with recovery from ataxia in conditional ATXN1[30Q]-D776 cerebella, one, *Anks1b*, we propose is particularly intriguing.

Anks1b, also know as amyloid b protein precursor intracellular domain associated protein-1 (AIDA-1), contains multiple conserved domains including ankyrin repeats, sterile alpha motif and a phosphor-tyrosine binding domain. *Anks1b/AIDA-1* has a complex genomic organization with several isoforms generated by alternative splicing with the various isoforms having specific subcellular localization, function and binding partners. In this regard, it is of note that *Anks1b* was unique in our analysis in that it had multiple exons with alternative splicing. In particular was mouse isoform 3, which was found to have decreased expression in each of four *SCA1* transgenic lines with ataxia. This isoform encodes a 510 amino acid protein highly similar to human isoform b (AIDA-1d in rat). AIDA-1d is reported to function in signaling from the synapse to nucleus in an activity dependent manner where it promotes protein synthesis regulating nucleolar assembly (Jordan et al., 2007).

The ability of a neuron to regulate and increase protein synthesis in response to persistent stimulation is suggested to be a critical process (Jordan et al., 2007). PCs do have to cope with a considerable level of stimulation from PF and CF synapses. The decrease in the amount of *Anks1b* isoform 3 seen with mutant ATXN1 expression could result in an inability to properly nucleolar numbers and protein synthesis in response to synaptic activity leading to PC dysfunction and ataxia.

Pathway Analysis of *condATXN1[30Q]-D776* RNA-seq Highlights Synaptic Changes

The *condATXN1[30Q]-D776* RNA-seq data was useful to narrow down potential targets that associated with ataxia. Pathway analysis identified axonal guidance signaling, synaptic long term depression (LTD) and synaptic long term potentiation (LTP) (Figure 3.10). This further emphasizes the importance of the synapse function, the development of ataxia and the potential to find targets to reverse ataxic phenotypes.

Chapter 4:

Recovery of Conditional *ATXN1[30Q]-D776* Mice

Introduction

Disease timecourse is well established in the SCA1 mouse model, *ATXN1[82Q].* This model expresses full length human *ATXN1* with 82 CAGs specifically in Purkinje cells driven by Purkinje cell-specific promoter Pcp2 (Burright et al., 1995). *ATXN1[82Q]* animals initially show reduced cage behavior and develop ataxic cage behavior around 12 weeks of age. They also exhibit Rotarod and gait abnormalities suggestive of ataxic motor impairments as early as 5 weeks of age. In addition, pathological changes resemble patient phenotypes such as cerebellar atrophy and Purkinje cell loss (Clark et al., 1997), as well as ^{1}H MRS biomarkers for neurochemical changes (Oz et al., 2010). However, pathological changes occur much later than neurological abnormalities suggesting PC dysfunction rather than cell death results in ataxia.

Prior studies described the ability of conditional *ATXN1[82Q]* to recover from disease after halting expression of mutant *ATXN1* (Zu et al., 2004). This study demonstrated dysfunctional neurons are able to recover if mutant *ATXN1* expression is blocked. However, the extent of recovery was decreased as animals increase in age. It is unclear if age dependence recovery is due to prolonged exposure to mutant ATXN1 or if older neurons are inherently less able to recover. In addition, delaying *ATXN1* expression until after cerebellar development (which is completed 3 weeks after birth) greatly decreases disease

severity (Serra et al., 2006).

Interestingly, adult mice expressing disease-causing forms of *ATXN1* in their PCs display alterations in CF innervation of PCs that include a lack of CF terminals on PC secondary and tertiary dendrites and a reduction in the CF-PC synaptic strength (Barnes et al., 2011; Duvick et al., 2010). In particular, the increased number of CF terminals present on the PC soma in *ATXN1[30Q]-D776* mice is reminiscent of the CF “pericellular nests” that form transiently during early postnatal cerebellar development (Altman, 1972).

We set out to determine recovery profiles of *ATXN1[30Q]-D776* mice since the progressive feature of disease is dependent on the presence of an expanded polyQ tract and these mice offer an opportunity to examine the regulation of CF innervation of PCs. This also allows us to assess the extent to which alteration PC-CF circuitry might contribute to disease.

Results

Generation of a conditional SCA1 model

We generated a conditional SCA1 model using the tetracycline-regulated system (Gossen and Bujard, 1992; Yamamoto et al., 2001). In the absence of tetracycline, the tetracycline transactivator (tTA) binds to tetracycline responsive elements (TRE), inducing expression of the respective downstream gene. In the presence of tetracycline or its derivative doxycycline (dox), the ability of the tTA protein to bind TRE sequences is abolished due to a conformational change in the tTA via the interaction of dox with the tTA. Thus, expression of the respective gene is suppressed (Figure 4.1). Conditional *ATXN1[30Q]-D776* mice were generated by adding a point mutation to *TRE-ATXN1[30Q]* construct in order to substitute an aspartic acid for the serine at amino acid 776. These were cloned in the same manner as *TRE-ATXN1[82Q]* mice as previously described (Zu et al., 2004). Embryo injections were performed by the Mouse Genetics Laboratory, University of Minnesota. PCR and Southern blot analyses were used to identify transgene positive animals. Pcp2-tTA mice (Zu et al., 2004) were crossed to *TRE-ATXN1[30Q]-D776* mice to place both genes in a single mouse.

Figure 4.1

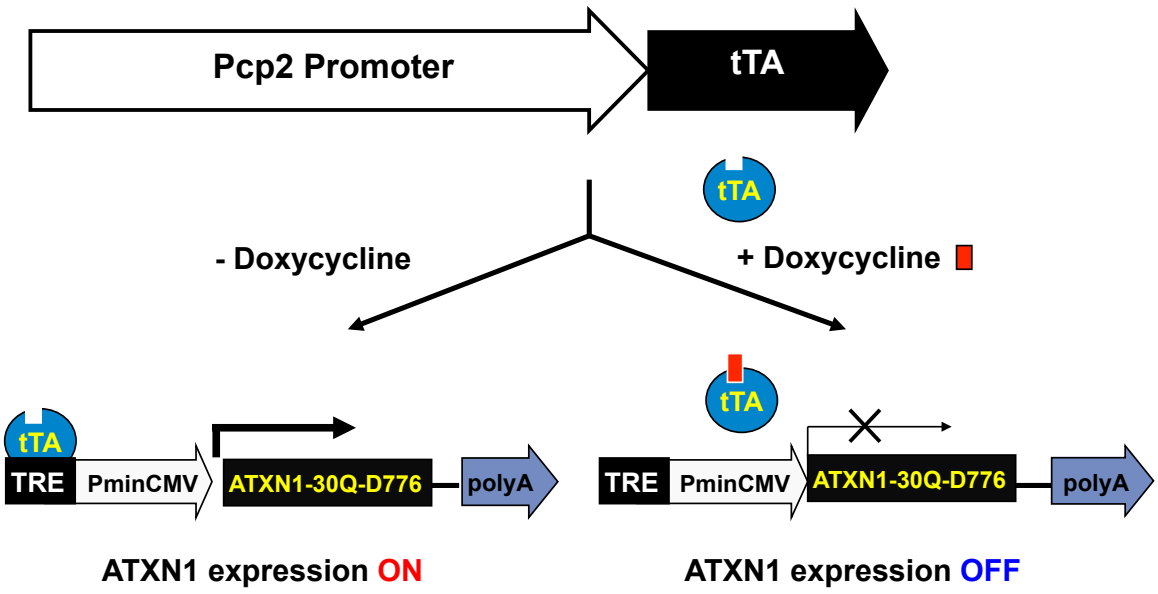

Figure 4.1: Tet-Off conditional model. Diagram of Tet-Off system used to design the *condATXN1[30Q]-D776* conditional model. Tetracycline transactivator (tTA) expression was driven only in PCs by the PC specific promoter Pcp2. Active tTA binds to the tetracycline response elements (TRE) to induce expression of the *ATXN1[30Q]-D776* transgene. The presence of doxycyclin inhibits expression of *ATXN1[30Q]-D776* by binding to the tTA and inactivating it.

To determine which line to use for recovery experiments, initial characterization was performed on the two lines with the highest expression line 2 (L2) and line 3 (L3), analyzed by qRT-PCR. Initial analysis by immunostaining was completed to ensure uniform expression in PCs (Figure 4.2). As both L2 and L3 had high and expression throughout the cerebellum, I tested the lines for ataxic behavior including motor function and hind stance width. Rotarod analysis indicated both lines were impaired compared to tTA/+ controls but not to nontransgenic FVB controls (Figure 4.3). In addition, hind stance width was increased in these lines (Figure 4.4). Since L2 had a greater Rotarod deficit and had a larger hind stance width I chose L2 to continue with future experiments.

ATXN1[30Q]-D776 mice have high mRNA expression (Duvick et al., 2010). In an effort to increase conditional *SCA1* mRNA levels, the mice were bred to homozygosity for the L2-*TRE-ATXN1[30Q]-D776* transgene. The resulting mice, *TRE-ATXN1[30Q]-D776/TRE-ATXN1[30Q]-D776;tTA/+* will henceforth be referred to as *condATXN1[30Q]-D776*. As illustrated and discussed below (Figure 4.6C), *condATXN1[30Q]-D776* expressed lower levels of the transgene than *ATXN1[30Q]-D776.*

Figure 4.2

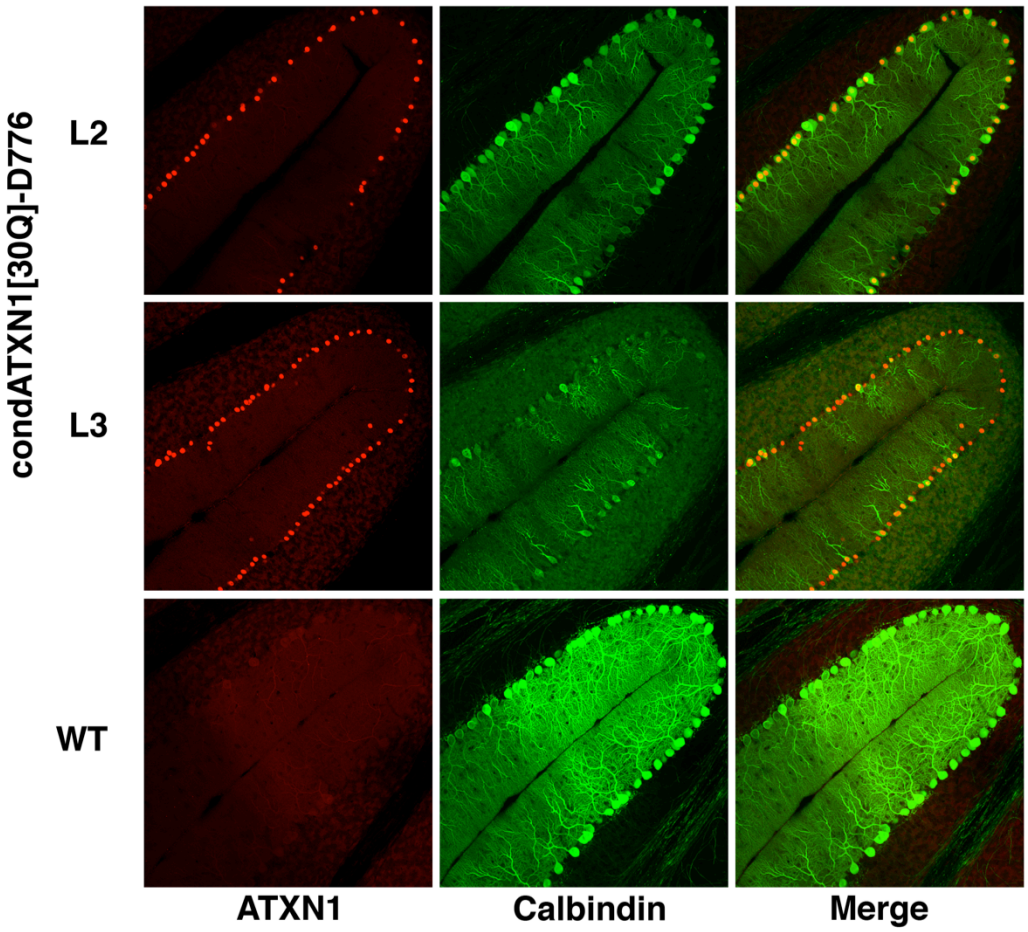

Figure 4.2: ATXN1 expression in *condATXN1[30Q]-D776* cerebella. Immunostaining of ATXN1 (red) and Purkinje cells (green, calbindin) to assess uniform expression of the transgene in the cerebellum.

Figure 4.3

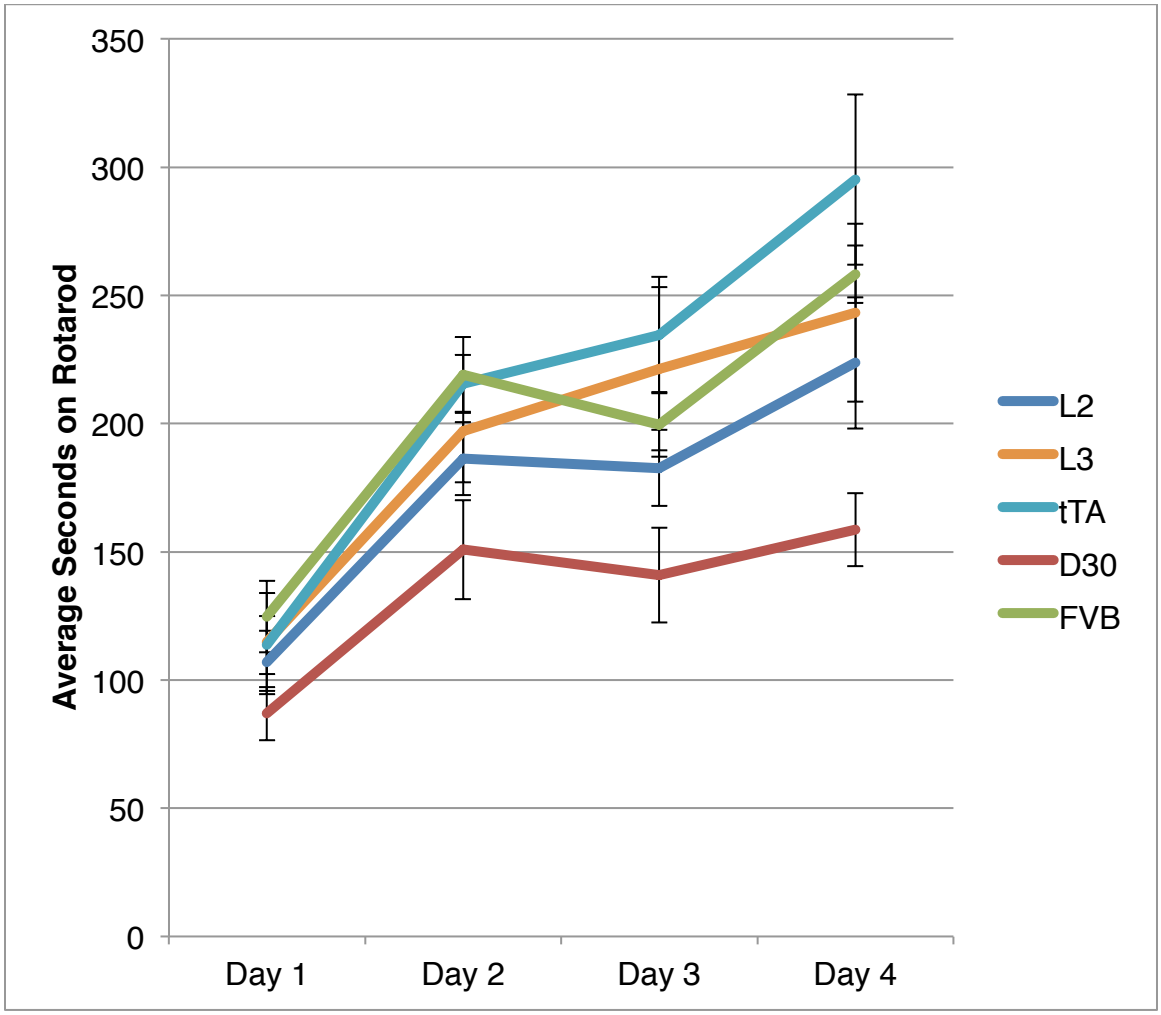

Figure 4.3: Motor coordination deficits in *condATXN1[30Q]-D776* lines. Line 2 and Line 3 of the conditional model show deficits by Rotarod analysis compared to the tTA control.

Figure 4.4

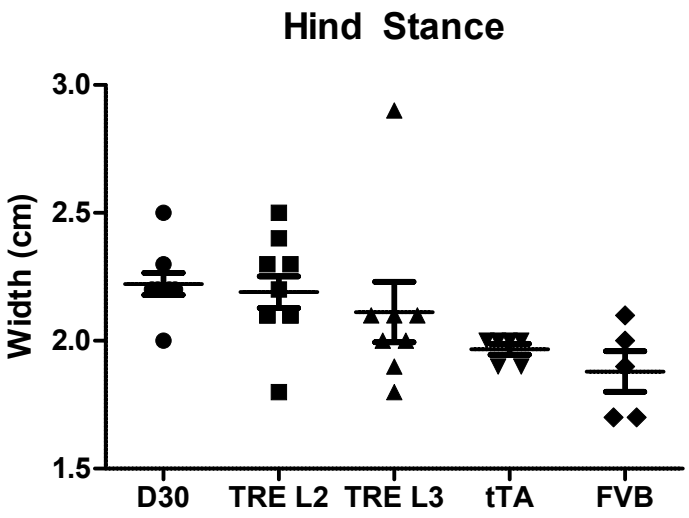

Figure 4.4: Hind Stance width in *condATXN1[30Q]-D776* lines. Line 2 and Line 3 of the conditional model show greater hind stance width compared to the tTA control.

As shown in Fig. 4.3 and 4.4, the tTA transgene, for some unknown reason, conferred some improvement to Rotarod ability and hindstance width, which is also seen in the *condATXN1[30Q]-D776* lines (hemizygous for the tTA transgene). Therefore, I chose tTA/+ as my control line to account for these differences in behavior.

The ability of dox to turn off gene expression in *condATXN1[30Q]-D776 mice* was assessed by giving 12-16 week old mice dox in their drinking water. Animals were sacrificed at 24 hours, 7 days, and 6 weeks post treatment. Total RNA was isolated from the cerebella and ATXN1 levels were analyzed by qRT-PCR. Dox administration via drinking water was successful in turning ATXN1 expression off after 24 hours and successive treatment for 6 weeks showed no increase in expression after long-term exposure (Figure 4.5).

Expression of mutant ATXN1 during development enhances disease

The first three postnatal weeks in mice are critical for PC and cerebellar development. During this time, a major input to PC called climbing fibers (CFs) mature from the inferior olive. The majority of PCs are innervated by a single CF whose synapses are located on the PC's primary, secondary, and tertiary dendrites. In addition, the cerebellum increases in size and transforms into a

highly foliated structure (Goldowitz and Hamre, 1998). Previous work indicated that blocking *ATXN1[82Q]* expression during development prevents neurological and pathological features that occur in animals expressing *ATXN1[82Q]* during postnatal development (Serra et al., 2006).

Figure 4.5

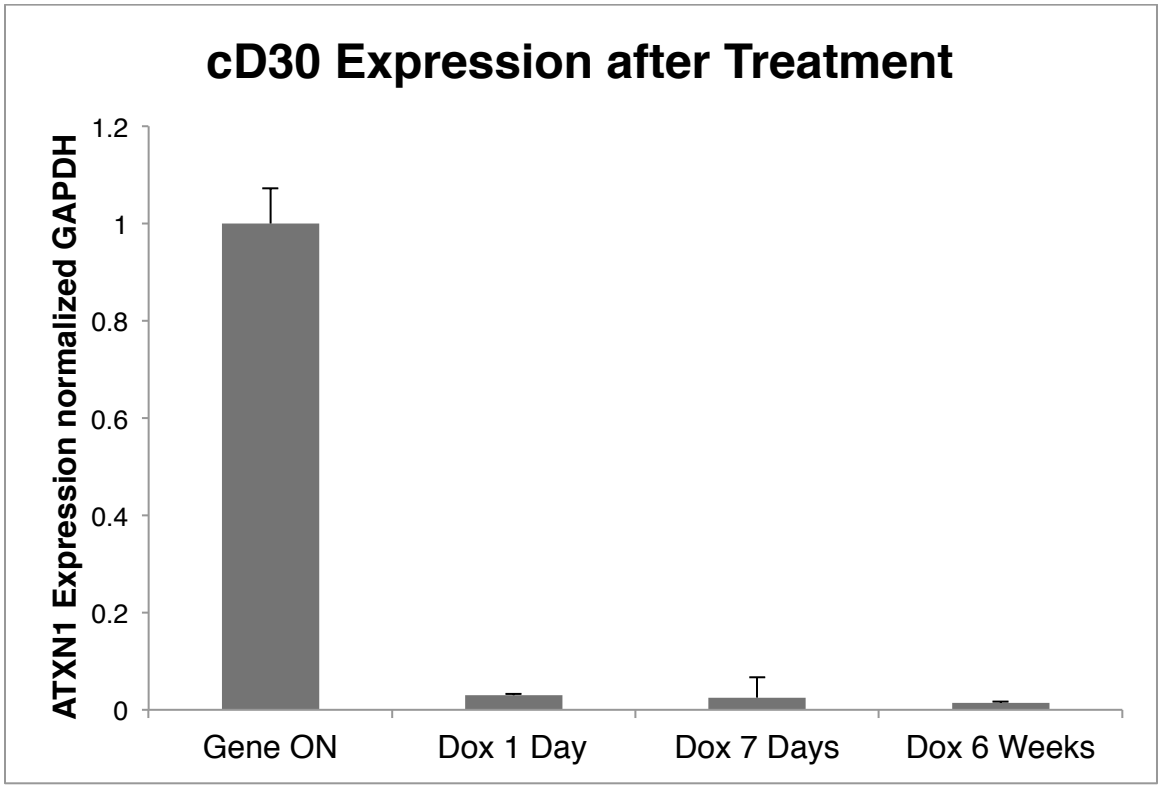

Figure 4.5: ATXN1 expression in *condATXN1[30Q]-D776* after dox administration. Graph of qRT-PCR mRNA levels showing sustained loss of *ATXN1[30Q]-D776* after dox administration for 1 day to 6 weeks. Error bars indicate SEM.

To determine if the changes observed at CF-PC synapses in *ATXN1[30Q]-D776* mice reflect the affect of *ATXN1* expression during a critical period of development we utilized the *condATXN1[30Q]-D776* model. For these studies, we examined CF extension using cerebellar sections from three groups of mice. The gene on control group, expressed *condATXN1[30Q]-D776* from birth until they were sacrificed at 7 weeks of age (Figure 4.6A). The gene off/gene on group was treated with doxycycline from birth until p21, at which time the gene was turned on and expressed for an additional 7 weeks of age (Figure 4.6A). Using this strategy, both groups of mice express *condATXN1[30Q]-D776* for 7 weeks. Cerebellar sections labeled with calbindin and VGLUT2 from mice in the gene on group, showed a high degree of both PC and CF terminal atrophy (Figure 4.6A). Conversely, cerebellar sections from mice in the gene off/gene on group showed healthy PC dendrites with a high density of CF terminals (Figure 4.6A). CF extension reached an average of 52% in the gene on *condATXN1[30Q]-D776* mice, notably lower than in *ATXN1[30Q]-D776* mice used in the previous studies (Figure 4.6B). The CF extension in the gene on *condATXN1[30Q]-D776* mice was significantly different from both the gene off/ gene on mice and the gene off mice ($p<0.01$ and $p< 0.001$, ANOVA followed by Bonferroni post hoc test). In the gene off/gene on mice, the CF terminals extended to a greater degree, 70%, and was not significantly different from *condATXN1[30Q]-D776* gene off mice ($p > 0.05$, ANOVA followed by Bonferroni post hoc test) (Figure 4.6B), suggesting that *ATXN1[30Q]-D776* affects CF

extensions during development when the distal CF terminals are being established.

Of note is the differences observed between the *ATXN1[30Q]-D776* and *condATXN1[30Q]-D776* mice. *ATXN1[30Q]-D776* mice retain CF synapses on the PC soma to a remarkable extent, while in *condATXN1[30Q]-D776* mice CF-PC somatic synapses were not evident (data not shown). Further, CF extension in *condATXN1[30Q]-D776* mice at 7 weeks of age was lower than that in *ATXN1[30Q]-D776* mice at any age. Considering that mutant *ATXN1* expression during development was critical for affecting the CF-PC synapses (Figure 4.6), we examined the developmental expression of the respective transgenes at p7, p9, p11, and p14. The expression of *condATXN1[30Q]-D776* mRNA was relatively constant through development (Figure 4.6C). Alternatively, *ATXN1[30Q]-D776* mice expression rises dramatically between p9 and p11 (Figure 4.6C). This data further supports the hypothesis that mutant *ATXN1* expression during development is critical for the alteration of CF-PC synapse and that the specific timing of expression during development alters the phenotypic profile.

Figure 4.6

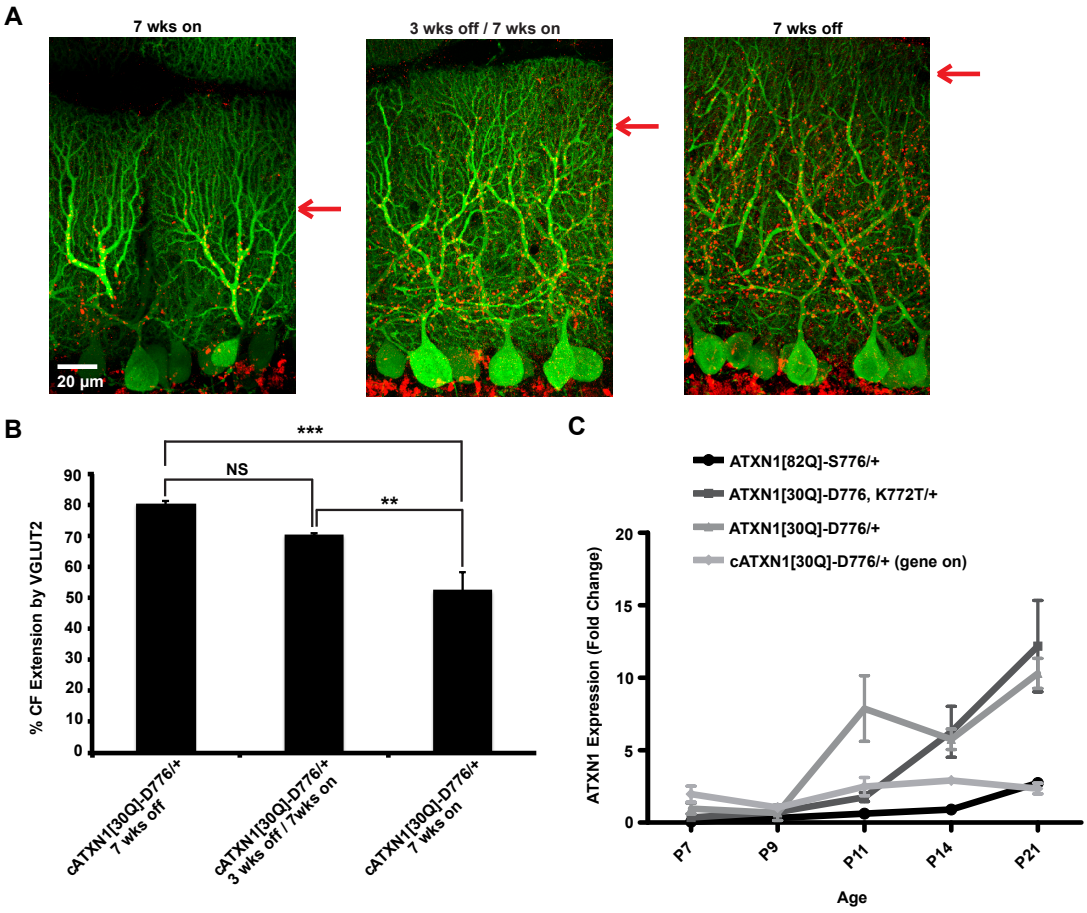

Figure 4.6: CF-PC Extension is Restored when *ATXN1[30Q]-D776* is Not Expressed During Cerebellar Development (A) 60X immunofluorescent images from primary fissure showing restored PC morphology (red) and CF extension (green) in mice not expressing *ATXN1[30Q]-D776* during the first three weeks of age. (B) Graph of distal extension of CF terminals onto the PC dendrites in *conditional ATXN1[30Q]-D776* mice. *Conditional ATXN1[30Q]-D776* Off N=4; *Conditional ATXN1[30Q]-D776* Off-On N= 3 animals; *Conditional ATXN1[30Q]-D776* On N = 4. (C) Graph of ATXN1 expression during development in *ATXN1[30Q]-D776/+* and *conditional ATXN1[30Q]-D776, ATXN1[82Q]-S776,* and *ATXN1[30Q]-D776-K772T/+*mice. Data are normalized to ATXN1 expression of *ATXN1[30Q]-D776/+* mice at p7. *p<0.05, **p<0.01, ***p<0.001.

Disease reversal: early stage disease

The ability of *condATXN1[30Q]-D776* mice to recover after cessation of transgene expression was assessed at early, mid and late stages of disease. For the early disease stage animals were allowed to age for 6 weeks with the *condATXN1[30Q]-D776* gene on. Animals were assessed for any neurological phenotype on the Rotarod apparatus. At six weeks the *condATXN1[30Q]-D776* animals were significantly impaired at each day tested (Figure 4.7). The group of animals was then split in half; the gene off group was administered dox and sucrose, and the control gene on group received sucrose only. At 12 weeks the animals were tested for Rotarod performance a second time. 6 week-old mice allowed to age an additional 6 weeks with the gene on displayed a Rotarod deficiency, though the animals' ability did not progressively deteriorate over the 6-12 week time period (Figure 4.7).

In contrast, *condATXN1[30Q]-D776* animals treated with dox for 6 weeks perform as well as Pcp2-tTA/+ controls. This data is similar to historical data, in which conditional ATXN[82Q] animals (cSCA1) could recover after expressing *ATXN1* for only 6 weeks (Figure 4.7 dark gray bars). However, the *condATXN1[30Q]-D776* animals treated with dox recover equally to wild-type counterparts and cSCA1 recover to 84.5% of wild-type (Zu et al., 2004).

Purkinje cells at early stage disease show signs of moderate pathology including dendritic atrophy as measured by reduced molecular layer thickness after calbindin immunostaining (Figure 4.8, quantified in Figure 4.7B). In addition, CF extension is reduced from wild-type levels and disease severity was rated at a moderate level (Figure 4.8, quantified in Figure 4.7C and D). Interestingly, after turning the gene off for 6 weeks these measures do not significantly improve even though animals completely recover the ataxic phenotype as measured by Rotarod analysis. It may be that at this age point that only PC dysfunction is rescued after turning the gene off. Alternatively, since the histological abnormalities are relatively minor at this age we may not have sensitive enough measures to quantify any rescue of pathology.

Figure 4.7

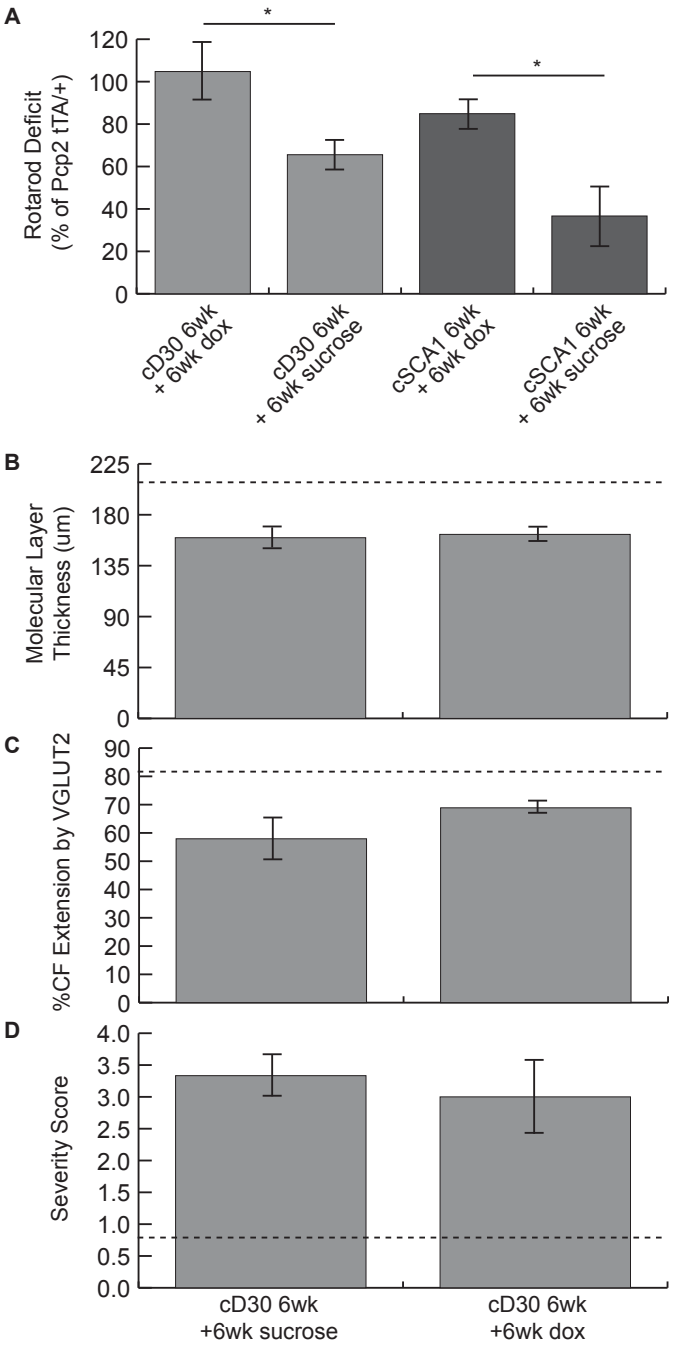
A
Rotarod Deficit
(% of Pcp2 tTA/+)
120
100
80
60
40
20
0
*
*
cD30 6wk
+ 6wk dox
cD30 6wk
+ 6wk sucrose
cSCA1 6wk
+ 6wk dox
cSCA1 6wk
+ 6wk sucrose
B
Molecular Layer
Thickness (um)
225
180
135
90
45
0
C
%CF Extension by VGLUT2
90
80
70
60
50
40
30
20
10
0
D
Severity Score
4.0
3.5
3.0
2.5
2.0
1.5
1.0
0.5
0.0
cD30 6wk
+6wk sucrose
cD30 6wk
+6wk dox

Figure 4.7: Early stage disease recovery. (A) Restoration of a normal performance level on the Rotarod in condATXN1[30Q]-D776 mice treated with dox beginning at 6 weeks of age. Quantified histological graphs of molecular layer length (B), distal extension of CF terminals onto the PC dendrites (C) and severity scores (D) in condATXN1[30Q]-D776 6 weeks with gene on and 6 weeks of indicated treatment. Dotted line indicates Pcp2 tTA/+ treated with dox (WT control) levels. Error bars indicate SEM. *p<0.05, **p<0.01, ***p<0.001.

Figure 4.8

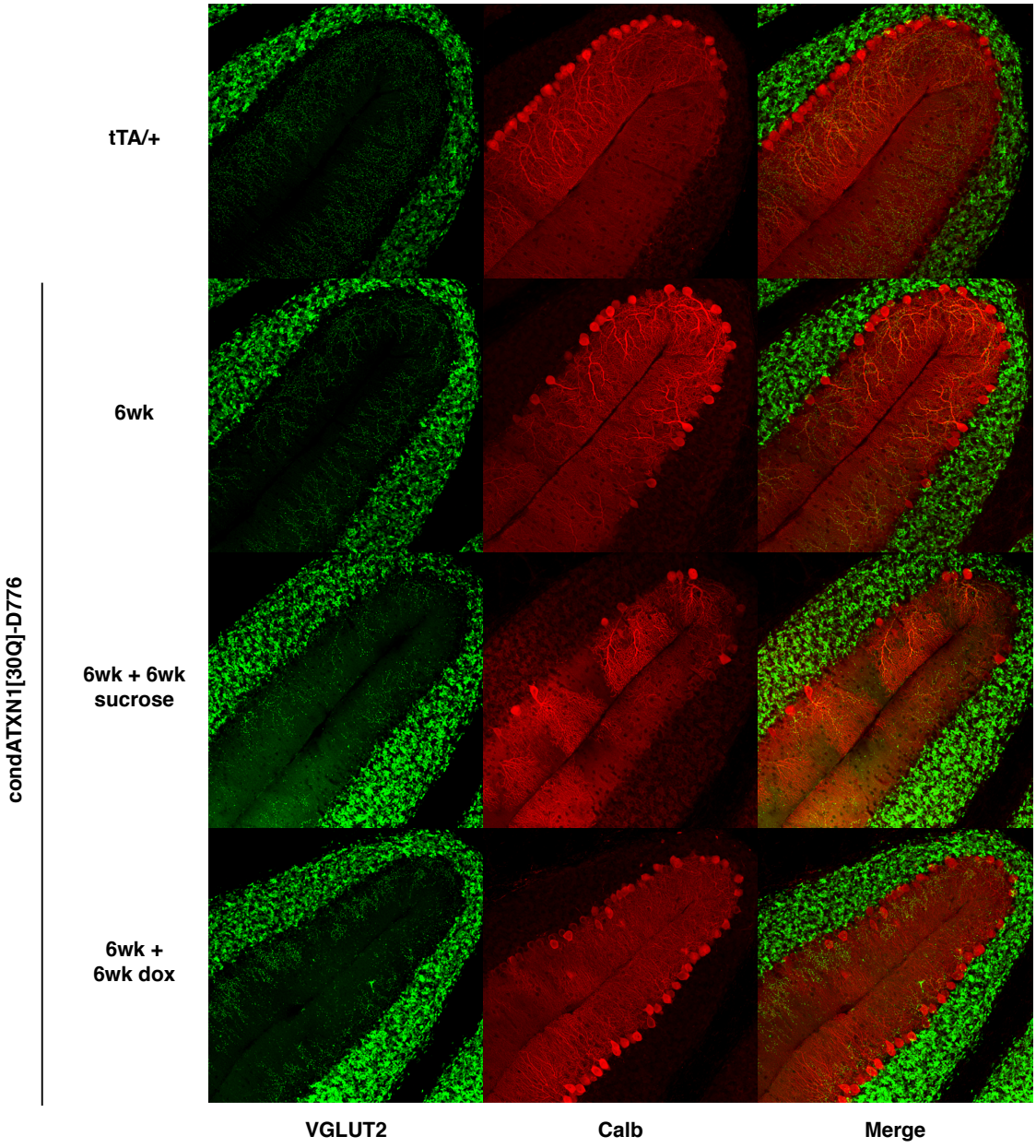

Figure 4.8: Early stage disease histology in *condATXN1[30Q]-D776* cerebella. Immunofluorescent images of the primary fissure showing minor pathology in *condATXN1[30Q]-D776* including slight molecular layer thinning and decreased CF extension. PC pathology measured by calbindin staining (red) and CF extension measured by VGLUT2 staining (green).

Disease reversal: mid stage disease

For the mid disease stage animals were allowed to age for 16 weeks with the c*ATXN1[30Q]-D776* gene on. At 16 weeks animals were assessed for baseline neurological phenotype on the Rotarod apparatus. After 16 week behavioral testing, the group of animals was split in half; the gene off group was administered dox and sucrose, and the control gene on group received sucrose only. At 20 and 24 weeks the animals were tested for Rotarod performance a second and third time. At 16, 20 and 24 weeks the condATXN1[30Q]-D776 gene on animals were significantly impaired compared to tTA controls (Figure 4.9A). However, after dox treatment for 4 weeks animals recover Rotarod defects completely. This trend continues after 8 weeks of treatment, though by student t-test comparing 8 weeks of dox treatment cohort to 8 weeks of sucrose treatment cohort is not significant. This may be due to variability in animal performance after repeated rounds of Rotarod testing as animal's inherent fear of falling from the Rotarod and test compliance reduces. The ability of the condATXN1[30Q]-D776 to recover at 16 weeks is a significant change from previous data in which cSCA1 mice were able to recover partially (about 60% of WT controls) at a slightly earlier time point of 12 weeks. In addition, improvement was significantly better than sucrose treated controls only after 12 weeks of dox treatment as opposed to condATXN1[30Q]-D776 improvement after 4 weeks of dox treatment (Figure 4.9A gray bars).

At mid-stage disease restoration of a normal neurological phenotype correlated with a reversal of PC pathology (Figure 4.10). At 16 weeks, CF extension is dramatically reduced (Figure 4.9B and Figure 4.10). This extension returns after 4 weeks of dox treatment and continues to improve with longer treatment of 8 and 12 weeks (Figure 4.9B and Figure 4.10). Molecular layer thickness also improves over the duration of treatment and severity scores significantly improve.

Figure 4.9

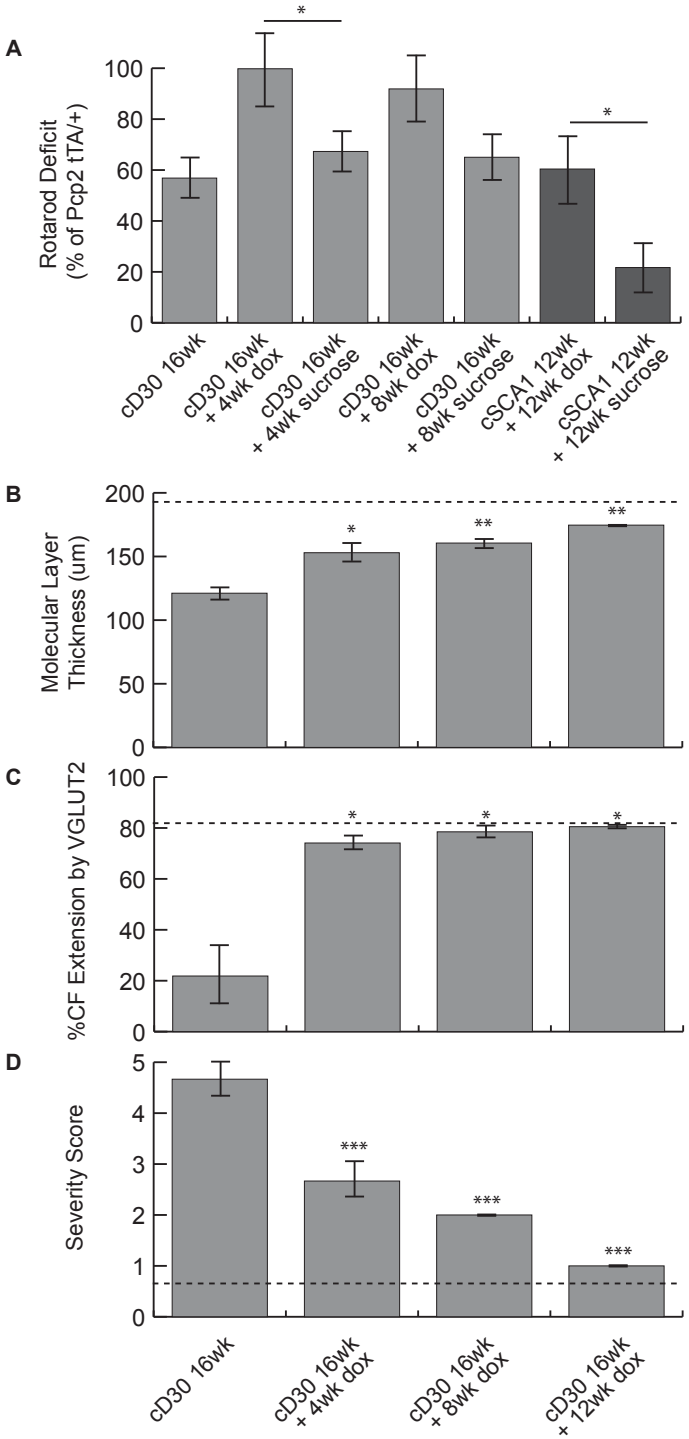
A
Rotarod Deficit
(% of Pcp2 tTA/+)
100
80
60
40
20
0
*
*
cD30 16wk
cD30 16wk + 4wk dox
cD30 16wk + 4wk sucrose
cD30 16wk + 8wk dox
cD30 16wk + 8wk sucrose
cSCA1 12wk + 12wk dox
cSCA1 12wk + 12wk sucrose
B
Molecular Layer Thickness (um)
200
150
100
50
0
*
**
**
C
%CF Extension by VGLUT2
100
80
60
40
20
0
*
*
*
D
Severity Score
5
4
3
2
1
0
***
***
***
cD30 16wk
cD30 16wk + 4wk dox
cD30 16wk + 8wk dox
cD30 16wk + 12wk dox

Figure 4.9: Mid stage disease recovery. (A) Restoration of a normal performance level on the Rotarod in condATXN1[30Q]-D776 mice treated with dox beginning at 16 weeks of age. Quantified histological graphs of molecular layer length (B), distal extension of CF terminals onto the PC dendrites (C) and severity scores (D) in condATXN1[30Q]-D776 16 weeks with gene on and 4-12 weeks of indicated treatment. Dotted line indicates Pcp2 tTA/+ treated with dox (WT control) levels. Error bars indicate SEM. *p<0.05, **p<0.01, ***p<0.001.

Figure 4.10

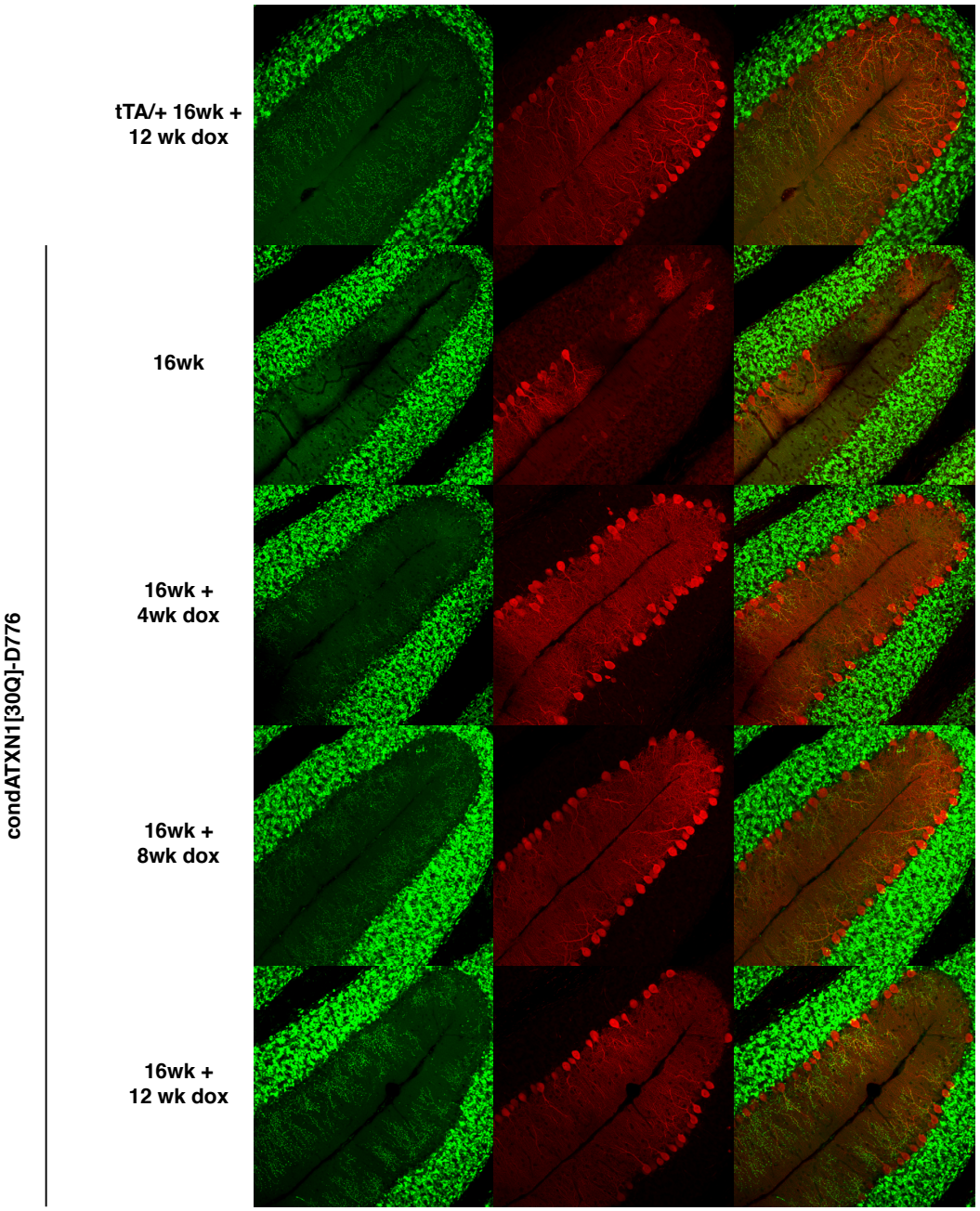

Figure 4.10: Mid stage disease histology in *condATXN1[30Q]-D776* cerebella. Immunofluorescent images of the primary fissure showing minor pathology in *condATXN1[30Q]-D776* including slight molecular layer thinning and decreased CF extension. PC pathology measured by calbindin staining (red) and CF extension measured by VGLUT2 staining (green).

Disease reversal: late stage disease

For the late disease stage animals were allowed to age for 32 weeks with the c*ATXN1[30Q]-D776* gene-on. At 32 weeks animals were assessed for baseline neurological phenotype on the Rotarod apparatus. After 32 week behavioral testing, the group of animals was split in half; the gene off group was administered dox and sucrose, and the control gene-on group received sucrose only. At 36, 40 and 44 weeks the animals were tested for Rotarod performance. At all ages the condATXN1[30Q]-D776 gene-on animals were significantly impaired compared to tTA controls (Figure 4.11A). In addition, dox treatment for 4-12 weeks does not result in a significant improvement in Rotarod performace.

Though ataxia persisted in late-stage animals even after ATXN1 expressed ceased, some aspects of PC pathology improved. Molecular layer thickness improved after 4 and 8 weeks of dox treatment, though thickness continued to decrease even with treatment until after 12 weeks of dox treatment there was no longer a significant increase in molecular layer thickness compared to 32 weeks gene-on. In addition, CF extension is dramatically reduced and did not significantly recover at any point in the treatment. Histology measurements were complicated by the fact that calbindin, a marker for PCs (Barski et al., 2003), was extensively downreguated resulting in poor PC staining. After treatment with dox, calbindin mRNA levels moderately recovered, which resulted in better imaging of

the cerebellar structure and PCs suggesting that lack of PC staining was a result of downregulation and not the loss of PCs from the molecular layer. In addition, while severity scores decreased after only 4 weeks of dox treatment, additional treatment time did not further improve disease severity.

Figure 4.11

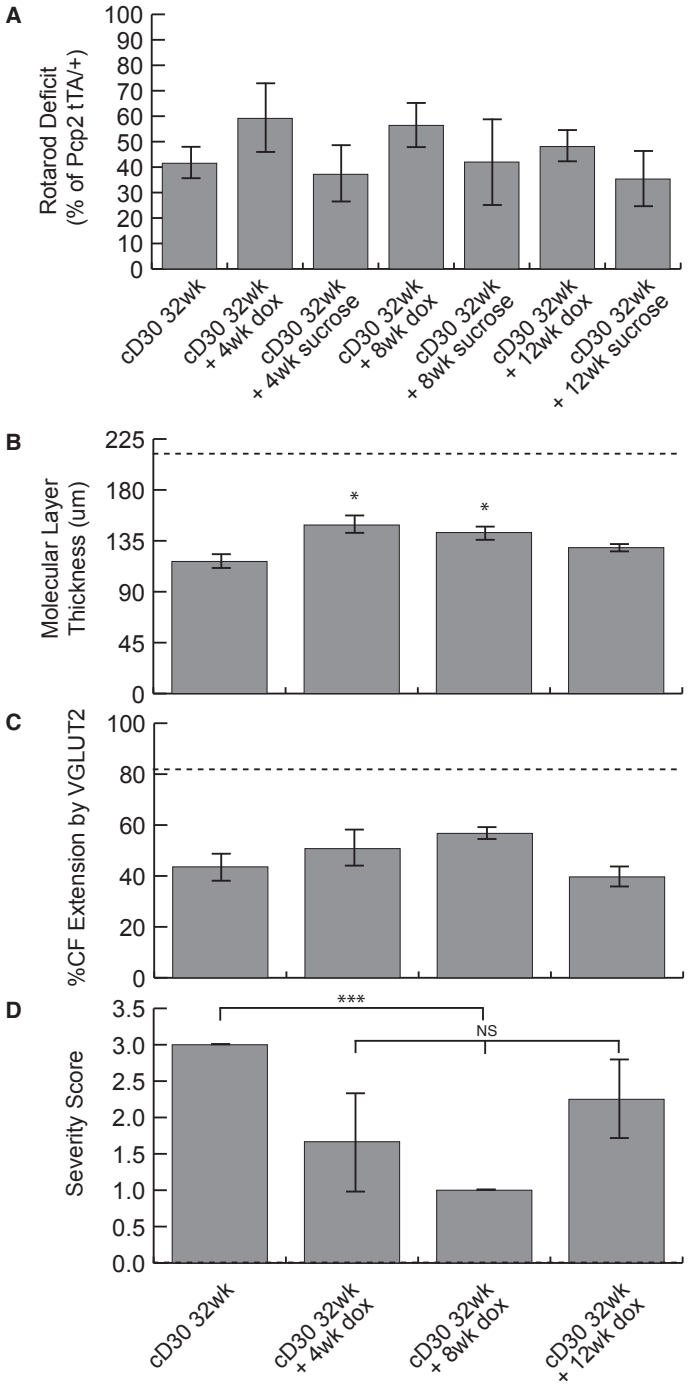
A
Rotarod Deficit
(% of Pcp2 tTA/+)
100
90
80
70
60
50
40
30
20
10
0
cD30 32wk
cD30 32wk + 4wk dox
cD30 32wk + 4wk sucrose
cD30 32wk + 8wk dox
cD30 32wk + 8wk sucrose
cD30 32wk + 12wk dox
cD30 32wk + 12wk sucrose
B
Molecular Layer Thickness (um)
225
180
135
90
45
0
*
*
C
%CF Extension by VGLUT2
100
80
60
40
20
0
D
Severity Score
3.5
3.0
2.5
2.0
1.5
1.0
0.5
0.0
***
NS
cD30 32wk
cD30 32wk + 4wk dox
cD30 32wk + 8wk dox
cD30 32wk + 12wk dox

Figure 4.11: Late-stage disease recovery. (A) Abnormal performance level on the Rotarod in condATXN1[30Q]-D776 mice treated with dox beginning at 32 weeks of age. Histological graphs of molecular layer length (B), distal extension of CF terminals onto the PC dendrites (C) and severity scores (D) in condATXN1[30Q]-D776 32 weeks with gene on and 4-12 weeks of indicated treatment. Dotted line indicates Pcp2 tTA/+ treated with dox (WT control) levels. Error bars indicate SEM.

Figure 4.12

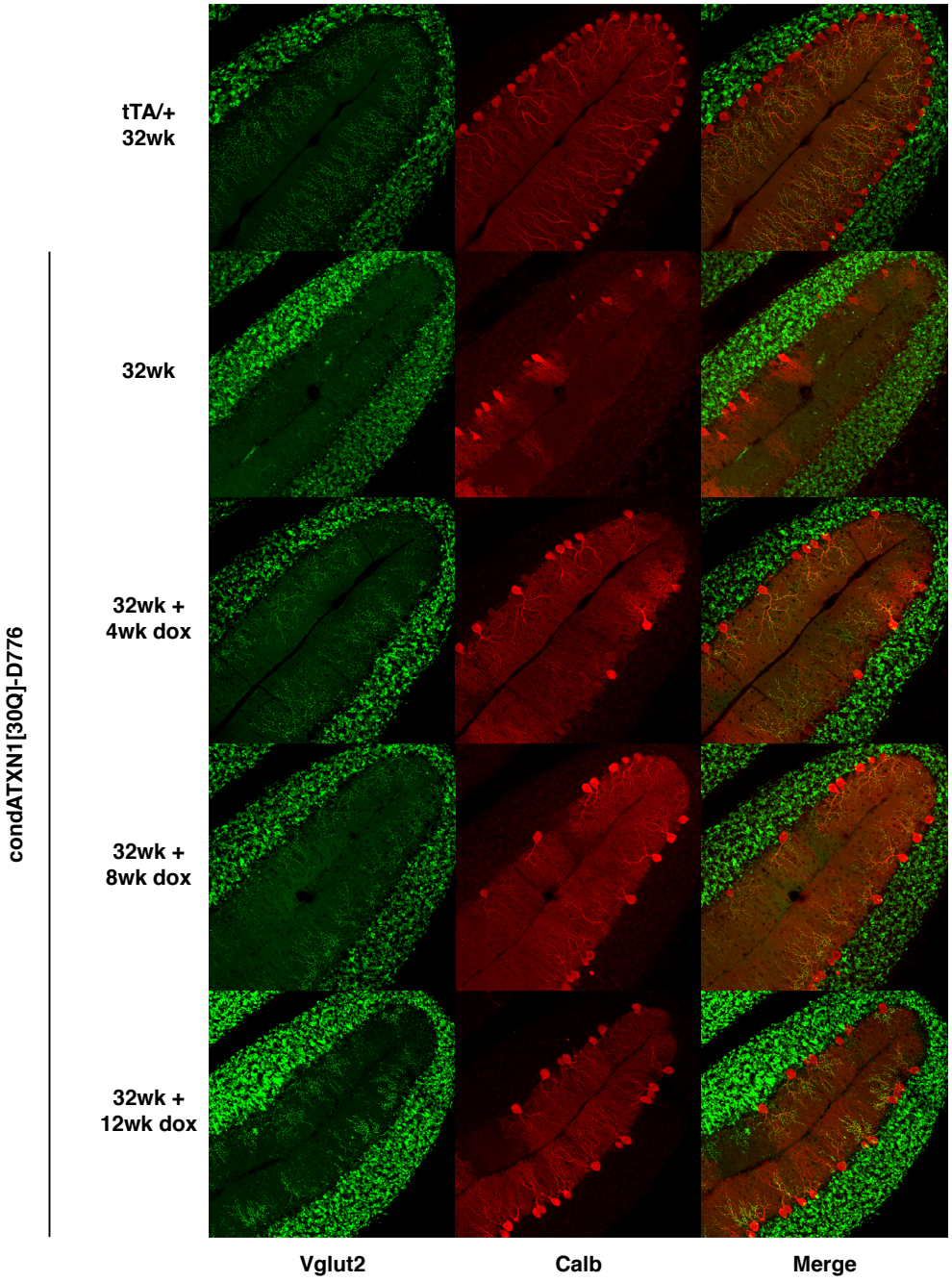

Figure 4.12: Late stage disease histology in *condATXN1[30Q]-D776* cerebella. Immunofluorescent images of the primary fissure showing pathology in *condATXN1[30Q]-D776* including molecular layer thinning and decreased CF extension and decreased calb immunostaining. PC pathology measured by calbindin staining (red) and CF extension measured by VGLUT2 staining (green).

Discussion

Conditional Model of *ATXN1[30Q]-D776*

I developed a conditional model of *ATXN1[30Q]-D776* using a tet-off system to control expression of the transgene in PCs. Similar to previous results (Zu et al., 2004), the pathogenic effects of ATXN1[30Q]-D776 could be reversed after cessation of gene expression with dox treatment. I examined the ability of PCs to recover at three stages of disease. This included an early stage after 6 weeks, mid-stage after 16 weeks and late-stage at 32 weeks. In addition, I examined the effects of *condATXN1[30Q]-D776* expression during development.

CF Development Altered by *condATXN1[30Q]-D776* Expression Pattern

Normally, early in the postnatal life of a mouse each PC soma is innervated by multiple CFs from different inferior olivary neurons. During the first postnatal week the somatic synapses of one CF functionally become stronger (Hashimoto and Kano, 2003). Subsequently, the terminals of this strong CF translocate up from the cell body and along the proximal PC dendritic shaft. During the late phase in development, the dominant CF begins its climb up the PC dendritic tree. During the second postnatal week, the synapses on the PC soma from both the dominant and other weaker CFs are eliminated. By the end of the third postnatal

week one CF forms hundreds of synapses along a PC primary dendrite, with essentially no synapses remaining on the PC soma (Cesa and Strata, 2009; Kano and Hashimoto, 2009).

The capacity of ATXN1 to disrupt CF innervation is shown here to depend upon the timing of ATXN1 expression during development. In *ATXN1*[*30Q*]*-D776* cerebella, CF translocation is normal at p14 and subsequently CF terminals fail to translocate beyond that point and the number of CF synapses on PC somata remain high. The failure of CFs to develop properly after p14 is synchronized with the expression of *ATXN1*[*30Q*]*-D776* increasing dramatically after p9. During this period, the late phase CF development has begun and *ATXN1*[*30Q*]*-D776* expression altered the normally proceeding CF translocation and CF synapse elimination. Further, using a *condATXN1[30Q]-D776* model we show that by delaying expression until p21, CF extension is restored compared with mice that express ATXN1 during development, supporting the hypothesis that ATXN1 expression during development alters CF–PC innervation. Unlike the *ATXN1*[*30Q*]*-D776* model, *condATXN1[30Q]-D776* mice express ATXN1 as early as p7 and these mice display a dramatically decreased CF extension compared with the other SCA1 models. The expression of ATXN1 at p7 in *conditional ATXN1*[*30Q*]*-D776* mice resulted in improved CF–PC somatic synapse elimination. These data reinforce the hypothesis that the altered CF development

is dependent upon the temporal pattern of ATXN1 expression during development.

Early Stage Disease Recovery

At the early stage, *condATXN1[30Q]-D776* animals completely recovered any ataxic phenotype by cage behavior and rotarod analysis (Figure 4.7A). At this stage of disease, there was mild PC including a reduced molecular layer thickness and a decrease in CF extension. The reduced molecular layer thickness at this age is a characteristic of the *ATXN1[30Q]-D776* model in that the molecular layer never fully reaches wild type thickness, but also does not progressively decrease in thickness (data not shown). Altered distribution of CFs on PCs is another characteristic feature of *ATXN1[30Q]-D776* (Duvick et al., 2010). Therefore, these phenotypes were anticipated. Interestingly, despite the reversal of ataxia, using measurements of molecular layer, CF extension and severity scores, I could not find any significant difference in pathology after 6 weeks of dox treatment. Objectively, after examining a minimum of three cerebella from each cohort I found there to be a slight difference, but it could be the increase in calbindin staining after dox treatment rather than reversal of pathology. It may also be that the pathology was not extensive enough at this time-point to see any change after gene cessation.

Mid Stage Disease Recovery

At 16 weeks, *condATXN1[30Q]-D776* had significant pathology (Figure 4.9). Some animals had areas where CF extension appeared normal, and other areas where there were no VGLUT2 positive stained CF to measure. After quantification, the CF extension as a percentage of the molecular layer ranged from 0-42% with an average of 22%. The molecular layer was also significantly reduced from Pcp2-tTA/+ controls. However, despite the level pathology when dox treatment was started, *condATXN1[30Q]-D776* mice were able to completely recover all Rotarod deficits and performed the task as well as controls after only 4 weeks of treatment. The recovery correlated with an increased molecular layer, an increase in CF extension and a decrease in severity scores. The neurological improvement continued as the longer the animals were given dox, from four to twelve weeks, the better the scores.

The extent of the *condATXN1[30Q]-D776* to recover at this time point is markedly different than *condATXN1[82]* mice (Zu et al., 2004). When *condATXN1[82]* mice were examined at 12 weeks of age, followed by four to twelve weeks of dox treatment, they exhibited only partial recovery. By Rotarod analysis, *condATXN1[82]* significantly improved from sucrose only controls but only recovered to roughly 60% of wild-type controls and it took eight weeks of treatment to see an improvement and did not see further Rotarod improvement

when treated for the full twelve weeks. This is as opposed to the *condATXN1[30Q]-D776* which recovered to almost 100% of the controls after only four weeks of dox treatment. In addition, it took twelve weeks of dox treatment in *condATXN1[82Q]* to see a significant increase in molecular layer thickness as opposed to the *condATXN1[30Q]-D776* which saw improvements after four.

Late Stage Disease Recovery

Somewhat surprisingly, despite a lack of PC death, *condATXN1[30Q]-D776* mice in which transgene expression was halted by dox after 32 weeks of age still had coordination deficits by cage behavior and performed poorly on the Rotarod as compared to Pcp2-tTA/+ controls. There was a trend for the dox treated cohort to perform better by accelerating Rotarod, however the improvement never reached statistical significance. There were also some signs of improved neurological phenotype, including a slight increase in molecular layer after four and eight weeks of treatment, and a decrease in severity scores after eight weeks of dox administration. In addition, CF extension trended upward but also never reached significance. There was also no correlation with longer dox treatment and better performance or neurological status.

PC Recovery Impacted by Age Despite Lack of polyQ Tract

Prior studies described the ability of conditional *ATXN1[82Q]* to recover from disease after halting expression of mutant *ATXN1* (Zu et al., 2004). Generally, the results support prior findings that coordination and PC pathology are reversible (Yamamoto et al., 2000; Zu et al., 2004). However, the extent of recovery was decreased as animals increase in age. Similarly, younger *condATXN1[30Q]-D776* mice were more able to recover motor deficits and neurological pathology. However, even at a slightly later time point, sixteen weeks as opposed to twelve, the *condATXN1[30Q]-D776* were more able to recover from disease than previous studies using *condATXN1[82Q]* mice. Despite the ability of *condATXN1[30Q]-D776* mice to recover completely at mid-stage disease, once disease was allowed to progress to 32 weeks mice were markedly less able to recover.

It was previously unclear if age dependence recovery was due to prolonged exposure to the polyQ expansion in mutant ATXN1, or if older neurons are inherently less able to recover. This was also complicated by late-stage disease features in *condATXN1[82Q]* mice such as the onset of PC death. The advantage of using *condATXN1[30Q]-D776* to assess recovery was that they do not have progressive features of disease such as PC death and provided a way to tease apart the previous question. The recovery profile of *condATXN1[30Q]-*

D776 suggests that PCs have a sustained ability to recover but there is a limit to recovery that is unaffected by the presence or absence of an expanded polyQ tract. Rather, it seems that age is the primary factor influencing recovery. It may be older neurons are less able to respond or alter gene expression needed for recovery.

Chapter 5: Discussion

Major Findings

The use of RNA-sequencing provided a non-biased molecular approach to examine the cerebellar transcriptome of *ATXN1[82Q]* and *ATXN1[30Q]-D776* relative to wt/FVB. Perhaps the most substantial finding of my thesis work was how similar the *ATXN1[82Q]* and *ATXN1[30Q]-D776* models were by both gene expression and splicing analysis. In both cases, most of the genes were downregulated compared to wt/FVB gene levels similar to previous SCA1 gene expression studies (Crespo-Barreto et al., 2010; Lin et al., 2000; Serra, 2004). In addition, there was extensive overlap in the gene lists for splicing and gene expression, 4615 and 4459 overlapping genes respectively. This led to subsequent identification of similar pathways and networks.

These findings emphasize how important ATXN1 native function is for the SCA1 disease process. As previously discussed, ATXN1 interacts with a variety of nuclear components including RNA, regulators of transcription and proteins involved in RNA processing. Clearly, phosphorylation status of ATXN1 at serine 776 dramatically impacts the function of ATXN1, leading to many expression changes, as well as altering splicing. Additionally, this suggests the ATXN1[30Q]-D776 protein is involved in SCA1 pathology in a similar mechanism as ATXN1[82Q], and not causing disease or ataxia via a distinct pathway. This also gives credibility to using *ATXN1[30Q]-D776* as a model of SCA1, and suggests

the aspartic acid substitution is mimicking the normal phosphorylation process.

While phosphorylation at site 776 modulates the stability of ATXN1, it also increases the level of RBM17 binding. A phosphomimetic aspartic acid mutation at this site increases the interaction with RBM17 to levels comparable to ATXN1[82Q]. Thus, I hypothesize that ATXN1 binding of RBM17, which leads to alternative splicing of RBM17 targets, is a major factor in the disease process. This mechanism is illustrated in Figure 5.1. I used *Anks1b* to demonstrate the splicing similarities in *ATXN1[82Q]* and *ATXN1[30Q]-D776*. In fact, every SCA1 model tested showed a decrease in *Anks1b* isoform 3. However, it remains to be seen if *Anks1b* is a target of RBM17 alternative splicing regulation.

I observed implications for climbing fiber and synapse abnormalities in SCA1 disease throughout my experiments. Using RNA-sequencing, I identified several interesting targets, including *Cck* and *Col18a1* as candidate genes for disease aspects that differ between *ATXN1[82Q]* and *ATXN1[30Q]-D776*. Both were involved in synapse maintenance or formation. *Col18a1*, and its proteolytically derived fragment endostatin, are necessary and sufficient for proper formation of CF synapses on the dendrites of PCs. In addition, my studies using a genetic approach to ablate *Cck* expression show a reduced number of CF puncta on the PC body. My *condATXN1[30Q]-D776* recovery studies illustrated that PC recovery diminishes over time. Interestingly, recovery is unaffected by the

presence or absence of an expanded polyQ tract. Rather, it seems that age is the primary factor influencing recovery. It is important to note that CF extension was one measurement that clearly improved at mid stage disease, but did not recover at later stages. Similarly, *Anks1b* isoform 3 reported to function in signaling from the synapse to nucleus in an activity dependent manner where it promotes protein synthesis regulating nucleolar assembly.

A major hallmark of SCA1 disease death is cerebellar atrophy caused by PC dendritic pruning and eventual cell death. However, my findings support the idea that PC dysfunction, and PC interaction with CF and other cerebellar cell types, is much more central to the disease process than previously appreciated. Thus, in order to develop successful therapies for SCA1 in the future, it will be essential to target the native function of ATXN1.

Figure 5.1

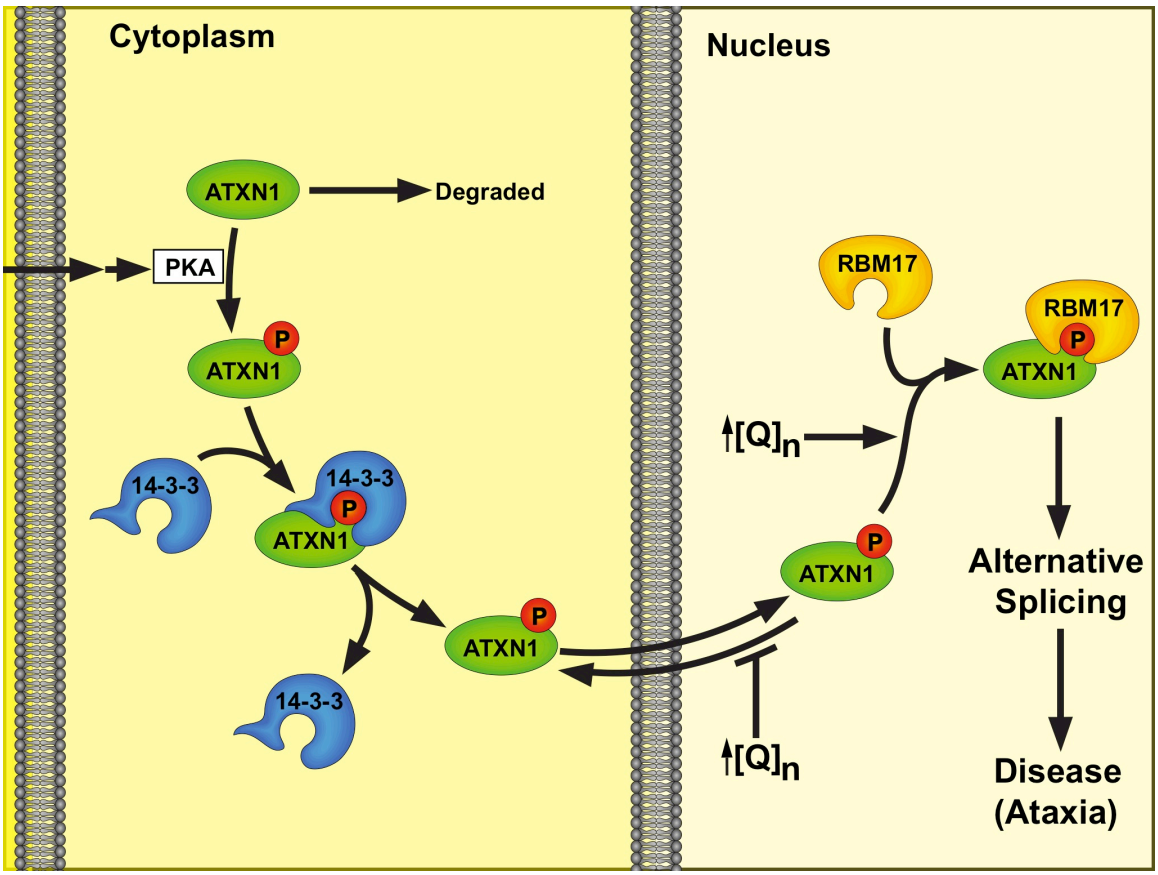

Figure 5.1: Model of ATXN1 disease mechanism. Phosphorylation status impacts ATXN1 stability and RBM17 binding. The ATXN1-RBM17 complex leads to alternative splicing and ataxia. An expanded PolyQ tract inhibits ATXN1 nuclear export as well as increasing RBM17 binding.

Future Directions

For the RNA-sequencing experiments, I used *ATXN1[82Q], ATXN1[30Q]-D776,* and *condATXN1[30Q]-D776* whole cerebella. While the transgenes were overexpressed specifically in the PCs, the gene expression and splicing findings illustrated here could be direct effects from PCs as well as nonautonomous effects from other cell types in the cerebellum. I attempted to address these concerns by filtering my datasets though a list of 1000 PC enriched mRNA (Heiman et al., 2008) and by using Allen Brain Atlas *in situ* hybridization to examine mRNA localization (Lein et al., 2007). Now that we have several targets there are other methods we could use to ascertain direct verses non-direct effects including laser microdisection microscopy and using a bacTRAP mouse model. We could use laser microdisection to collect tissue from the PC layer only or the entire molecular layer (to include PC dendrites), and use RNA collected from the tissue to measure splicing and gene expression changes. Alternatively, we could use the bacTRAP, *t*ranslating *r*ibosome *a*ffinity *p*urification, approach to study translated mRNAs in PCs (Doyle et al., 2008; Heiman et al., 2008). In this way, we could use Pcp2-bacTRAP mice crossed to used *ATXN1[82Q]* and *ATXN1[30Q]-D776* mice to examine only actively translated mRNA from PCs and look for gene expression and splicing changes identified by the RNA-seq.

Another question that remains to be answered is how does ATXN1 regulate the

gene changes we see in the RNA-seq data? As previously mentioned, ATXN1 interacts with several regulators of transcription including SMRT (Tsai et al., 2004), Capicua (Kim et al., 2013; Lam et al., 2006), Gfi-1 (Tsuda et al., 2005), and the Rora/Tip60 complex (Gehrking et al., 2011; Serra et al., 2006). The Orr lab is currently generating *ATXN1[82Q]* transgenic mice in which the binding sites for Capicua is mutated. It will be intriguing to see in these mice if *Cck* or *Col18a1* levels are altered in these models to better understand the role of Capicua as a transcription factor for these genes.

Finally, the initial goal of this project was to identify molecules and pathways specific to progressive disease in SCA1 including PC death. While the RNA-seq studies lead to the discovery of several potential targets and led to the discovery that splicing correlates with ataxia in our models, I could not identify any specific molecules or pathways that lead to cell death in PCs expressing *ATXN1[82Q].* It may be that our choice to study animals at 12 weeks, when ataxia is present but PC pathology is relatively intact hampered these efforts. Future aging studies are planned for the *ATXN1[30Q]-D776*;*Cck*$^{-/-}$ mice to examine how *Cck* expression levels impact disease progression including assessing motor ability by Rotarod and examining pathology at one year of age.

Bibliography

Altman, J. (1972). Postnatal development of the cerebellar cortex in the rat. II. Phases in the maturation of Purkinje cells and of the molecular layer. J. Comp. Neurol. *145*, 399–463.

Anders, S., Reyes, A., and Huber, W. (2012). Detecting differential usage of exons from RNA-seq data. Genome Res. *22*, 2008–2017.

Andrews, S. Babraham Bioinformatics - FastQC A Quality Control tool for High Throughput Sequence Data.

Banfi, S., Servadio, A., Chung, M.Y., Kwiatkowski, T.J., Jr, McCall, A.E., Duvick, L.A., Shen, Y., Roth, E.J., Orr, H.T., and Zoghbi, H.Y. (1994). Identification and characterization of the gene causing type 1 spinocerebellar ataxia. Nat. Genet. *7*, 513–520.

Barclay, S.S., Tamura, T., Ito, H., Fujita, K., Tagawa, K., Shimamura, T., Katsuta, A., Shiwaku, H., Sone, M., Imoto, S., et al. (2013). Systems biology analysis of Drosophila in vivo screen data elucidates core networks for DNA damage repair in SCA1. Hum. Mol. Genet. ddt524.

Barnes, J.A., Ebner, B.A., Duvick, L.A., Gao, W., Chen, G., Orr, H.T., and Ebner, T.J. (2011). Abnormalities in the Climbing Fiber-Purkinje Cell Circuitry Contribute to Neuronal Dysfunction in ATXN1[82Q] Mice. J. Neurosci. *31*, 12778–12789.

Barski, J.J., Hartmann, J., Rose, C.R., Hoebeek, F., Mörl, K., Noll-Hussong, M., De Zeeuw, C.I., Konnerth, A., and Meyer, M. (2003). Calbindin in cerebellar Purkinje cells is a critical determinant of the precision of motor coordination. J. Neurosci. *23*, 3469–3477.

Blankenberg, D., Von Kuster, G., Coraor, N., Ananda, G., Lazarus, R., Mangan, M., Nekrutenko, A., and Taylor, J. (2010). Galaxy: a web-based genome analysis tool for experimentalists. Curr. Protoc. Mol. Biol. Ed. Frederick M Ausubel Al *Chapter 19*, Unit 19.10.1–21.

Bowman, A.B., Lam, Y.C., Jafar-Nejad, P., Chen, H.-K., Richman, R., Samaco, R.C., Fryer, J.D., Kahle, J.J., Orr, H.T., and Zoghbi, H.Y. (2007). Duplication of Atxn1l suppresses SCA1 neuropathology by decreasing incorporation of polyglutamine-expanded ataxin-1 into native complexes. Nat. Genet. *39*, 373–379.

Burright, E.N., Brent Clark, H., Servadio, A., Matilla, T., Feddersen, R.M., Yunis, W.S., Duvick, L.A., Zoghbi, H.Y., and Orr, H.T. (1995). SCA1 transgenic mice: A model for neurodegeneration caused by an expanded CAG trinucleotide repeat. Cell *82*, 937–948.

Burright, E.N., Davidson, J.D., Duvick, L.A., Koshy, B., Zoghbi, H.Y., and Orr, H.T. (1997). Identification of a self-association region within the SCA1 gene product, ataxin-1. Hum. Mol. Genet. *6*, 513–518.

Carlson, K.M., Melcher, L., Lai, S., Zoghbi, H.Y., Clark, H.B., and Orr, H.T. (2009). Characterization of the Zebrafish atxn1/axh Gene Family. J. Neurogenet. *23*, 313–323.

Cesa, R., and Strata, P. (2009). Axonal competition in the synaptic wiring of the cerebellar cortex during development and in the mature cerebellum. Neuroscience *162*, 624–632.

Chen, H.-K., Fernandez-Funez, P., Acevedo, S.F., Lam, Y.C., Kaytor, M.D., Fernandez, M.H., Aitken, A., Skoulakis, E., Orr, H.T., and Botas, J. (2003). Interaction of Akt-phosphorylated ataxin-1 with 14-3-3 mediates neurodegeneration in spinocerebellar ataxia type 1. Cell *113*, 457–468.

Chen, Y.W., Allen, M.D., Veprintsev, D.B., Löwe, J., and Bycroft, M. (2004). The Structure of the AXH Domain of Spinocerebellar Ataxin-1. J. Biol. Chem. *279*, 3758–3765.

De Chiara, C., Giannini, C., Adinolfi, S., de Boer, J., Guida, S., Ramos, A., Jodice, C., Kioussis, D., and Pastore, A. (2003). The AXH module: an independently folded domain common to ataxin-1 and HBP1. FEBS Lett. *551*, 107–112.

De Chiara, C., Menon, R.P., Strom, M., Gibson, T.J., and Pastore, A. (2009). Phosphorylation of S776 and 14-3-3 Binding Modulate Ataxin-1 Interaction with Splicing Factors. PLoS ONE *4*, e8372.

Chung, M.Y., Ranum, L.P., Duvick, L.A., Servadio, A., Zoghbi, H.Y., and Orr, H.T. (1993). Evidence for a mechanism predisposing to intergenerational CAG repeat instability in spinocerebellar ataxia type I. Nat. Genet. *5*, 254–258.

Clark, H.B., and Orr, H.T. (2000). Spinocerebellar ataxia type 1-modeling the pathogenesis of a polyglutamine neurodegenerative disorder in transgenic mice. J. Neuropathol. Exp. Neurol. *59*, 265–270.

Clark, H.B., Burright, E.N., Yunis, W.S., Larson, S., Wilcox, C., Hartman, B., Matilla, A., Zoghbi, H.Y., and Orr, H.T. (1997). Purkinje Cell Expression of a Mutant Allele of SCA1in Transgenic Mice Leads to Disparate Effects on Motor Behaviors, Followed by a Progressive Cerebellar Dysfunction and Histological Alterations. J. Neurosci. *17*, 7385–7395.

Corsini, L., Bonnal, S., Bonna, S., Basquin, J., Hothorn, M., Scheffzek, K., Valcárcel, J., and Sattler, M. (2007). U2AF-homology motif interactions are required for alternative splicing regulation by SPF45. Nat. Struct. Mol. Biol. *14*, 620–629.

Crespo-Barreto, J., Fryer, J.D., Shaw, C.A., Orr, H.T., and Zoghbi, H.Y. (2010). Partial Loss of Ataxin-1 Function Contributes to Transcriptional Dysregulation in Spinocerebellar Ataxia Type 1 Pathogenesis. PLoS Genet. *6*, e1001021.

Cummings, C.J., Mancini, M.A., Antalffy, B., DeFranco, D.B., Orr, H.T., and Zoghbi, H.Y. (1998). Chaperone suppression of aggregation and altered subcellular proteasome localization imply protein misfolding in SCA1. Nat. Genet. *19*, 148–154.

Cummings, C.J., Sun, Y., Opal, P., Antalffy, B., Mestril, R., Orr, H.T., Dillmann, W.H., and Zoghbi, H.Y. (2001). Over-expression of inducible HSP70 chaperone suppresses neuropathology and improves motor function in SCA1 mice. Hum. Mol. Genet. *10*, 1511–1518.

Doyle, J.P., Dougherty, J.D., Heiman, M., Schmidt, E.F., Stevens, T.R., Ma, G., Bupp, S., Shrestha, P., Shah, R.D., Doughty, M.L., et al. (2008). Application of a Translational Profiling Approach for the Comparative Analysis of CNS Cell Types. Cell *135*, 749–762.

Duvick, L., Barnes, J., Ebner, B., Agrawal, S., Andresen, M., Lim, J., Giesler, G.J., Zoghbi, H.Y., and Orr, H.T. (2010). SCA1-like Disease in Mice Expressing Wild-Type Ataxin-1 with a Serine to Aspartic Acid Replacement at Residue 776. Neuron *67*, 929–935.

Ebner, B.A., Ingram, M.A., Barnes, J.A., Duvick, L.A., Frisch, J.L., Clark, H.B., Zoghbi, H.Y., Ebner, T.J., and Orr, H.T. (2013). Purkinje cell ataxin-1 modulates climbing fiber synaptic input in developing and adult mouse cerebellum. J. Neurosci. Off. J. Soc. Neurosci. *33*, 5806–5820.

Emamian, E.S., Kaytor, M.D., Duvick, L.A., Zu, T., Tousey, S.K., Zoghbi, H.Y., Clark, H.B., and Orr, H.T. (2003). Serine 776 of Ataxin-1 Is Critical for Polyglutamine-Induced Disease in SCA1 Transgenic Mice. Neuron *38*, 375–387.

Fernandez-Funez, P., Nino-Rosales, M.L., de Gouyon, B., She, W.C., Luchak, J.M., Martinez, P., Turiegano, E., Benito, J., Capovilla, M., Skinner, P.J., et al. (2000). Identification of genes that modify ataxin-1-induced neurodegeneration. Nature *408*, 101–106.

Gatchel, J.R., Watase, K., Thaller, C., Carson, J.P., Jafar-Nejad, P., Shaw, C., Zu, T., Orr, H.T., and Zoghbi, H.Y. (2008). The insulin-like growth factor pathway is altered in spinocerebellar ataxia type 1 and type 7. Proc. Natl. Acad. Sci. *105*, 1291–1296.

Gehrking, K.M., Andresen, J.M., Duvick, L., Lough, J., Zoghbi, H.Y., and Orr, H.T. (2011). Partial loss of Tip60 slows mid-stage neurodegeneration in a spinocerebellar ataxia type 1 (SCA1) mouse model. Hum. Mol. Genet. *20*, 2204–2212.

Giardine, B., Riemer, C., Hardison, R.C., Burhans, R., Elnitski, L., Shah, P., Zhang, Y., Blankenberg, D., Albert, I., Taylor, J., et al. (2005). Galaxy: A platform for interactive large-scale genome analysis. Genome Res. *15*, 1451–1455.

Goecks, J., Nekrutenko, A., and Taylor, J. (2010). Galaxy: a comprehensive approach for supporting accessible, reproducible, and transparent computational research in the life sciences. Genome Biol. *11*, R86.

Goldowitz, D., and Hamre, K. (1998). The cells and molecules that make a cerebellum. Trends Neurosci. *21*, 375–382.

Gossen, M., and Bujard, H. (1992). Tight control of gene expression in mammalian cells by tetracycline-responsive promoters. Proc. Natl. Acad. Sci. U. S. A. *89*, 5547–5551.

Haines, J.L., Schut, L.J., Weitkamp, L.R., Thayer, M., and Anderson, V.E. (1984). Spinocerebellar ataxia in a large kindred: age at onset, reproduction, and genetic linkage studies. Neurology *34*, 1542–1548.

Hashimoto, K., and Kano, M. (2003). Functional differentiation of multiple climbing fiber inputs during synapse elimination in the developing cerebellum. Neuron *38*, 785–796.

Heiman, M., Schaefer, A., Gong, S., Peterson, J.D., Day, M., Ramsey, K.E., Suárez-Fariñas, M., Schwarz, C., Stephan, D.A., Surmeier, D.J., et al. (2008). A Translational Profiling Approach for the Molecular Characterization of CNS Cell Types. Cell *135*, 738–748.

Hong, S., Ka, S., Kim, S., Park, Y., and Kang, S. (2003). p80 coilin, a coiled body-specific protein, interacts with ataxin-1, the SCA1 gene product. Biochim. Biophys. Acta BBA - Mol. Basis Dis. *1638*, 35–42.

Hourez, R., Servais, L., Orduz, D., Gall, D., Millard, I., de Kerchove d'Exaerde, A., Cheron, G., Orr, H.T., Pandolfo, M., and Schiffmann, S.N. (2011).

Aminopyridines correct early dysfunction and delay neurodegeneration in a mouse model of spinocerebellar ataxia type 1. J. Neurosci. Off. J. Soc. Neurosci. *31*, 11795–11807.

Huang, D.W., Sherman, B.T., and Lempicki, R.A. (2008). Systematic and integrative analysis of large gene lists using DAVID bioinformatics resources. Nat. Protoc. *4*, 44–57.

Huang, D.W., Sherman, B.T., and Lempicki, R.A. (2009). Bioinformatics enrichment tools: paths toward the comprehensive functional analysis of large gene lists. Nucleic Acids Res. *37*, 1–13.

Irwin, S., Vandelft, M., Pinchev, D., Howell, J.L., Graczyk, J., Orr, H.T., and Truant, R. (2005). RNA association and nucleocytoplasmic shuttling by ataxin-1. J. Cell Sci. *118*, 233–242.

Jafar-Nejad, P., Ward, C.S., Richman, R., Orr, H.T., and Zoghbi, H.Y. (2011). Regional rescue of spinocerebellar ataxia type 1 phenotypes by 14-3-3ε haploinsufficiency in mice underscores complex pathogenicity in neurodegeneration. Proc. Natl. Acad. Sci. *108*, 2142–2147.

Jordan, B.A., Fernholz, B.D., Khatri, L., and Ziff, E.B. (2007). Activity-dependent AIDA-1 nuclear signaling regulates nucleolar numbers and protein synthesis in neurons. Nat. Neurosci. *10*, 427–435.

Jorgensen, N.D., Andresen, J.M., Lagalwar, S., Armstrong, B., Stevens, S., Byam, C.E., Duvick, L.A., Lai, S., Jafar-Nejad, P., Zoghbi, H.Y., et al. (2009). Phosphorylation of ATXN1 at Ser776 in the cerebellum. J. Neurochem. *110*, 675–686.

Kano, M., and Hashimoto, K. (2009). Synapse elimination in the central nervous system. Curr. Opin. Neurobiol. *19*, 154–161.

Kim, E., Lu, H.-C., Zoghbi, H.Y., and Song, J.-J. (2013). Structural basis of protein complex formation and reconfiguration by polyglutamine disease protein Ataxin-1 and Capicua. Genes Dev. *27*, 590–595.

Klement, I.A., Skinner, P.J., Kaytor, M.D., Yi, H., Hersch, S.M., Clark, H.B., Zoghbi, H.Y., and Orr, H.T. (1998). Ataxin-1 Nuclear Localization and Aggregation: Role in Polyglutamine-Induced Disease in SCA1 Transgenic Mice. Cell *95*, 41–53.

Klement, I.A., Zoghbi, H.Y., and Orr, H.T. (1999). Pathogenesis of Polyglutamine-Induced Disease: A Model for SCA1. Mol. Genet. Metab. *66*, 172–178.

Koeppen, A.H. (1998). The hereditary ataxias. J. Neuropathol. Exp. Neurol. *57*, 531–543.

Lam, Y.C., Bowman, A.B., Jafar-Nejad, P., Lim, J., Richman, R., Fryer, J.D., Hyun, E.D., Duvick, L.A., Orr, H.T., and Botas, J. (2006). ATAXIN-1 Interacts with the Repressor Capicua in Its Native Complex to Cause SCA1 Neuropathology. Cell *127*, 1335–1347.

Langmead, B., Trapnell, C., Pop, M., and Salzberg, S.L. (2009). Ultrafast and memory-efficient alignment of short DNA sequences to the human genome. Genome Biol. *10*, R25.

Lein, E.S., Hawrylycz, M.J., Ao, N., Ayres, M., Bensinger, A., Bernard, A., Boe, A.F., Boguski, M.S., Brockway, K.S., Byrnes, E.J., et al. (2007). Genome-wide atlas of gene expression in the adult mouse brain. Nature *445*, 168–176.

Lim, J., Crespo-Barreto, J., Jafar-Nejad, P., Bowman, A.B., Richman, R., Hill, D.E., Orr, H.T., and Zoghbi, H.Y. (2008). Opposing effects of polyglutamine expansion on native protein complexes contribute to SCA1. Nature *452*, 713–718.

Lin, X., Antalffy, B., Kang, D., Orr, H.T., and Zoghbi, H.Y. (2000). Polyglutamine expansion down-regulates specific neuronal genes before pathologic changes in SCA1. Nat. Neurosci. *3*, 157–163.

Matilla, A., Roberson, E.D., Banfi, S., Morales, J., Armstrong, D.L., Burright, E.N., Orr, H.T., Sweatt, J.D., Zoghbi, H.Y., and Matzuk, M.M. (1998). Mice Lacking Ataxin-1 Display Learning Deficits and Decreased Hippocampal Paired-Pulse Facilitation. J. Neurosci. *18*, 5508–5516.

Matsui, K., Masui, A., Kato, N., and Adachi, K. (1993). Levels of somatostatin and cholecystokinin in the brain of ataxic mutant mice. Life Sci. *53*, 333–340.

Mortazavi, A., Williams, B.A., McCue, K., Schaeffer, L., and Wold, B. (2008). Mapping and quantifying mammalian transcriptomes by RNA-Seq. Nat. Methods *5*, 621–628.

Oberdick, J., Smeyne, R.J., Mann, J.R., Zackson, S., and Morgan, J.I. (1990). A promoter that drives transgene expression in cerebellar Purkinje and retinal bipolar neurons. Science *248*, 223–226.

Orr, H. (2000). The Ins and Outs of a Polyglutamine Neurodegenerative Disease: Spinocerebellar Ataxia Type 1 (SCA1). Neurobiol. Dis. *7*, 129–134.

Oz, G., Nelson, C.D., Koski, D.M., Henry, P.-G., Marjanska, M., Deelchand, D.K., Shanley, R., Eberly, L.E., Orr, H.T., and Clark, H.B. (2010). Noninvasive Detection of Presymptomatic and Progressive Neurodegeneration in a Mouse Model of Spinocerebellar Ataxia Type 1. J. Neurosci. *30*, 3831–3838.

Öz, G., Hutter, D., Tkáč, I., Clark, H.B., Gross, M.D., Jiang, H., Eberly, L.E., Bushara, K.O., and Gomez, C.M. (2010). Neurochemical alterations in spinocerebellar ataxia type 1 and their correlations with clinical status. Mov. Disord. *25*, 1253–1261.

Paisán-Ruiz, C., Scopes, G., Lee, P., and Houlden, H. (2009). Homozygosity mapping through whole genome analysis identifies a COL18A1 mutation in an Indian family presenting with an autosomal recessive neurological disorder. Am. J. Med. Genet. B Neuropsychiatr. Genet. *150B*, 993–997.

Ross, C.A. (1997). Intranuclear neuronal inclusions: a common pathogenic mechanism for glutamine-repeat neurodegenerative diseases? Neuron *19*, 1147–1150.

Schut, J.W. (1950). Hereditary ataxia: Clinical study through six generations. Arch. Neurol. Psychiatry *63*, 535–568.

Serra, H.G. (2004). Gene profiling links SCA1 pathophysiology to glutamate signaling in Purkinje cells of transgenic mice. Hum. Mol. Genet. *13*, 2535–2543.

Serra, H.G., Duvick, L., Zu, T., Carlson, K., Stevens, S., Jorgensen, N., Lysholm, A., Burright, E., Zoghbi, H.Y., and Clark, H.B. (2006). RORα-Mediated Purkinje Cell Development Determines Disease Severity in Adult SCA1 Mice. Cell *127*, 697–708.

Servadio, A., Koshy, B., Armstrong, D., Antalffy, B., Orr, H.T., and Zoghbi, H.Y. (1995). Expression analysis of the ataxin-1 protein in tissues from normal and spinocerebellar ataxia type 1 individuals. Nat. Genet. *10*, 94–98.

Smeyne, R.J., Oberdick, J., Schilling, K., Berrebi, A.S., Mugnaini, E., and Morgan, J.I. (1991). Dynamic organization of developing Purkinje cells revealed by transgene expression. Science *254*, 719–721.

Su, J., Stenbjorn, R.S., Gorse, K., Su, K., Hauser, K.F., Ricard-Blum, S., Pihlajaniemi, T., and Fox, M.A. (2012). Target-Derived Matricryptins Organize Cerebellar Synapse Formation through α3β1 Integrins. Cell Rep. *2*, 223–230.

Trapnell, C., Pachter, L., and Salzberg, S.L. (2009). TopHat: discovering splice junctions with RNA-Seq. Bioinformatics *25*, 1105–1111.

Trapnell, C., Williams, B.A., Pertea, G., Mortazavi, A., Kwan, G., van Baren, M.J., Salzberg, S.L., Wold, B.J., and Pachter, L. (2010). Transcript assembly and quantification by RNA-Seq reveals unannotated transcripts and isoform switching during cell differentiation. Nat. Biotechnol. *28*, 511–515.

Tsai, C.-C., Kao, H.-Y., Mitzutani, A., Banayo, E., Rajan, H., McKeown, M., and Evans, R.M. (2004). Ataxin 1, a SCA1 neurodegenerative disorder protein, is functionally linked to the silencing mediator of retinoid and thyroid hormone receptors. Proc. Natl. Acad. Sci. U. S. A. *101*, 4047–4052.

Tsuda, H., Jafar-Nejad, H., Patel, A.J., Sun, Y., Chen, H.-K., Rose, M.F., Venken, K.J.T., Botas, J., Orr, H.T., Bellen, H.J., et al. (2005). The AXH Domain of Ataxin-1 Mediates Neurodegeneration through Its Interaction with Gfi-1/Senseless Proteins. Cell *122*, 633–644.

Vandaele, S., Nordquist, D.T., Feddersen, R.M., Tretjakoff, I., Peterson, A.C., and Orr, H.T. (1991). Purkinje cell protein-2 regulatory regions and transgene expression in cerebellar compartments. Genes Dev. *5*, 1136–1148.

Watase, K., Weeber, E.J., Xu, B., Antalffy, B., Yuva-Paylor, L., Hashimoto, K., Kano, M., Atkinson, R., Sun, Y., Armstrong, D.L., et al. (2002). A long CAG repeat in the mouse Sca1 locus replicates SCA1 features and reveals the impact of protein solubility on selective neurodegeneration. Neuron *34*, 905–919.

Watase, K., Venken, K.J.T., Sun, Y., Orr, H.T., and Zoghbi, H.Y. (2003). Regional differences of somatic CAG repeat instability do not account for selective neuronal vulnerability in a knock-in mouse model of SCA1. Hum. Mol. Genet. *12*, 2789–2795.

Wishart, T.M., Parson, S.H., and Gillingwater, T.H. (2006). Synaptic vulnerability in neurodegenerative disease. J. Neuropathol. Exp. Neurol. *65*, 733–739.

Wood, P.L., Steel, D.J., Kim, H.S., Petrack, B., and Altar, C.A. (1988). Inhibition of climbing and mossy fiber input to mouse cerebellar Purkinje cells by cholecystokinin. J. Pharmacol. Exp. Ther. *244*, 58–62.

Wu, T.D., and Watanabe, C.K. (2005). GMAP: a genomic mapping and alignment program for mRNA and EST sequences. Bioinformatics *21*, 1859–1875.

Yamamoto, A., Lucas, J.J., and Hen, R. (2000). Reversal of neuropathology and motor dysfunction in a conditional model of Huntington's disease. Cell *101*, 57–66.

Yamamoto, A., Hen, R., and Dauer, W.T. (2001). The ons and offs of inducible transgenic technology: a review. Neurobiol. Dis. *8*, 923–932.

Yue, S., Serra, H.G., Zoghbi, H.Y., and Orr, H.T. (2001). The spinocerebellar ataxia type 1 protein, ataxin-1, has RNA-binding activity that is inversely affected by the length of its polyglutamine tract. Hum. Mol. Genet. *10*, 25–30.

Zoghbi, H.Y., and Orr, H.T. (1995). Spinocerebellar ataxia type 1. Semin. Cell Biol. *6*, 29–35.

Zu, T., Duvick, L.A., Kaytor, M.D., Berlinger, M.S., Zoghbi, H.Y., Clark, H.B., and Orr, H.T. (2004). Recovery from Polyglutamine-Induced Neurodegeneration in Conditional SCA1 Transgenic Mice. J. Neurosci. *24*, 8853–8861.

Appendix 1. CuffDiff Data from ATXN1[82Q] vs ATXN1[30Q]-D776

gene	locus	status	B05_value_1	D30_value_2	log2(fold_change)	test_stat	p_value	q_value	significant
1700037H04Rik	chr2:130972060-130985756	OK	26.2265	39.5108	0.591222	2.44783	0.00015	0.0072806	yes
2900026A02Rik	chr5:113515342-113592333	OK	2.59206	4.45534	0.781438	2.61104	5.00E-05	0.00280638	yes
2900052N01Rik	chr9:46721685-46735449	OK	0.629979	3.05058	2.27571	3.9455	5.00E-05	0.00280638	yes
3110035E14Rik	chr1:9538126-9621173	OK	2.77251	7.22868	1.38254	2.88246	5.00E-05	0.00280638	yes
3830431G21Rik	chr12:81793587-81825203	OK	18.8968	27.5451	0.543657	2.36147	5.00E-05	0.00280638	yes
4933407C03Rik	chr8:119780918-119985405	OK	23.8064	34.6475	0.541402	2.34844	5.00E-05	0.00280638	yes
5930403L14Rik	chr4:153690233-154010982	OK	1.00927	2.25502	1.15983	2.1824	0.00055	0.0208374	yes
6030405A18Rik	chr3:54700990-54719809	OK	0.781596	2.14286	1.45504	2.73007	5.00E-05	0.00280638	yes
6330403A02Rik	chr1:182362503-182413635	OK	3.19122	5.45	0.772147	2.71019	5.00E-05	0.00280638	yes
6330403K07Rik	chr11:70845442-70847119	OK	31.9982	54.6397	0.77196	3.30286	5.00E-05	0.00280638	yes
6330512M04Rik	chr7:149512014-149558164	OK	10.9018	7.60404	-0.519734	-1.94847	0.00085	0.0292756	yes
6330527O06Rik	chr2:135883662-135895653	OK	1.24596	5.7581	2.20833	4.36965	5.00E-05	0.00280638	yes
A730017C20Rik	chr18:59222034-59236614	OK	5.60294	8.98787	0.681795	1.97308	0.00085	0.0292756	yes
A830018L16Rik	chr1:11404185-11965983	OK	1.02392	1.98132	0.952364	2.06316	0.00065	0.0238316	yes
AI593442	chr9:52481146-52487534	OK	7.09628	14.8112	1.06156	4.35995	5.00E-05	0.00280638	yes
AW551984	chr9:39394980-39411709	OK	0.810798	1.91261	1.23812	2.47215	0.0001	0.00520573	yes
Accn4	chr1:75447084-75470915	OK	0.988779	2.87343	1.53905	2.96681	0.0001	0.00520573	yes
Acsl5	chr19:55327858-55371118	OK	5.24842	7.87088	0.584642	1.97392	0.001	0.0331849	yes
Adamts18	chr8:116222036-116372739	OK	5.45308	3.71707	-0.552906	-1.89488	0.0016	0.0478561	yes
Agfg2	chr5:138092081-138125921	OK	11.8684	18.0996	0.608829	2.15867	0.00015	0.0072806	yes
Ajap1	chr4:152747329-152856939	OK	6.44683	9.48489	0.557041	1.98654	0.00065	0.0238316	yes
Akap2	chr4:57858119-57909856	OK	9.52796	13.318	0.483139	2.02389	0.0005	0.0192099	yes
Akap7	chr10:24888895-25018969	OK	29.8504	21.9594	-0.442913	-1.92283	0.0013	0.0406667	yes
Alas2	chrX:146981959-147005165	OK	5.69776	10.9119	0.937436	2.79894	5.00E-05	0.00280638	yes
Aldh1b1	chr4:45811893-45817480	OK	0.834251	1.97849	1.24585	2.14852	0.00155	0.0467709	yes
Alms1	chr6:85537524-85652745	OK	6.17806	4.46764	-0.467642	-1.89954	0.0011	0.0354678	yes
Ankrd33b	chr15:31221234-31297514	OK	1.43327	2.55277	0.832758	2.14915	0.0003	0.0125512	yes
Apold1	chr6:134932018-134936854	OK	0.760403	2.47032	1.69986	3.31385	5.00E-05	0.00280638	yes
Aqp4	chr18:15547902-15562193	OK	98.9746	72.7236	-0.444636	-1.88895	0.0012	0.0384197	yes
Arap1	chr7:108496582-108561100	OK	8.78381	12.426	0.500438	1.98594	0.00025	0.0108246	yes
Arhgap30	chr1:173319090-173340370	OK	0.546031	1.31519	1.26821	2.33685	0.0002	0.00915369	yes
Arhgap32	chr9:31923720-32073096	OK	10.815	16.6331	0.621019	2.67286	5.00E-05	0.00280638	yes
Arhgap33	chr7:31307244-31320028	OK	6.63263	10.3814	0.646346	2.47522	5.00E-05	0.00280638	yes
Arhgdib	chr6:136872229-136890238	OK	4.02637	11.1692	1.47198	3.48291	5.00E-05	0.00280638	yes
Arhgdig	chr17:26336127-26338295	OK	10.0255	17.5535	0.808088	2.53264	0.0003	0.0125512	yes
Arhgef33	chr17:80706746-80788029	OK	24.8254	37.0676	0.57834	2.43723	5.00E-05	0.00280638	yes
Arpc1b	chr5:145875124-145889055	OK	11.4636	27.0033	1.23608	4.21861	5.00E-05	0.00280638	yes
Atp2b4	chr1:135599250-135650324	OK	4.3639	7.10313	0.702838	2.70767	5.00E-05	0.00280638	yes

B230120H23Rik	chr2:72123693-72280667	OK	2.01198	3.30399	0.715597	2.03489	0.00025	0.0108246	yes
B3gat1	chr9:26559146-26568923	OK	15.8868	24.9249	0.649753	2.77403	5.00E-05	0.00280638	yes
Basp1	chr15:25293031-25343519	OK	13.4895	43.6928	1.69556	6.49814	5.00E-05	0.00280638	yes
Baz1a	chr12:55993975-56087323	OK	0.286488	0.952203	1.73279	2.95218	5.00E-05	0.00280638	yes
Bcar1	chr8:114234374-114267749	OK	33.6422	55.4065	0.719783	3.10499	5.00E-05	0.00280638	yes
Bcl11b	chr12:109148612-109241624	OK	0.382229	1.26367	1.72512	3.48233	5.00E-05	0.00280638	yes
Begain	chr12:110270391-110306427	OK	10.0989	15.7193	0.638341	2.47901	0.0001	0.00520573	yes
Beta-s	chr7:110975036-110976442	OK	117.783	201.054	0.771451	3.70943	5.00E-05	0.00280638	yes
Btk	chrX:131076879-131117679	OK	0.189368	1.14218	2.59253	3.02788	0.0002	0.00915369	yes
Bub1b	chr2:118423946-118467328	OK	0.094328	1.06905	3.5025	3.96901	5.00E-05	0.00280638	yes
C1ql2	chr1:122237158-122239751	OK	0.39691	1.61955	2.02871	2.84829	5.00E-05	0.00280638	yes
Cacna1g	chr11:94269704-94335512	OK	21.8406	43.8501	1.00557	4.30422	5.00E-05	0.00280638	yes
Cacna1h	chr17:25507497-25570728	OK	0.94674	1.56306	0.723336	1.91242	0.00125	0.0395563	yes
Camk2a	chr18:61085285-61147806	OK	15.7058	63.2754	2.01035	6.88188	5.00E-05	0.00280638	yes
Camk2n1	chr4:138011062-138016041	OK	82.0617	119.592	0.543337	2.34153	5.00E-05	0.00280638	yes
Camkv	chr9:107838250-107852022	OK	4.64994	22.6028	2.28122	7.3493	5.00E-05	0.00280638	yes
Car4	chr11:84771255-84779556	OK	145.931	104.419	-0.482901	-2.24159	0.00035	0.0142073	yes
Casq2	chr3:101890432-101950435	OK	11.298	7.62723	-0.566833	-2.01524	0.0008	0.0279059	yes
Casz1	chr4:148178500-148329001	OK	0.586149	1.06045	0.855339	1.88091	0.0014	0.0433968	yes
Cbln2	chr18:86882439-86887675	OK	0.894522	2.31923	1.37445	2.32859	0.00025	0.0108246	yes
Cbln4	chr2:171861835-171868966	OK	0.741408	2.1767	1.5538	2.81696	0.0001	0.00520573	yes
Ccdc88b	chr19:6919112-6932701	OK	0.481452	1.16017	1.26888	2.32574	0.00025	0.0108246	yes
Cck	chr9:121398941-121404807	OK	21.2067	272.003	3.68103	14.4227	5.00E-05	0.00280638	yes
Cckbr	chr7:112574333-112584852	OK	1.11184	2.58982	1.2199	2.36492	0.0006	0.0224203	yes
Ccl9	chr11:83386418-83392138	OK	0.479215	1.4809	1.62773	2.58994	0.0001	0.00520573	yes
Ccnb1	chr13:101548693-101556441	OK	0.119241	1.34189	3.49232	3.51874	0.00025	0.0108246	yes
Ccnb2	chr9:70255495-70269361	OK	0.776071	2.38603	1.62035	2.50346	0.00045	0.0175359	yes
Ccnd2	chr6:127075726-127162437	OK	2.65565	4.60045	0.79271	2.6161	5.00E-05	0.00280638	yes
Cd24a	chr10:43298974-43304071	OK	5.9659	11.5345	0.951139	2.94354	5.00E-05	0.00280638	yes
Cd33	chr7:50782825-50788541	OK	0.582239	2.55482	2.13354	3.48946	5.00E-05	0.00280638	yes
Cd37	chr7:52489001-52494209	OK	1.10262	3.84155	1.80075	2.99822	0.00025	0.0108246	yes
Cdca7	chr2:72314275-72324947	OK	0.327942	1.70517	2.3784	3.40962	5.00E-05	0.00280638	yes
Cdca8	chr4:124595708-124614161	OK	0.283598	1.25978	2.15125	2.47839	0.0013	0.0406667	yes
Cdh13	chr8:120807654-121847348	OK	4.98483	8.35601	0.74527	2.32588	0.00025	0.0108246	yes
Cdh7	chr1:111880313-112035578	OK	9.52312	6.51073	-0.548615	-1.97648	0.0009	0.0307647	yes
Cdk1	chr10:68799382-68815660	OK	0.0920037	0.846908	3.20244	3.04235	0.0007	0.0250585	yes
Cdk5r2	chr1:74901602-74904306	OK	42.7474	61.1764	0.51714	2.31567	0.0001	0.00520573	yes
Cdk6	chr5:3344311-3522225	OK	0.1409	0.824372	2.54862	2.76326	0.00065	0.0238316	yes
Cdr1	chrX:58436420-58438733	OK	200.267	119.299	-0.747343	-3.27819	5.00E-05	0.00280638	yes

Cenpa	chr5:30969274-30977199	OK	0.429375	1.94234	2.17749	2.72235	0.0002	0.00915369	yes
Chd5	chr4:151712759-151764303	OK	9.33637	15.4669	0.728247	3.14971	5.00E-05	0.00280638	yes
Chn1	chr2:73434582-73613403	OK	24.6143	37.5038	0.607541	2.556	5.00E-05	0.00280638	yes
Chn2	chr6:53989925-54380215	OK	223.947	158.462	-0.499025	-2.11892	0.0003	0.0125512	yes
Chrm1	chr19:8738494-8758092	OK	0.186544	1.83264	3.29634	5.12699	5.00E-05	0.00280638	yes
Chrm3	chr13:9875858-10360049	OK	0.604597	1.71044	1.50032	2.60888	5.00E-05	0.00280638	yes
Chrna4	chr2:180757015-180773882	OK	2.06307	3.49844	0.76192	2.19041	0.00015	0.0072806	yes
Cks1b	chr3:89219393-89222213	OK	2.4771	5.94351	1.26266	2.29363	0.00135	0.042038	yes
Clmn	chr12:106001323-106103286	OK	6.82538	10.0087	0.552272	2.36745	5.00E-05	0.00280638	yes
Cmtm7	chr9:114665953-114691111	OK	3.33762	11.4864	1.78304	3.73141	5.00E-05	0.00280638	yes
Cnih3	chr1:183282758-183390772	OK	1.34714	3.62192	1.42686	2.98937	5.00E-05	0.00280638	yes
Cnksr3	chr10:3134303-3227479	OK	24.1496	17.1584	-0.493084	-2.08661	0.00095	0.0320719	yes
Cntn6	chr6:104443037-104813399	OK	16.1312	10.6758	-0.59551	-2.4276	5.00E-05	0.00280638	yes
Cntnap5b	chr1:101669341-102382519	OK	1.5724	3.16768	1.01046	2.80808	5.00E-05	0.00280638	yes
Cobl	chr11:12136678-12364963	OK	1.0026	2.24704	1.16428	2.85774	5.00E-05	0.00280638	yes
Coch	chr12:52694327-52706760	OK	4.79773	2.04687	-1.22893	-2.90431	5.00E-05	0.00280638	yes
Col18a1	chr10:76514923-76629275	OK	6.16143	37.1679	2.59272	10.4229	5.00E-05	0.00280638	yes
Col25a1	chr3:129883762-130302801	OK	0.580572	1.49758	1.36709	3.05381	5.00E-05	0.00280638	yes
Col4a1	chr8:11198422-11312826	OK	4.10703	11.3249	1.46333	5.7511	5.00E-05	0.00280638	yes
Col4a2	chr8:11312828-11449287	OK	3.70422	8.88737	1.26258	4.81537	5.00E-05	0.00280638	yes
Col5a1	chr2:27741944-27895030	OK	0.619068	5.19826	3.06986	8.11426	5.00E-05	0.00280638	yes
Col6a1	chr10:76171536-76188789	OK	3.73589	5.47733	0.552019	1.81763	0.0013	0.0406667	yes
Cpeb1	chr7:88491911-88599644	OK	5.96616	8.92786	0.581511	1.99922	0.0008	0.0279059	yes
Cpne4	chr9:104472117-104936874	OK	0.517626	1.70881	1.72301	3.01467	0.0001	0.00520573	yes
Cpne5	chr17:29293465-29374735	OK	0.50687	2.59925	2.35841	4.43811	5.00E-05	0.00280638	yes
Cpne6	chr14:56129284-56136268	OK	4.19322	14.8318	1.82256	5.17062	5.00E-05	0.00280638	yes
Cpne7	chr8:125641273-125659085	OK	0.337704	4.34612	3.6859	5.51283	5.00E-05	0.00280638	yes
Creg2	chr1:39675250-39708027	OK	1.81689	3.51256	0.95105	2.86713	5.00E-05	0.00280638	yes
Crhbp	chr13:96201330-96214786	OK	0.380103	1.60906	2.08175	2.75262	0.00025	0.0108246	yes
Crtac1	chr19:42357526-42506273	OK	4.30885	7.04077	0.708431	2.17309	0.00035	0.0142073	yes
Csrnp1	chr9:119880283-119893776	OK	3.96137	6.33663	0.677714	2.0987	0.0006	0.0224203	yes
Ctxn1	chr8:4257645-4259274	OK	5.04311	30.0865	2.57673	6.92377	5.00E-05	0.00280638	yes
Cx3cl1	chr8:97296079-97306326	OK	28.0665	44.8745	0.677048	2.95728	5.00E-05	0.00280638	yes
Cyb561	chr11:105795017-105805461	OK	5.37196	8.8242	0.716016	2.31091	0.00025	0.0108246	yes
Cyr61	chr3:145309934-145312949	OK	1.35639	3.98873	1.55616	3.12315	5.00E-05	0.00280638	yes
D430019H16Rik	chr12:106692065-106731305	OK	1.8437	4.35116	1.2388	3.79484	5.00E-05	0.00280638	yes
Dact2	chr17:14332236-14340838	OK	3.4215	5.52146	0.690421	2.01309	0.00125	0.0395563	yes
Dagla	chr19:10319754-10379367	OK	11.0777	26.1565	1.23952	5.34072	5.00E-05	0.00280638	yes
Dapk1	chr13:60703307-60864547	OK	2.92411	5.22283	0.836832	2.83965	5.00E-05	0.00280638	yes

Dbh	chr2:27021026-27038724	OK	0.489184	2.37755	2.28103	3.36865	5.00E-05	0.00280638	yes
Ddc	chr11:11714103-11798147	OK	2.18529	6.14477	1.49153	3.30604	5.00E-05	0.00280638	yes
Ddit4	chr10:59412422-59414518	OK	30.1322	41.4701	0.460764	1.98889	0.00105	0.0342606	yes
Ddn	chr15:98634212-98638356	OK	0.853997	31.2284	5.19248	10.3496	5.00E-05	0.00280638	yes
Dgkh	chr14:78969415-79124896	OK	1.92075	3.83819	0.998751	2.67789	5.00E-05	0.00280638	yes
Dgkz	chr2:91772978-91803720	OK	134.7	181.301	0.428632	1.79795	0.001	0.0331849	yes
Dhcr24	chr4:106233642-106261718	OK	18.8537	33.3145	0.821304	3.57579	5.00E-05	0.00280638	yes
Dkk3	chr7:119259532-119302571	OK	8.9549	16.2896	0.863205	3.32068	5.00E-05	0.00280638	yes
Dlgap2	chr8:14095874-14847686	OK	0.455003	1.12036	1.30002	2.19648	0.0004	0.0159988	yes
Dlk1	chr12:110691032-110701546	OK	1.00214	3.22821	1.68765	3.62839	5.00E-05	0.00280638	yes
Dmrtb1	chr4:107348894-107356767	OK	0.238469	1.80195	2.91769	3.31873	0.00025	0.0108246	yes
Dock8	chr19:25074018-25276922	OK	0.43297	0.912833	1.07608	2.15977	0.0007	0.0250585	yes
Dok2	chr14:71174187-71178301	OK	0.150313	1.3798	3.19842	3.27179	0.0007	0.0250585	yes
Dpf3	chr12:84370184-84828658	OK	28.0894	19.7438	-0.50863	-1.98134	0.0016	0.0478561	yes
Dusp1	chr17:26642535-26645417	OK	39.0718	69.6039	0.833039	3.68637	5.00E-05	0.00280638	yes
Dusp6	chr10:98725864-98730123	OK	4.17579	6.60662	0.661863	2.0622	0.0006	0.0224203	yes
E130012A19Rik	chr11:97488700-97491030	OK	2.22491	5.1842	1.22037	2.96157	5.00E-05	0.00280638	yes
Egr1	chr18:35020860-35024610	OK	18.738	26.6142	0.50623	2.1607	0.00015	0.0072806	yes
Egr3	chr14:70477251-70479964	OK	0.199923	2.38738	3.57791	3.7187	0.0002	0.00915369	yes
Egr4	chr6:85461115-85463536	OK	2.04351	4.48489	1.13402	2.57105	0.00015	0.0072806	yes
Elfn1	chr5:140383896-140450678	OK	0.889266	2.18928	1.29977	2.70863	5.00E-05	0.00280638	yes
Elfn2	chr15:78500436-78548543	OK	2.80936	6.55114	1.2215	4.0989	5.00E-05	0.00280638	yes
Enc1	chr13:98011059-98022995	OK	4.28984	14.4649	1.75356	6.07747	5.00E-05	0.00280638	yes
Epha10	chr4:124559028-124595044	OK	2.7788	4.33562	0.641775	1.84379	0.00165	0.0492437	yes
Epha4	chr1:77363759-77511663	OK	5.30418	7.95503	0.584736	2.24639	0.0002	0.00915369	yes
Ephb3	chr16:21204867-21223377	OK	0.970045	2.06513	1.09011	2.37789	0.0002	0.00915369	yes
Ephb6	chr6:41555480-41570506	OK	3.02071	6.34464	1.07065	3.30094	5.00E-05	0.00280638	yes
Eps8	chr6:137425765-137597641	OK	37.673	24.4205	-0.625437	-2.73019	5.00E-05	0.00280638	yes
Erf	chr7:26027578-26035777	OK	5.5247	8.17923	0.56607	2.00897	0.001	0.0331849	yes
Espn	chr4:151494984-151526316	OK	1.31235	2.919	1.15332	1.90793	0.0013	0.0406667	yes
Etv5	chr16:22381385-22439643	OK	14.6214	22.2426	0.605245	2.58149	5.00E-05	0.00280638	yes
Extl1	chr4:133912287-133928462	OK	2.35474	4.24974	0.851806	2.50662	5.00E-05	0.00280638	yes
Fam107b	chr2:3630729-3699406	OK	18.4441	28.3677	0.621086	2.67878	5.00E-05	0.00280638	yes
Fam111a	chr19:12648014-12671056	OK	0.332136	1.41049	2.08635	2.26701	0.00095	0.0320719	yes
Fam160a1	chr3:85463984-85550131	OK	0.470866	1.05515	1.16405	2.02433	0.00125	0.0395563	yes
Fam163b	chr2:26965898-26997997	OK	7.97654	13.8834	0.799526	3.01428	5.00E-05	0.00280638	yes
Fam174b	chr7:80885192-80921805	OK	7.75514	12.6529	0.706246	2.59549	5.00E-05	0.00280638	yes
Fam19a2	chr10:122701131-123178260	OK	1.17856	2.64689	1.16728	2.72375	5.00E-05	0.00280638	yes
Fam40b	chr6:29867012-29909680	OK	16.7995	9.99443	-0.749224	-3.12799	5.00E-05	0.00280638	yes

Fam65b	chr13:24706478-24825675	OK	2.19606	3.54423	0.690553	1.96092	0.0011	0.0354678	yes
Fam70a	chrX:35550477-35605658	OK	14.4838	4.71793	-1.61821	-5.65615	5.00E-05	0.00280638	yes
Fbl	chr7:28954766-28964288	OK	30.725	42.9296	0.482563	2.01895	0.001	0.0331849	yes
Fbxo2	chr4:147534776-147540526	OK	62.0838	85.5474	0.462506	2.106	0.0007	0.0250585	yes
Fgd3	chr13:49358478-49404577	OK	3.36203	5.57218	0.728912	2.20274	0.00035	0.0142073	yes
Fgf13	chrX:56315327-56387613	OK	7.89719	11.8649	0.587289	2.02786	0.0008	0.0279059	yes
Fibcd1	chr2:31668809-31701525	OK	0.238075	0.940962	1.98272	2.98286	5.00E-05	0.00280638	yes
Fos	chr12:86814850-86818219	OK	10.3431	36.5413	1.82086	6.98052	5.00E-05	0.00280638	yes
Fosb	chr7:19888044-19895394	OK	0.333528	1.76151	2.40094	3.99616	5.00E-05	0.00280638	yes
Fosl2	chr5:32438844-32460212	OK	1.75902	3.82576	1.12098	3.43797	5.00E-05	0.00280638	yes
Foxo3	chr10:41905591-41996548	OK	35.6426	25.1777	-0.501456	-2.13407	0.00015	0.0072806	yes
Fstl4	chr11:52578207-53000849	OK	2.13198	3.617	0.762598	1.91332	0.0015	0.0457685	yes
Fstl5	chr3:75878482-76513927	OK	6.09899	3.34602	-0.866126	-2.89495	5.00E-05	0.00280638	yes
Fxyd7	chr7:31827533-31836473	OK	11.1999	21.3158	0.928436	2.71922	0.0003	0.0125512	yes
Fzd7	chr1:59538990-59543799	OK	21.3079	13.6429	-0.643237	-2.75657	5.00E-05	0.00280638	yes
Gabra5	chr7:64642641-64765379	OK	0.620756	2.18818	1.81763	2.81019	0.0001	0.00520573	yes
Gar1	chr3:129527829-129534314	OK	10.0716	16.0908	0.675947	2.2165	0.00045	0.0175359	yes
Garnl3	chr2:32841885-32942724	OK	23.914	14.3318	-0.738639	-3.10446	5.00E-05	0.00280638	yes
Gda	chr19:21465796-21547151	OK	0.462462	3.43024	2.8909	5.66067	5.00E-05	0.00280638	yes
Gm12824	chr4:114079328-114287703	OK	0.64663	2.62406	2.02079	4.81147	5.00E-05	0.00280638	yes
Gm14169	chr2:156434933-156439158	OK	2.30133	4.85574	1.07722	2.73015	5.00E-05	0.00280638	yes
Gm20594	chr6:79768024-79768358	OK	52.5482	114.398	1.12235	4.90279	5.00E-05	0.00280638	yes
Gm2694	chr8:89996710-90049453	OK	106.176	71.7038	-0.566331	-2.63252	5.00E-05	0.00280638	yes
Gmfg	chr7:29222465-29231914	OK	1.19066	3.39444	1.51141	2.13106	0.00055	0.0208374	yes
Gng13	chr17:25854116-25864360	OK	127.191	230.076	0.855117	3.38983	5.00E-05	0.00280638	yes
Gng4	chr13:13876805-13920162	OK	0.83667	3.03906	1.86089	3.60745	5.00E-05	0.00280638	yes
Gpr137c	chr14:45839391-45900651	OK	17.8432	12.0077	-0.571413	-2.21946	0.0003	0.0125512	yes
Gpr153	chr4:151648470-151659446	OK	13.2647	9.43056	-0.492179	-1.97739	0.00085	0.0292756	yes
Gpr26	chr7:139158142-139177316	OK	0.87337	1.95997	1.16617	2.15025	0.00095	0.0320719	yes
Gpr63	chr4:24900565-24936380	OK	3.71442	6.43998	0.793921	2.27681	0.0003	0.0125512	yes
Gpr88	chr3:115952571-115956402	OK	0.19023	1.10792	2.54204	3.42473	5.00E-05	0.00280638	yes
Gpx3	chr11:54716354-54723889	OK	4.70151	10.1106	1.10467	2.77731	5.00E-05	0.00280638	yes
Gria3	chrX:38754480-39031778	OK	16.0522	23.2112	0.532047	2.30743	0.00015	0.0072806	yes
Grid2ip	chr5:144119016-144153477	OK	7.26951	12.9748	0.835787	3.15515	5.00E-05	0.00280638	yes
Grik4	chr9:42328494-42752454	OK	4.05822	7.29553	0.846166	2.81832	5.00E-05	0.00280638	yes
Grin2b	chr6:135679822-136123529	OK	0.568296	1.46214	1.36336	3.05383	5.00E-05	0.00280638	yes
Grm5	chr7:94732677-95283573	OK	1.72135	3.11594	0.856129	2.76158	5.00E-05	0.00280638	yes
Hap1	chr11:100208640-100217455	OK	37.077	54.7161	0.56144	2.35511	5.00E-05	0.00280638	yes
Hba-a1,Hba-a2	chr11:32196488-32197310	OK	143.633	252.697	0.815015	3.17944	5.00E-05	0.00280638	yes

Hbb-b2	chr7:110961037-110962437	OK	357.179	714.227	0.999736	3.9339	5.00E-05	0.00280638	yes
Hmgb2	chr8:59990639-59994796	OK	3.43634	6.46566	0.911926	2.54653	5.00E-05	0.00280638	yes
Homer3	chr8:72806897-72826351	OK	83.3146	113.676	0.448282	1.83306	0.00135	0.042038	yes
Hpcal1	chr12:17697619-17798732	OK	74.4703	131.318	0.818328	3.75532	5.00E-05	0.00280638	yes
Hpcal4	chr4:122860746-122871942	OK	12.5698	28.5258	1.1823	4.50034	5.00E-05	0.00280638	yes
Hrh3	chr2:179834177-179838927	OK	5.94013	11.7093	0.979087	3.33541	5.00E-05	0.00280638	yes
Hs3st4	chr7:131126694-131542503	OK	0.836915	3.24397	1.95461	3.74763	5.00E-05	0.00280638	yes
Hspa14	chr2:3406125-3430086	OK	29.4721	48.4252	0.716409	3.12456	5.00E-05	0.00280638	yes
Htr1a	chr13:106233772-106238213	OK	0.267459	1.04289	1.96319	3.03786	5.00E-05	0.00280638	yes
Icam5	chr9:20836481-20843480	OK	0.624267	6.50575	3.38148	5.9097	5.00E-05	0.00280638	yes
Igfbp4	chr11:98902573-98913957	OK	4.50514	9.74629	1.11328	3.31653	5.00E-05	0.00280638	yes
Igfbp5	chr1:72904638-72921439	OK	30.0367	42.5753	0.503293	2.22115	0.0002	0.00915369	yes
Ikzf1	chr11:11586215-11672929	OK	0.377389	1.75361	2.2162	3.87871	5.00E-05	0.00280638	yes
Il34	chr8:113265728-113329803	OK	4.2854	7.75181	0.855104	2.24105	0.0001	0.00520573	yes
Ildr2	chr1:168184269-168246963	OK	2.67343	4.37793	0.711559	2.59076	5.00E-05	0.00280638	yes
Inpp5d	chr1:89516886-89617083	OK	1.29824	2.35983	0.862127	2.06687	0.00045	0.0175359	yes
Irf8	chr8:123260275-123280592	OK	1.4194	2.78469	0.972235	2.08066	0.00105	0.0342606	yes
Islr2	chr9:58044103-58056615	OK	0.503595	1.89026	1.90825	3.07094	5.00E-05	0.00280638	yes
Itgal	chr7:134439773-134478651	OK	0.373968	1.27971	1.77482	3.08847	5.00E-05	0.00280638	yes
Itih3	chr14:31721759-31736773	OK	49.5222	33.484	-0.564603	-2.51343	5.00E-05	0.00280638	yes
Itpka	chr2:119568072-119576989	OK	18.4935	28.907	0.644406	2.58066	5.00E-05	0.00280638	yes
Junb	chr8:87500807-87502647	OK	12.6882	22.5888	0.832118	3.15438	5.00E-05	0.00280638	yes
Kalrn	chr16:33969158-34514113	OK	4.33651	9.65295	1.15444	3.67333	5.00E-05	0.00280638	yes
Kat2b	chr17:53706295-53812046	OK	25.7859	19.0794	-0.434566	-1.81866	0.0015	0.0457685	yes
Kcna6	chr6:126658346-126690692	OK	13.0243	20.5569	0.658417	2.84	5.00E-05	0.00280638	yes
Kcnab2	chr4:151764848-151851658	OK	54.4014	72.2513	0.40938	1.78389	0.0016	0.0478561	yes
Kcnc2	chr10:111708178-111903360	OK	1.80148	3.58695	0.993572	3.06185	5.00E-05	0.00280638	yes
Kcnf1	chr12:17178905-17183694	OK	0.121885	1.6805	3.7853	5.02958	5.00E-05	0.00280638	yes
Kcnip2	chr19:45868159-45890293	OK	1.764	5.91553	1.74565	2.4244	0.00025	0.0108246	yes
Kcnj4	chr15:79314143-79335671	OK	0.497158	3.89316	2.96917	4.66259	5.00E-05	0.00280638	yes
Kcnn4	chr7:25155281-25170231	OK	0.187895	1.1774	2.64761	2.58258	0.00025	0.0108246	yes
Kcnq5	chr1:21388483-21952023	OK	0.404605	1.22587	1.59922	3.09614	5.00E-05	0.00280638	yes
Kcnv1	chr15:44937829-44946480	OK	0.0781372	0.834642	3.41708	3.67555	0.0002	0.00915369	yes
Kctd13	chr7:134072392-134089123	OK	40.8218	55.6775	0.447753	1.99459	0.00105	0.0342606	yes
Khdrbs3	chr15:68758849-68923948	OK	12.3606	19.2891	0.642036	2.3929	0.0001	0.00520573	yes
Kif11	chr19:37450892-37496349	OK	0.353236	1.05856	1.5834	2.63062	5.00E-05	0.00280638	yes
Kif15	chr9:122860198-122927851	OK	0.316647	0.807338	1.3503	2.16282	0.00085	0.0292756	yes
Klf2	chr8:74842960-74845553	OK	2.74944	6.62881	1.26961	3.10508	5.00E-05	0.00280638	yes
Klhdc7a	chr4:139518087-139523941	OK	2.08799	3.26385	0.644459	1.98797	0.0008	0.0279059	yes

Laptm5	chr4:130469248-130492063	OK	6.64935	13.6673	1.03945	3.45905	5.00E-05	0.00280638	yes
Lat2	chr5:135076134-135090893	OK	1.60751	3.78768	1.23649	2.20554	0.0009	0.0307647	yes
Lcp1	chr14:75530929-75630649	OK	2.67383	5.62234	1.07226	3.07847	5.00E-05	0.00280638	yes
Ldb2	chr5:44863371-45190946	OK	1.35773	3.3188	1.28946	2.618	5.00E-05	0.00280638	yes
Lgals1	chr15:78757154-78760895	OK	20.9705	33.7312	0.685727	2.43889	0.00015	0.0072806	yes
Lhx2	chr2:38206827-38225248	OK	0.386063	3.38991	3.13434	4.39414	5.00E-05	0.00280638	yes
Lin7a	chr10:106708886-106862199	OK	26.8288	19.3229	-0.473476	-2.0475	0.00025	0.0108246	yes
Lmo3	chr6:138313001-138530489	OK	1.48298	3.58903	1.27509	2.59438	0.00015	0.0072806	yes
Lmo4	chr3:143851493-143868219	OK	19.7421	29.4133	0.575194	2.17789	0.0002	0.00915369	yes
Lmo7	chr14:102129144-102333910	OK	2.11251	4.12074	0.963949	3.10297	5.00E-05	0.00280638	yes
Lor	chr3:91884192-91887064	OK	0.733984	1.97799	1.43021	2.25337	0.00085	0.0292756	yes
Lrfn2	chr17:49071906-49236915	OK	0.5207	1.50494	1.53118	2.50359	0.0002	0.00915369	yes
Lrmp	chr6:145070258-145159490	OK	0.522105	2.27944	2.12627	2.62915	0.00025	0.0108246	yes
Lrp4	chr2:91297687-91354058	OK	3.66773	5.3258	0.538111	2.01264	0.0006	0.0224203	yes
Lrrn1	chr6:107479719-107520222	OK	44.5558	30.73	-0.535965	-2.34683	5.00E-05	0.00280638	yes
Ly6h	chr15:75395174-75397612	OK	19.0874	38.5069	1.0125	3.3944	5.00E-05	0.00280638	yes
Lyl1	chr8:87225355-87228615	OK	0.544188	2.01052	1.88539	2.72016	0.00015	0.0072806	yes
Lzts1	chr8:71659401-71664852	OK	1.8692	4.04491	1.11369	2.29985	0.0005	0.0192099	yes
Mal2	chr15:54402920-54434401	OK	1.98876	5.18385	1.38216	3.46561	5.00E-05	0.00280638	yes
7-Mar	chr2:60047992-60086442	OK	19.8774	14.0687	-0.498638	-2.02098	0.00105	0.0342606	yes
Mcm3	chr1:20793094-20810294	OK	1.48168	3.08137	1.05634	2.32149	0.00035	0.0142073	yes
Mcm5	chr8:77633426-77652338	OK	3.6911	6.18873	0.745593	2.31067	5.00E-05	0.00280638	yes
Mcm6	chr1:130228167-130256233	OK	0.550107	3.67803	2.74115	4.79775	5.00E-05	0.00280638	yes
Mef2a	chr7:74378716-74517744	OK	32.4767	22.8934	-0.504472	-2.11597	0.00035	0.0142073	yes
Mef2c	chr13:83643032-83806684	OK	6.0457	9.28015	0.618239	2.30965	5.00E-05	0.00280638	yes
Megf11	chr9:64233432-64557012	OK	37.06	26.9842	-0.457748	-1.9532	0.0003	0.0125512	yes
Meis2	chr2:115686999-115890794	OK	1.86487	3.6191	0.956554	2.70272	5.00E-05	0.00280638	yes
Mesdc1	chr7:91029004-91032851	OK	12.7587	17.6173	0.465507	1.94925	0.0007	0.0250585	yes
Miat	chr5:112642247-112657968	OK	2.70531	8.88124	1.71497	6.38818	5.00E-05	0.00280638	yes
Midn	chr10:79611034-79621112	OK	12.9155	18.2331	0.497456	2.07962	0.0007	0.0250585	yes
Mira	chr6:52164489-52165287	OK	0	1.66534	inf	#NAME?	5.00E-05	0.00280638	yes
Mki67	chr7:142881470-142908062	OK	0.123557	1.46904	3.57162	5.82376	5.00E-05	0.00280638	yes
Mlec	chr5:115592989-115608185	OK	27.0694	36.714	0.439667	1.93402	0.00105	0.0342606	yes
Mlph	chr1:92811676-92847719	OK	0.993015	2.56213	1.36745	3.17516	5.00E-05	0.00280638	yes
Mmp15	chr8:97876236-97898193	OK	7.02959	9.80518	0.480105	1.86218	0.00115	0.0369926	yes
Mpped1	chr15:83610452-83688904	OK	1.9114	7.06738	1.88655	4.87175	5.00E-05	0.00280638	yes
Mrc2	chr11:105153959-105212459	OK	1.73909	2.78127	0.677409	1.97465	0.00125	0.0395563	yes
Myb	chr10:20844735-20880790	OK	0.196038	1.554	2.98678	3.82652	5.00E-05	0.00280638	yes
Mybpc3	chr2:90958300-90976673	OK	21.4983	15.2886	-0.491769	-2.10576	0.00035	0.0142073	yes

Myc	chr15:61816895-61821916	OK	1.04995	2.70963	1.36778	2.46341	0.00015	0.0072806	yes
Myl4	chr11:104411976-104448533	OK	0.85794	2.99472	1.80347	2.5682	0.001	0.0331849	yes
Myo10	chr15:25552304-25743426	OK	6.05792	9.18183	0.599958	2.49245	0.0001	0.00520573	yes
Myo1g	chr11:6406550-6420961	OK	0.134428	1.09735	3.02913	3.55806	5.00E-05	0.00280638	yes
Myo5b	chr18:74602272-74931131	OK	0.501429	1.22795	1.29214	2.5703	0.0001	0.00520573	yes
Myo7a	chr7:105199563-105268003	OK	0.837884	1.52589	0.864826	2.06226	0.0007	0.0250585	yes
Napsa	chr7:51827814-51842216	OK	0.519944	1.94125	1.90055	2.56448	0.00075	0.0266387	yes
Ncan	chr8:72616983-72644743	OK	4.52298	7.62946	0.754308	2.97226	5.00E-05	0.00280638	yes
Ncf1	chr5:134696129-134705495	OK	1.11473	2.84928	1.35391	2.69612	5.00E-05	0.00280638	yes
Ncf4	chr15:78075240-78093010	OK	0.381541	1.7153	2.16855	2.71091	0.00055	0.0208374	yes
Ndst3	chr3:123229083-123375310	OK	20.364	14.5123	-0.488739	-2.10493	0.00025	0.0108246	yes
Neat1	chr19:5842301-5845478	OK	30.7817	41.5641	0.433265	1.91237	0.0009	0.0307647	yes
Neb	chr2:51992166-52194318	OK	1.67359	1.12217	-0.57666	-2.09853	0.0002	0.00915369	yes
Necab1	chr4:14857787-15076278	OK	3.46294	5.23801	0.597022	1.92382	0.00095	0.0320719	yes
Necab2	chr8:121970618-121996535	OK	1.53527	5.00379	1.70453	3.56514	5.00E-05	0.00280638	yes
Nek2	chr1:193645351-193656928	OK	2.84683	1.40894	-1.01475	-2.3098	0.00045	0.0175359	yes
Nell1	chr7:57230719-58118659	OK	6.90545	15.9764	1.21013	4.33483	5.00E-05	0.00280638	yes
Neto1	chr18:86564343-86671289	OK	0.78263	1.80494	1.20555	2.30871	5.00E-05	0.00280638	yes
Neurl1b	chr17:26551909-26583287	OK	0.212293	0.888783	2.06577	3.31334	5.00E-05	0.00280638	yes
Neurod6	chr6:55627812-55631257	OK	1.60319	3.77707	1.23632	2.55042	5.00E-05	0.00280638	yes
Nfyc	chr4:120430039-120504180	OK	43.5416	31.1458	-0.483357	-2.00965	0.00055	0.0208374	yes
Ngb	chr12:88438480-88443489	OK	0.873314	3.44804	1.9812	3.22642	5.00E-05	0.00280638	yes
Ngef	chr1:89373403-89470445	OK	7.09521	16.1489	1.18651	4.1267	5.00E-05	0.00280638	yes
Nnat	chr2:157382097-157392097	OK	113.349	172.824	0.608539	1.99234	0.0005	0.0192099	yes
Nog	chr11:89161951-89163873	OK	2.80097	5.04144	0.847908	2.0538	0.001	0.0331849	yes
Npas4	chr19:4984354-4989971	OK	1.22188	4.40429	1.84981	4.29072	5.00E-05	0.00280638	yes
Nptx2	chr5:145306755-145318347	OK	0.71619	1.98023	1.46725	2.54161	0.0003	0.0125512	yes
Nr4a1	chr15:101097276-101105225	OK	5.10156	25.8712	2.34234	8.09617	5.00E-05	0.00280638	yes
Nr4a2	chr2:56959636-56976414	OK	2.01643	8.27019	2.03612	5.38368	5.00E-05	0.00280638	yes
Nr4a3	chr4:48064119-48096224	OK	1.24247	4.92669	1.98741	3.90613	5.00E-05	0.00280638	yes
Nrarp	chr2:25036277-25038852	OK	1.84503	4.31249	1.22488	2.90111	5.00E-05	0.00280638	yes
Nrgn	chr9:37352077-37360330	OK	23.4397	94.9195	2.01775	7.47306	5.00E-05	0.00280638	yes
Nrk	chrX:135448968-135543629	OK	1.84426	0.53178	-1.79414	-3.92177	5.00E-05	0.00280638	yes
Nrsn1	chr13:25343907-25361865	OK	52.4698	72.951	0.475442	2.12362	0.0003	0.0125512	yes
Nsg1	chr5:38528431-38550706	OK	250.38	402.525	0.684956	2.94255	5.00E-05	0.00280638	yes
Nsg2	chr11:31900458-31959202	OK	90.7052	125.43	0.467628	2.10157	0.00035	0.0142073	yes
Ntm	chr9:28803548-29770714	OK	118.621	88.1805	-0.427832	-1.92939	0.00105	0.0342606	yes
Odz1	chrX:39885569-40627963	OK	11.8761	8.44265	-0.492291	-2.02673	0.00045	0.0175359	yes
Odz2	chr11:35820170-36757745	OK	2.87444	4.57034	0.66902	2.54061	5.00E-05	0.00280638	yes

Odz4	chr7:103359146-104057064	OK	2.79067	4.18787	0.585603	2.23346	5.00E-05	0.00280638	yes
Olfm2	chr9:20472429-20532658	OK	7.74501	13.1469	0.763387	2.44837	0.0001	0.00520573	yes
Olfm3	chr3:114607280-114828174	OK	36.1946	27.0608	-0.419566	-1.78374	0.00145	0.0445418	yes
Otof	chr5:30669350-30764305	OK	0.23995	0.953048	1.98981	3.37664	5.00E-05	0.00280638	yes
Padi2	chr4:140462274-140513817	OK	27.1569	18.9331	-0.520405	-2.22978	0.00015	0.0072806	yes
Pak6	chr2:118489312-118523756	OK	1.42287	3.43117	1.26989	3.05518	5.00E-05	0.00280638	yes
Pam	chr1:99717670-99992209	OK	16.0421	21.8521	0.445905	1.87893	0.0012	0.0384197	yes
Parvg	chr15:84155149-84173408	OK	0.965964	4.03941	2.0641	3.97313	5.00E-05	0.00280638	yes
Pcdh19	chrX:130117399-130223532	OK	0.553498	1.00661	0.862856	2.05897	0.0008	0.0279059	yes
Pcdh8	chr14:80166578-80171119	OK	0.941787	2.62054	1.47639	3.08464	5.00E-05	0.00280638	yes
Pcp2	chr8:3621550-3625545	OK	544.538	880.152	0.692721	2.79466	5.00E-05	0.00280638	yes
Pcp4	chr16:96689212-96747400	OK	464.123	740.477	0.673948	3.37103	5.00E-05	0.00280638	yes
Pde1a	chr2:79674609-79969569	OK	1.39336	4.53135	1.70137	2.96265	5.00E-05	0.00280638	yes
Pde2a	chr7:108570204-108661343	OK	11.3342	19.3132	0.768909	3.01907	5.00E-05	0.00280638	yes
Pdzrn3	chr6:101099600-101327891	OK	0.980705	2.07721	1.08276	2.34565	0.0002	0.00915369	yes
Per1	chr11:68912457-68923459	OK	13.7338	21.2507	0.629779	2.66985	5.00E-05	0.00280638	yes
Perp	chr10:18564876-18576878	OK	3.20569	5.78562	0.851836	2.15895	0.00105	0.0342606	yes
Pgrmc2	chr3:40870247-40886968	OK	26.8483	37.1522	0.468617	2.05749	0.00045	0.0175359	yes
Pkia	chr3:7366603-7445365	OK	59.2507	38.91	-0.606692	-2.67804	5.00E-05	0.00280638	yes
Plcb4	chr2:135567565-135838804	OK	64.6432	46.933	-0.461896	-2.00769	0.0004	0.0159988	yes
Plcg2	chr8:120022190-120159042	OK	1.10881	3.62692	1.70973	3.95344	5.00E-05	0.00280638	yes
Pld3	chr7:28317036-28338131	OK	47.0529	69.1748	0.555962	2.48333	5.00E-05	0.00280638	yes
Plekhg5	chr4:151470827-151489509	OK	2.49286	4.89262	0.972807	2.94185	5.00E-05	0.00280638	yes
Plxdc1	chr11:97784550-97847760	OK	13.6272	21.4103	0.651811	2.62166	5.00E-05	0.00280638	yes
Pou4f1	chr14:104861540-104867216	OK	0.0816129	1.83166	4.48821	4.76599	5.00E-05	0.00280638	yes
Ppapdc2	chr19:28997553-29041291	OK	13.0011	18.2845	0.491981	1.91035	0.00075	0.0266387	yes
Ppp1r14b	chr19:7049537-7051814	OK	27.9664	40.5905	0.537448	2.15506	0.00095	0.0320719	yes
Ppp1r16b	chr2:158492468-158592070	OK	26.7871	43.4482	0.697757	3.0467	5.00E-05	0.00280638	yes
Prss12	chr3:123149830-123209520	OK	0.299441	1.37197	2.1959	3.06267	0.00015	0.0072806	yes
Psd2	chr18:36124488-36174369	OK	38.7714	55.3692	0.51409	2.27726	0.00015	0.0072806	yes
Psg16	chr7:17659388-17684320	OK	7.98546	5.15588	-0.631156	-1.97308	0.00125	0.0395563	yes
Psmb8	chr17:34335139-34338399	OK	2.53796	8.33508	1.71552	3.617	5.00E-05	0.00280638	yes
Ptch1	chr13:63612840-63666828	OK	30.866	21.5323	-0.519517	-2.23383	5.00E-05	0.00280638	yes
Ptk2b	chr14:66772093-66899889	OK	1.31415	10.9734	3.06181	7.32357	5.00E-05	0.00280638	yes
Ptpn4	chr1:121554669-121733648	OK	16.7275	12.0759	-0.470088	-1.9232	0.0015	0.0457685	yes
Ptpn5	chr7:54333169-54389054	OK	8.22884	14.0832	0.775215	2.87934	5.00E-05	0.00280638	yes
Ptpn6	chr6:124670735-124688727	OK	1.38205	3.43347	1.31285	2.50785	0.0001	0.00520573	yes
Ptprc	chr1:139959437-140071882	OK	0.469655	1.3359	1.50814	2.78609	5.00E-05	0.00280638	yes
Pvalb	chr15:78021547-78034586	OK	729.727	995	0.44734	2.03388	0.0016	0.0478561	yes

Rac2	chr15:78389598-78403213	OK	0.760928	2.39474	1.65404	3.05934	5.00E-05	0.00280638	yes
Rasal1	chr5:121098830-121129602	OK	2.50797	4.38566	0.806272	2.17578	0.0006	0.0224203	yes
Rasgrf2	chr13:92020011-92901449	OK	1.24307	3.54977	1.51381	4.41474	5.00E-05	0.00280638	yes
Rasgrp2	chr19:6400582-6415216	OK	3.87488	6.95207	0.843293	2.35332	0.0002	0.00915369	yes
Rbm38	chr2:172847402-172860232	OK	1.41251	3.14522	1.1549	2.18115	0.0007	0.0250585	yes
Rcc2	chr4:140257387-140279135	OK	22.9239	34.2841	0.580688	2.52155	0.0001	0.00520573	yes
Resp18	chr1:75268776-75274955	OK	31.3058	55.4247	0.824102	3.26561	5.00E-05	0.00280638	yes
Rgs14	chr13:55471092-55486048	OK	0.10546	1.47561	3.80655	3.86869	0.00065	0.0238316	yes
Rgs4	chr1:171671607-171677773	OK	7.46514	12.669	0.763056	2.76109	5.00E-05	0.00280638	yes
Rgs8	chr1:155500166-155544795	OK	63.7924	133.224	1.06239	4.47895	5.00E-05	0.00280638	yes
Rhobtb2	chr14:70184796-70205352	OK	12.803	22.5075	0.813924	3.51498	5.00E-05	0.00280638	yes
Rimbp2	chr5:129266275-129459237	OK	1.73594	4.12125	1.24737	3.42742	5.00E-05	0.00280638	yes
Rlf	chr4:120817977-120861139	OK	6.52871	4.69323	-0.476218	-1.84075	0.00155	0.0467709	yes
Rprm	chr2:53936503-53937963	OK	1.4053	5.67799	2.0145	3.82022	5.00E-05	0.00280638	yes
Rprml	chr11:103510822-103511894	OK	1.15233	4.20478	1.86748	3.00734	5.00E-05	0.00280638	yes
Rrm2	chr12:25393118-25399011	OK	0.486772	1.98259	2.02607	3.0724	0.0001	0.00520573	yes
Rspo2	chr15:42852340-43002364	OK	0.474619	1.50872	1.66848	2.74712	5.00E-05	0.00280638	yes
Ryr1	chr7:29788358-29910170	OK	2.45707	3.49155	0.506929	2.01006	0.0004	0.0159988	yes
S100a4	chr3:90407691-90409967	OK	0.822634	14.4201	4.13169	5.35458	5.00E-05	0.00280638	yes
Satb2	chr1:56850824-57028178	OK	0.19776	0.927935	2.23027	3.34507	5.00E-05	0.00280638	yes
Scn3b	chr9:40076800-40099203	OK	1.91528	4.48021	1.22601	3.37838	5.00E-05	0.00280638	yes
Sema7a	chr9:57787941-57810672	OK	59.6127	83.8736	0.492596	2.19036	0.00025	0.0108246	yes
Sept9	chr11:117060974-117223639	OK	4.64929	9.77337	1.07184	3.46324	5.00E-05	0.00280638	yes
Sez6l	chr5:112848170-113006218	OK	43.3756	59.8792	0.46517	2.04292	0.00055	0.0208374	yes
Shank2	chr7:151361424-151608580	OK	22.9882	30.6581	0.415373	1.81252	0.0011	0.0354678	yes
Shisa7	chr7:4777153-4796298	OK	1.80386	3.20925	0.831146	2.50615	5.00E-05	0.00280638	yes
Sik1	chr17:31981194-31992737	OK	2.10429	5.26162	1.32217	4.00183	5.00E-05	0.00280638	yes
Six3	chr17:86020173-86025531	OK	0.394561	1.03206	1.38721	2.02829	0.00145	0.0445418	yes
Skor2	chr18:77095143-77139081	OK	3.59611	1.97519	-0.864444	-2.19201	0.00075	0.0266387	yes
Slc10a4	chr5:73398142-73404194	OK	0.276387	1.22295	2.1456	2.59733	0.00065	0.0238316	yes
Slc11a1	chr1:74421776-74432625	OK	1.09831	2.501	1.18722	2.19233	0.00065	0.0238316	yes
Slc18a2	chr19:59335367-59370502	OK	1.12136	2.72941	1.28334	2.89301	5.00E-05	0.00280638	yes
Slc1a3	chr15:8584123-8660807	OK	282.35	183.339	-0.622968	-2.47805	5.00E-05	0.00280638	yes
Slc1a5	chr7:17366694-17383623	OK	0.712085	1.96879	1.46719	2.56143	0.00025	0.0108246	yes
Slc20a1	chr2:129024508-129037348	OK	51.0335	70.9291	0.474935	2.02002	0.001	0.0331849	yes
Slc2a13	chr15:91098121-91403692	OK	8.78549	13.8934	0.661207	2.78455	5.00E-05	0.00280638	yes
Slc30a3	chr5:31388478-31395900	OK	1.64036	5.52597	1.75222	3.75529	5.00E-05	0.00280638	yes
Slc43a3	chr2:84776802-84798666	OK	0.257116	1.19917	2.22154	2.9868	0.00015	0.0072806	yes
Slc5a1	chr5:33446867-33505348	OK	1.57157	0.491741	-1.67624	-2.99807	5.00E-05	0.00280638	yes

Slc6a11	chr6:114081234-114199880	OK	29.5685	47.4558	0.682526	2.85708	5.00E-05	0.00280638	yes
Slc6a17	chr3:107270465-107320936	OK	60.8221	86.3972	0.506388	2.18238	0.0002	0.00915369	yes
Slc6a2	chr8:95484945-95525566	OK	0.346444	1.11007	1.67995	2.89042	5.00E-05	0.00280638	yes
Slc6a7	chr18:61155033-61173853	OK	5.95225	9.02472	0.600447	2.14745	0.00045	0.0175359	yes
Slc7a1	chr5:149138985-149211480	OK	5.37221	7.54134	0.489306	1.9581	0.0008	0.0279059	yes
Slit1	chr19:41674746-41818346	OK	0.521228	2.47053	2.24483	4.55081	5.00E-05	0.00280638	yes
Slitrk4	chrX:61522618-61530171	OK	6.31878	4.29327	-0.55757	-1.8791	0.00145	0.0445418	yes
Slpi	chr2:164179805-164182243	OK	0.301711	2.21627	2.87689	2.96658	0.00155	0.0467709	yes
Smad3	chr9:63494573-63605801	OK	17.8838	13.1329	-0.445471	-1.90568	0.0011	0.0354678	yes
Smc6	chr12:11272691-11326591	OK	14.1022	10.4027	-0.438965	-1.8581	0.00145	0.0445418	yes
Sncg	chr14:35183459-35187855	OK	7.60243	14.7794	0.959057	2.47018	0.0003	0.0125512	yes
Snhg11	chr2:158201373-158211881	OK	83.2535	128.872	0.630359	2.6494	5.00E-05	0.00280638	yes
Sorcs2	chr5:36359829-36740788	OK	2.98311	6.87943	1.20547	4.19902	5.00E-05	0.00280638	yes
Sphkap	chr1:83252355-83404775	OK	106.273	75.5452	-0.492369	-2.00203	0.00065	0.0238316	yes
Spn	chr7:134276977-134281331	OK	0.106114	1.35848	3.67832	3.2019	5.00E-05	0.00280638	yes
Spnb3	chr19:4711222-4752352	OK	116.616	197.619	0.760962	2.95642	5.00E-05	0.00280638	yes
Spry4	chr18:38745918-38760922	OK	1.78815	3.37036	0.914435	2.55076	0.0001	0.00520573	yes
Sst	chr16:23889666-23890930	OK	21.1049	67.4118	1.67542	6.03847	5.00E-05	0.00280638	yes
Sstr1	chr12:59312790-59317023	OK	0.829294	2.00696	1.27506	2.59004	5.00E-05	0.00280638	yes
St18	chr1:6477311-6851021	OK	15.7726	11.6157	-0.441352	-1.81183	0.00155	0.0467709	yes
St3gal1	chr15:66934436-67008444	OK	1.00797	1.97132	0.96771	2.38719	0.0002	0.00915369	yes
St6galnac5	chr3:152483673-152645171	OK	1.38226	4.4553	1.68849	3.40783	5.00E-05	0.00280638	yes
Stk3	chr15:34805253-35085561	OK	9.32688	5.85588	-0.671508	-2.33635	0.00015	0.0072806	yes
Stk32b	chr5:37838063-38108392	OK	0.224242	0.997436	2.15317	2.86004	0.00015	0.0072806	yes
Stk32c	chr7:146289536-146428872	OK	5.46305	11.3954	1.06067	2.98491	5.00E-05	0.00280638	yes
Stx1a	chr5:135499441-135526969	OK	2.54769	12.234	2.26363	5.68797	5.00E-05	0.00280638	yes
Stxbp6	chr12:45953472-46175470	OK	2.94782	4.57458	0.63399	1.9886	0.0014	0.0433968	yes
Sv2b	chr7:82259780-82476305	OK	58.5851	43.1251	-0.442007	-1.87695	0.0013	0.0406667	yes
Sv2c	chr13:96729397-96902532	OK	5.96176	3.73547	-0.674449	-2.27804	0.00015	0.0072806	yes
Sycp1	chr3:102622421-102740023	OK	3.74612	1.71338	-1.12855	-2.85962	5.00E-05	0.00280638	yes
Synpo	chr18:60753643-60783959	OK	3.60058	6.96487	0.951866	3.1664	5.00E-05	0.00280638	yes
Syt10	chr15:89612823-89672291	OK	7.04726	3.97225	-0.827108	-2.23228	0.0004	0.0159988	yes
Syt16	chr12:75098747-75368903	OK	0.951361	2.84199	1.57884	3.02992	5.00E-05	0.00280638	yes
Syt5	chr7:4491366-4498169	OK	5.88658	16.3573	1.47443	4.62874	5.00E-05	0.00280638	yes
Tbr1	chr2:61642509-61652170	OK	0.163061	1.41686	3.11921	4.24525	5.00E-05	0.00280638	yes
Tex261	chr6:83720407-83725806	OK	20.3751	29.1378	0.516085	2.0748	0.0008	0.0279059	yes
Tifab	chr13:56275063-56280246	OK	0.51202	1.24225	1.27869	2.07662	0.0007	0.0250585	yes
Timp2	chr11:118162374-118216725	OK	30.9749	43.2988	0.483226	2.11418	0.0002	0.00915369	yes
Tmem130	chr5:145496783-145522447	OK	48.1574	67.7708	0.492906	2.17583	0.00015	0.0072806	yes

Tmem132b	chr5:126012787-126272953	OK	2.20518	3.50103	0.666884	2.27182	5.00E-05	0.00280638	yes
Tmem179	chr12:113738394-113749371	OK	9.20511	17.6403	0.938366	3.50268	5.00E-05	0.00280638	yes
Tmem191c	chr16:17276392-17278754	OK	7.95621	13.6007	0.773529	2.44654	5.00E-05	0.00280638	yes
Tmem40	chr6:115679156-115712484	OK	0.186414	1.74937	3.23025	1.89674	0.00035	0.0142073	yes
Tmem56	chr3:120904927-120966234	OK	15.5599	11.2544	-0.467351	-1.98231	0.00045	0.0175359	yes
Top2a	chr11:98854260-98885503	OK	0.14861	2.06082	3.79362	5.46363	5.00E-05	0.00280638	yes
Tox2	chr2:163051189-163148838	OK	3.00857	5.99125	0.993778	2.37536	0.0003	0.0125512	yes
Tph2	chr10:114515696-114622078	OK	0.161358	4.90317	4.92538	6.29709	5.00E-05	0.00280638	yes
Trim62	chr4:128561383-128588570	OK	79.8025	55.9109	-0.513304	-2.28579	5.00E-05	0.00280638	yes
Trpc3	chr3:36519403-36589089	OK	14.9136	21.2089	0.508038	2.13851	0.00045	0.0175359	yes
Tshz2	chr2:169459145-169714004	OK	3.1134	4.78632	0.620426	2.08182	0.0005	0.0192099	yes
Tspan11	chr6:127837639-127903049	OK	1.7204	4.14764	1.26954	3.49924	5.00E-05	0.00280638	yes
Tspan14	chr14:41719732-41780096	OK	11.4478	17.071	0.576483	2.25561	0.0004	0.0159988	yes
Tubb2a	chr13:34166146-34169877	OK	84.8675	116.432	0.456204	2.08405	0.0005	0.0192099	yes
Uchl1	chr5:67067359-67078473	OK	153.998	221.127	0.521963	2.45083	0.0001	0.00520573	yes
Uhrf1	chr17:56442759-56462909	OK	0.239706	1.57813	2.71888	3.76822	5.00E-05	0.00280638	yes
Vav1	chr17:57418522-57468659	OK	0.557717	1.47782	1.40586	2.50986	0.00035	0.0142073	yes
Vav3	chr3:109143600-109488612	OK	3.9815	6.40018	0.6848	2.08392	0.00035	0.0142073	yes
Vgf	chr5:137506164-137509221	OK	12.8911	34.935	1.4383	5.80132	5.00E-05	0.00280638	yes
Vip	chr10:4698926-4707323	OK	0.911832	3.45696	1.92266	3.00168	5.00E-05	0.00280638	yes
Was	chrX:7658591-7667617	OK	0.456389	1.66521	1.86737	2.69543	5.00E-05	0.00280638	yes
Wdfy4	chr14:33772732-33998252	OK	0.198718	0.961546	2.27463	3.70462	5.00E-05	0.00280638	yes
Wnt3	chr11:103635488-103679335	OK	4.43862	7.92897	0.837022	2.77072	5.00E-05	0.00280638	yes
Wsb2	chr5:117807313-117828598	OK	66.1497	88.7748	0.424417	1.91336	0.0011	0.0354678	yes
Ywhah	chr5:33361464-33370615	OK	388.608	554.77	0.513573	2.19476	0.0001	0.00520573	yes
Zcchc12	chrX:33735898-33739153	OK	7.54798	17.1692	1.18566	4.08182	5.00E-05	0.00280638	yes
Zfp157	chr5:138882703-138901922	OK	5.07712	3.51983	-0.528504	-1.84227	0.00155	0.0467709	yes
Zfp238	chr1:179374791-179380897	OK	223.075	149.722	-0.575238	-2.33417	0.0002	0.00915369	yes
Zfp521	chr18:13845522-14131242	OK	35.0588	23.7515	-0.561758	-2.42854	5.00E-05	0.00280638	yes